REPORT DOCUMENTATION PAGE

Form Approved
OMB No. 0704-0188

1. AGENCY USE ONLY (Leave blank)	2. REPORT DATE	3. REPORT TYPE AND DATES COVERED
		FINAL REPORT 01 Nov 93 – 31 Aug 96

4. TITLE AND SUBTITLE
PHOTOREFRACTIVE TUNGSTEN BRONZE MATERIALS FOR OPTICAL COMPUTING

5. FUNDING NUMBERS

62712E
A492/03

6. AUTHOR(S)
Dr Neurgaonkar

7. PERFORMING ORGANIZATION NAME(S) AND ADDRESS(ES)
Rockwell Science Center
1049 Camino Dos Rios
Thousand Oaks, CA 91360

AFOSR-TR-96

0114   97

9. SPONSORING/MONITORING AGENCY NAME(S) AND ADDRESS(ES)
AFOSR/NE
110 Duncan Avenue Suite B115
Bolling AFB DC 20332-8050

10. SPONSORING/MONITORING AGENCY REPORT NUMBER

F49620-94-C-0005

11. SUPPLEMENTARY NOTES

12a. DISTRIBUTION/AVAILABILITY STATEMENT

APPROVED FOR PUBLIC RELEASE: DISTRIBUTION UNLIMITED

12b. DISTRIBUTION CODE

13. ABSTRACT (Maximum 200 words)

The optical tungsten bronze BSTN and BSKNN single crystals were investigated for photorefractive and guided-wave optical applications with considerable success. These materials have both high optical figure-of-merit and low dark conductivity, making them potentially important for pattern recognition and 3-D memory applications. Undopd crystals are advantageous for electro-optic devices such as guided-wave for telecommunication and signal processing. Under this effort, advances were made in growth of large size (4 cm diameter) BSTN and BSKNN crystals with possibility for large scale manufacturing. Also, investigations of guided-wave structures were carried out, which showed that the operating voltage and size can be much reduced compared to LiNbO3.

14. SUBJECT TERMS

15. NUMBER OF PAGES

16. PRICE CODE

17. SECURITY CLASSIFICATION OF REPORT	18. SECURITY CLASSIFICATION OF THIS PAGE	19. SECURITY CLASSIFICATION OF ABSTRACT	20. LIMITATION OF ABSTRACT
UNCLASSIFIED	UNCLASSIFIED	UNCLASSIFIED	

NSN 7540-01-280-5500

Standard Form 298 (Rev. 2-89)
Prescribed by ANSI Std. 239-18

SC71094.FR

PHOTOREFRACTIVE TUNGSTEN BRONZE CRYSTALS FOR OPTICAL COMPUTING

FINAL REPORT

For the Period November,1993 through August, 1996

CONTRACT NO. F49620-94-C-0005

Prepared for
Air Force Office of Scientific Research
Bolling AFB
Washington, D. C. 20332

R. R. Neurgaonkar
Principal Investigator

February 1997

Approved for public release; distribution unlimited

"The views and conclusions contained in this document are those of the authors and should not be interpreted as necessarily representing the official policies, either expressed or implied, of the Advanced Research Project Agency or the U.S. Government."

Rockwell

19970227 036

DISCLAIMER NOTICE
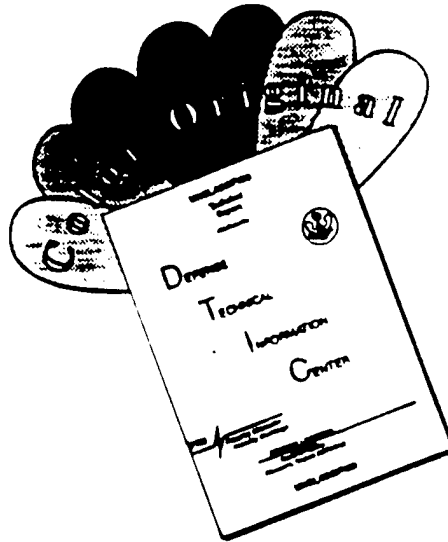
THIS DOCUMENT IS BEST QUALITY AVAILABLE. THE COPY FURNISHED TO DTIC CONTAINED A SIGNIFICANT NUMBER OF COLOR PAGES WHICH DO NOT REPRODUCE LEGIBLY ON BLACK AND WHITE MICROFICHE.

REPORT DOCUMENTATION PAGE	FORM APPROVED OMB No. 0704-0188

1a. REPORT SECURITY CLASSIFICATION **UNCLASSIFIED**	1b. RESTRICTIVE MARKINGS

2a. SECURITY CLASSIFICATION AUTHORITY	3. DISTRIBUTION/AVAILABILITY OF REPORT
2b. CLASSIFICATION/DOWNGRADING SCHEDULE	**Approved for public release; distribution unlimited**

4. PERFORMING ORGANIZATION REPORT NUMBER(S) **SC71094.FTR**	5. MONITORING ORGANIZATION REPORT NUMBER(S)

6a. NAME OF PERFORMING ORGANIZATION **ROCKWELL SCIENCE CENTER, INC.**	6b. OFFICE SYMBOL *(If Applicable)*	7a. NAME OF MONITORING ORGANIZATION

6c. ADDRESS *(City, State and ZIP Code)* **1049 Camino Dos Rios Thousand Oaks , CA 91360**	7b. ADDRESS *(City, State and ZIP Code)*

8a. NAME OF FUNDING/SPONSORING ORGANIZATION *AFOSR/NE* *Attn: Dr. Alan Craig*	8b. OFFICE SYMBOL *(If Applicable)*	9. PROCUREMENT INSTRUMENT IDENTIFICATION NUMBER *F49620-94-C-0005*

8C. ADDRESS *(City, State and ZIP Code)* *Directorate of Physics & Electronics* *110 Duncan Ave. Ste. B115* *Bolling AFB, DC 20332-001*	10. SOURCE OF FUNDING NOS.

PROGRAM ELEMENT NO.	PROJECT NO.	TASK NO.	WORK UNIT ACCESSION NO.

11. TITLE *(Include Security Classification)*

Photorefractive Tungsten Bronze Crystals for Optical Computing

12. PERSONAL AUTHOR(S)

Neurgaonkar, Ratnakar R.

13a. TYPE OF REPORT **Final Report**	13b. TIME COVERED FROM **11/01/93** TO **08/31/96**	14. DATE OF REPORT *(Year, Month, Day)* **February 7, 1997**	15. PAGE COUNT *20 + attachments*

16. SUPPLEMENTARY NOTATION

17. COSATI CODES			18. SUBJECT TERMS *(Continue on reverse if necessary and identify by block number)*
FIELD	GROUP	SUB-GROUP	*Electro-optic, photorefractive, guided-wave, pattern recognition, tungsten bronze, optical quality striation, single crystals, optical loss, modulators, switches, signal processing, 3-D memory.*

19. ABSTRACT *(Continue on reverse if necessary and identify by block number)*

The optical tungsten bronze BSTN and BSKNN single crystals were investigated for photorefractive and guided-wave optical applications with considerable success. These materials have both high optical figure-of-merit and low dark conductivity, making them potentially important for pattern recognition and 3-D memory applications. Undoped crystals are advantageous for electro-optic devices such as guided-wave for telecommunication and signal processing. Under this effort, advances were made in growth of large size (~4 cm diameter) BSTN and BSKNN crystals with possibility for large scale manufacturing. Also, investigations of guided-wave structures were carried out, which showed that the operating voltage and size can be much reduced compared to LiNbO3.

20. DISTRIBUTION/AVAILABILITY OF ABSTRACT UNCLASSIFIED/UNLIMITED ☐ SAME AS RPT. ☒ DTIC USERS ☐	21. ABSTRACT SECURITY CLASSIFICATION **UNCLASSIFIED**	
22a. NAME OF RESPONSIBLE INDIVIDUAL **R.R. Neurgaonkar**	22b. TELEPHONE NUMBER *(INCLUDE AREA CODE)* **805/373-4109**	22c. OFFICE SYMBOL **None**

DD FORM 1473   Previous editions are obsolete.

DTIC QUALITY INSPECTED 3

TABLE OF CONTENTS

LIST OF FIGURES

LIST OF TABLES

1.0   PROGRESS SUMMARY

This report covers the work on optical tungsten bronze crystals for photorefractive and optical wave-guide applications carried out over the period of November,1993, through September 31, 1996, in the Ferroelectric Materials Department of the Rockwell International Science Center under Contract No. F49620-94-C-0005. During this period, the superiority of new tungsten bronze materials in optical guided-wave structures has been demonstrated, and significant progress was made in the growth of tungsten bronze $(Ba,Sr)_6Ti_2Nb_8O_{30}$ (BSTN), and $Ba_{2-x}Sr_xK_{1-y}Na_yNb_5O_{15}$ (BSKNN) single crystals and the improvement of their photorefractive and guided-wave optical properties with respect to optical computing applications. At Caltech, Professor D. Psaltis and his group have characterized and studied the performance of these materials for a number of optical computing device configurations, including pattern recognition and 3-D holography with great success. Because BSTN and BSKNN have relatively lower dark conductivity, they retain holograms over a long period of time ($\sim$ 1 month) which is longer than SBN:60 (8 days).

Professor Henry Taylor at Texas A&M evaluated these tungsten bronze materials for guided-wave optics and found them superior to $LiNbO_3$ for many telecommunication and signal processing applications. The static strain-optics (SSO) effect has been used on the tungsten bronze BSTN and SBN:60 crystals in producing: (a) record low-loss channel waveguides in SBN:60 (< 1 dB/cm) and BSTN (< 2 dB/cm), (b) first self-poled electro-optic modulators in SBN:60 and BSTN, and (c) GHz electro-optic modulation at 1.3 μm wavelength in SBN:60 (1.03 GHz and 1.4 GHz).

The overall performance of the selected tungsten bronze SBN and BSTN single crystals meet the requirements set for both photorefractive and guided-wave optical applications, and these materials are promising for future system applications. The growth techniques for SBN and BSTN crystals have been well-established at the Rockwell Science Center and the crystals can be produced in large scale at relatively low cost. The advantages of low voltage operation and compact size compared to $LiNbO_3$ should have significant impact on future systems.

2.0 INTRODUCTION

The main objective of this work is to utilize the large photorefractive and electro-optic properties and variable spectral response available in high figure-of-merit ($n^3 r_{ij}/\varepsilon$) tungsten bronze $(Ba,Sr)_6Ti_2Nb_8O_{30}$ (BSTN), and $Ba_{2-x}Sr_xK_{1-y}Na_yNb_5O_{15}$ (BSKNN) single crystals to achieve exceptional performance in various short and long term holographic storage, pattern recognition, image processing and interconnect applications. Undoped BSTN and BSKNN crystal will also be used for guidedwave optical applications such as telecommunication and signal processing. Table 2.1 summarizes the ferroelectric and optical properties of these high figure-of-merit tungsten bronze crystals. The work includes the necessary modifications in crystal compositions, growth techniques and doping schemes to achieve the desired crystals size, quality and spectral range. This is the first time these tungsten bronze crystals are available for optical computing and guidedwave optical applications and they have distinct advantages over the current best candidates such as $LiNbO_3$, $BaTiO_3$ and SBN. We expect that these materials will provide the desired storage time and storage capacity needed for various applications.

Table 2.1
Ferroelectric Tungsten Bronze Crystals For Optical Applications

Composition	ε	r_{ij} ($\times 10^{-12}$ m/V)	$n^3 r_{ij}/\varepsilon$	Dark Conductivity (Ω^{-1} - cm^{-1})
$(Ba,Sr)_6Ti_2O_8O_{30}$ Sr:Ba = 3:2 (BSTN-1)	ε_{33} = 350	r_{33} = 225	8.3	$\times 10^{-16}$
$(Ba,Sr)_6Ti_2O_8O_{30}$ Sr:Ba = 1:2 (BSTN-2)	ε_{33} = 360	r_{33} = 245	8.2	$\times 10^{-16}$
$(Ba,Sr)_2(K,Na)Nb_5O_{15}$	ε_{11} = 1000	r_{51} = 410	7.5	$\times 10^{-16}$
$(Sr,Ca)_2NaNb_5O_{15}$	ε_{33} = 1740 ε_{11} = 1700	r_{33} = 750 r_{51} = 630	8.1 7.5	$\times 10^{-16}$ $\times 10^{-16}$
SBN:60	ε_{33} = 900	r_{33} = 420	5.1	$\times 10^{-15}$

ε = dielectric constant, r_{ij} = electro-optic coefficient.

Photorefractive single crystals developed under this program are being evaluated for optical computing applications at Caltech (D. Psaltis), UCSD (Sing Lee) and at Rockwell International (J.

Hong) and based on these results, the necessary modifications in photorefractive properties (the role of dopants) are being made to achieve the desired material performance. Recently, Psaltis and the Rockwell group demonstrated the fixing of holograms in tungsten bronze crystals such as SBN:75 and SBN:60 over the period of year, and now the efforts are being made to fix the hologram in high T_c tungsten bronze crystals like BSTN and BSKNN. The development of this fixing technique will allow us speed up holographic storage and pattern recognition work. They have also planned various configuration to build optical disks for these different applications.

Undoped tungsten bronze BSTN and SBN crystals have been evaluated at Texas A&M University for guided-wave optical applications. Their work shows superior performance in both SBN and BSTN crystals with significantly low optical losses. It is expected that with further improvement in crystal quality we will achieve even better performance in these materials to develop compact device designs. The overall goals of this program are summarized in Figure 2.1.

T. B. Crystals for Optical Devices

- Grow high optical FOM (r_{ij}/ε) crystals
- Crystal size and optical quality
- Reliability and manufacturability

Requirements

Photorefractive

- Fast Response ~ 1 ms
- High diffraction efficiency
- Long storage time (> 1 year)

Guided-Wave Optics

- Low dissipation energy
- Low optical loss
- Suppress space charge

Applications

- Pattern Recognition
- Interconnects
- 3-D Volume Holography

Applications

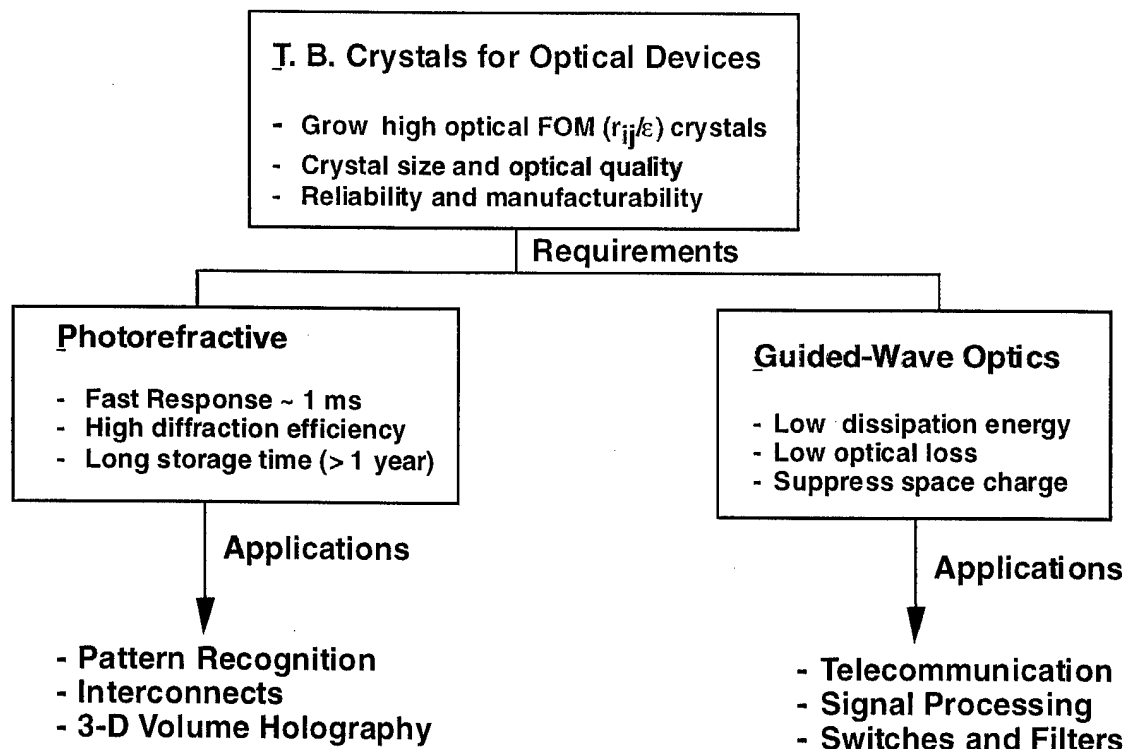- Telecommunication
- Signal Processing
- Switches and Filters

Figure 2.1 -- Photorefractive tungsten bronze crystals for optical computing and guidedwave optics.

3

3.0 PROGRESS

During the past 12 months, significant progress was made in the development of high optical figure-of-merit BSTN and BSKNN-5 tungsten bronze (T. B.) ferroelectric materials for optical computing and guidedwave optical applications. Since BSTN and BSKNN-5 crystals exhibit exceptionally good optical figures-of-merit and these crystals can be grown in decent size with optical quality, we have concentrated our efforts on these two materials. The advantages of these materials for photorefractive and guidedwave optical applications are as follows:

Photorefractive	**Guidedwave Optics**
- High n^3r_{ij}/ε : Fast speed of response	- High r_{ij}/ε : Operates at low voltages
- $T_c > 150°C$.	- $T_c > 150°C$.
- Exhibit low dark conductivity	- Exhibit low optical losses ~ 0.5 dB/cm
- Hologram fixing achievable.	- Exhibit low switching energy

> **Large size BSTN & BSKNN crystals are available in optical quality**

3.1 Accomplishments at Rockwell

Under this program, we have successfully grown and characterized tungsten bronze BSTN, and BSKNN-5 single crystals for optical computing and guidedwave optics. This work is a part of our continuing long-range effort to identify and grow high optical figure-of-merit tungsten bronze crystals. Figure 3.1 summarizes the classification established for tungsten bronze crystals in our laboratory. The new bronzes such as BSTN and BSKNN were identified and grown from this general scheme because they possess approximately two times larger optical figures-of-merit (Table 2.1) than the current best SBN, $LiNbO_3$ and $BaTiO_3$. The BSTN and BSKNN solid solution systems have been studied for the first time in our laboratory and they are extremely good candidates for photorefractive and guidedwave optical applications.
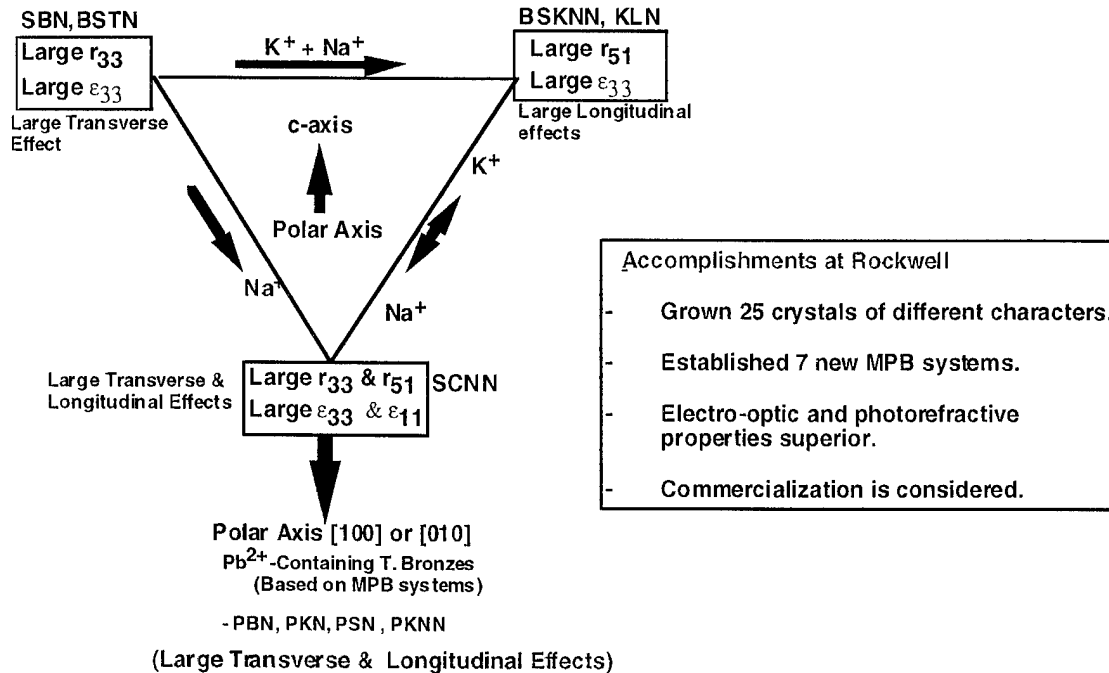
Figure 3.1 -- Classification established for tungsten bronze ferroelectric crystals.

The electro-optic and ferroelectric properties of filled tungsten bronze BSTN and BSKNN crystals are distinctly different from one another:

1. BSTN:
   - Large transverse electro-optic coefficient, r_{33}
   - Exhibit 4 mm symmetry at RT and no phase transition at low temperatures
   - Exhibit low dark conductivity and low optical losses

2. BSKNN
   - Large longitudinal electro-optic coefficient, r_{51}
   - Exhibit 4mm symmetry at RT and possibility of 4mm to mm2 transition at low temperatures.
   - Exhibit low dark conductivity and low optical losses

It is interesting to note that BSTN crystals behave like SBN in their electro-optic and photorefractive characters; however, the optical figure-of-merit for BSTN is almost two time better than SBN:60. The preliminary results indicate that BSTN crystals exhibit much faster response but at the same time the dark conductivity is almost an order of magnitude lower than

SBN:60. BSKNN crystals resembles to $BaTiO_3$ and they exhibit a strong longitudinal electro-optic (r_{51}) effect. Furthermore, BSKNN crystals have higher optical figure-of-merit and they can be grown in large sizes, currently up to 4 cm diameter in optical quality. For these reasons, BSKNN can form the base for large scale production of optical components where large r_{51} is required.

All of these BSTN and BSKNN-5 crystals have been grown by the Czochralski technique equipped with an automatic diameter controlled (ADC) unit and we have been successful in growing a number of doped and undoped crystals doped in optical quality. A brief summary of our growth experiments are given below:

Table 3.1
Growth of Tungsten Bronze BSTN and BSKNN Single Crystals

Composition	T_c (°C)	Growth Temp (°C)	Xtl Diam (cm)
1. Photorefractive Xtls			
BSTN: Rh^{3+} & Ce^{3+}	120	1470	3 - 4
BSKNN-5: Rh^{3+} & Ce^{3+}	180	1495	3 - 3.5
2. Electro-Optic			
BSTN	120	1465	` 4.5
SBN:60	80	1495	> 6
BSKNN-5	180	1488	> 3.5

Concentration of Rh & Ce was in the range of 0.01 to 0.03 wt%.

3.1.1 BSTN Crystals

Crystals grown in this study are tetragonal at room temperature and show almost no relaxor character. Ferroelectric and optical characterization of BSTN indicates that the optical figure-of-merit ($n^3 r_{ij}/\varepsilon$) is almost two times larger than for SBN:60 and $BaTiO_3$ crystals with significantly higher phase transition temperatures (100- 170°C). Because of such high $n^3 r_{ij}/\varepsilon$, BSTN crystals exhibit fast response, high diffraction efficiency and long dark storage time. Currently, these crystals are being grown in excess of 3.5 cm diameter in optical quality, and we expect that the size can be increased beyond 6 cm by scaling up our current growth processes. Figure 3.2 shows a 3.5 cm diameter BSTN crystal and its products .

Because BSTN crystals exhibit faster speed of response and lower dark conductivity than SBN:60, these crystals are attractive for optical computing applications. These BSTN crystals have been doped with Ce^{3+} and Rh^{3+} and currently we are optimizing the photorefractive properties of these dopants with respect the requirements set for data storage and optical pattern recognition.

The undoped BSTN crystals were evaluated at Texas A&M University and their results show that these crystals are also exceptionally good candidates for guidedwave optical applications. Since the transverse electro-optic coefficient ($r_{33} > 250$ x 10^{-12} m/V) for BSTN crystal is large, the operating voltage for this crystal in these applications is an order of magnitude lower than the current best $LiNbO_3$. At present the optical losses for BSTN are comparable with $LiNbO_3$ and they are in the range of 0.4 to 0.7 dB/cm. We expect that the optical losses for BSTN should reduce to the range of 0.2 to 0.4 dB/cm with further improvement in optical quality. Currently, we are introducing highly pure starting materials for this growth, and this should allow us to achieve the losses in the desired range. In parallel, we are up grading our growth process to increase crystal size beyond 4 cm diameter. Based on our current success of growing SBN:60 single crystals beyond 6.5 cm diameter, we do not anticipate any major problems in scaling up our current BSTN crystal growth processes
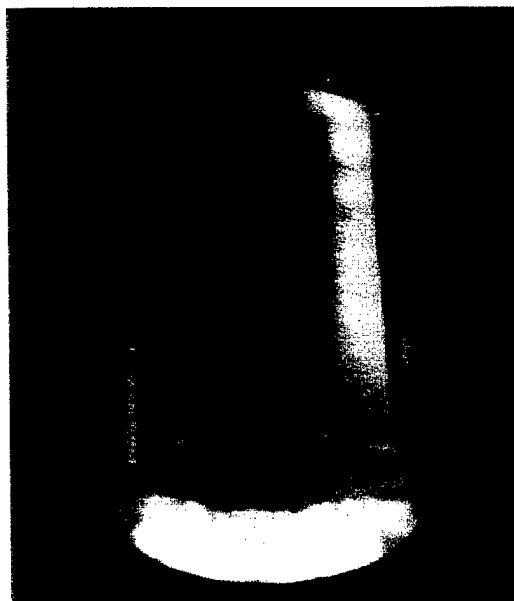
3 cm Diameter BSTN Crystals   BSTN Cube & Substrate
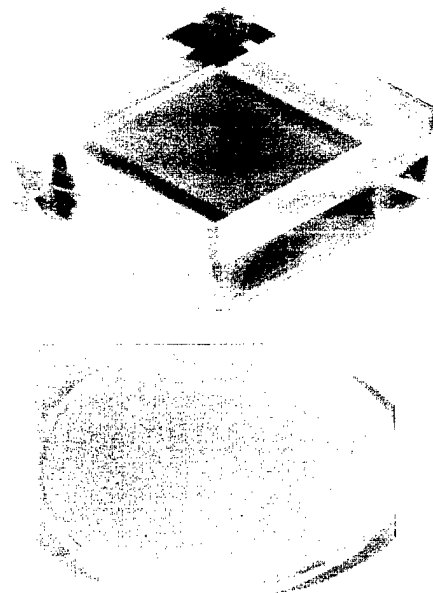
Figure 3.2 -- Czochralski grown undoped BSTN single crystal and its products

3.1.2   BSKNN-5 Crystals

This crystal is tetragonal at room temperature and it resembles $BaTiO_3$ in its electro-optic character. The speed and coupling are slightly better than $BaTiO_3$ and they also exhibit enhanced performance with the application of external field (~ 5 kV/cm). These crystals are easier to grow than BSKNN-1 and BSKNN-2 and currently we have grown these crystals in sizes up to 3 to 4 cm diameter with excellent optical quality (as shown in Figure 3.3).

BSKNN-5 crystal samples are being provided to Texas A&M University for guidedwave optical studies, and we will be especially interested in how the use of electro-optic r_{51} effect differs from our work on SBN and BSTN, where electro-optic r_{33} is used. This is the first instance where tungsten bronze crystals exhibiting large r_{51} has been available for guidedwave applications.
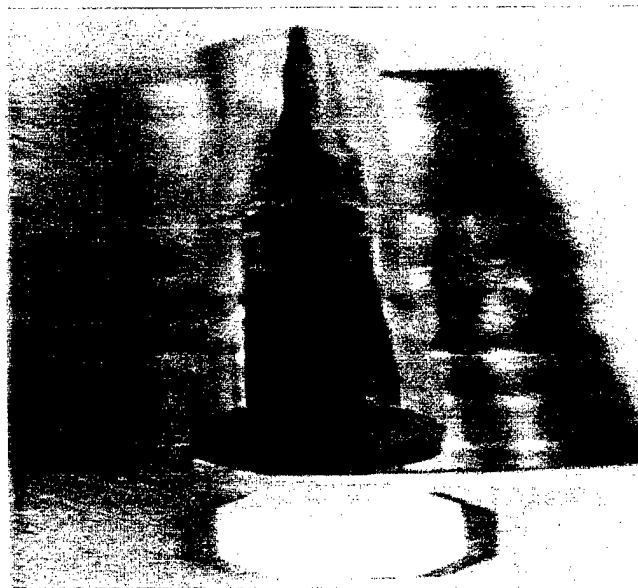
Figure 3.3 : BSKNN-5 crystals (3 cm diameter) grown along the [001] direction.

The $Sr_{1-x}Ba_xNbO_6$ (SBN) solid solution is the best example of a bronze system with strong transverse properties, including the dielectric constant (ε_{33}) , the electro-optic coefficient (r_{33}) and piezoelectric (d_{33}) coefficients, with the polar axis along [001]. BSTN has similar characteristics and both have distinct cylindrical growth habit with 24 well-defined facets, each facet corresponding to a definite crystallographic orientation as illustrated in Figure 3.4. On the other hand, BSKNN solid solution crystals exhibit strong longitudinal properties, including the dielectric constant

8

(ε_{11}), the electro-optic coefficient (r_{51}) and piezoelectric (d_{15}) coefficients, with the polar axis along [001]. The striking differences between BSKNN and BSTN (or SBN) crystals are in their growth habits and ferroelectric properties. BSKNN single crystal crystals grow either with a square or octahedral cross-section depending on the unit cell dimensions. Figure 3.4 shows the growth habit for small unit cell BSKNN-5 crystal which exhibits 8 well-defined facets. We expect that the 4mm to mm2 phase transitions in BSKNN single crystals are similar to $Ba_2NaNb_5O_{15}$, but this transition should occur below 100K (Xu et al).
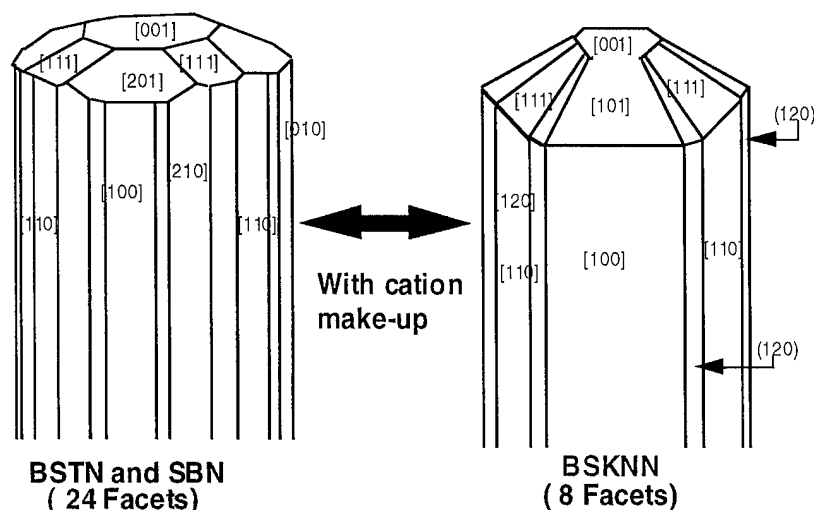
Figure 3.4 : Growth habits for tetragonal tungsten bronze crystals.

3.2 Accomplishments at Caltech

3.2.1 Photorefractive Characterization

Ce-doped BSTN has been experimentally characterized in terms of photorefractive sensitivity and two-wave coupling gain. Figure 3.3 shows typical experimental data for the intensity of diffracted light as a function of time. The sensitivity derived from this measurement for BSTN is about 64 mJ/cm^2. This sensitivity is much better than that of the best Ce-doped SBN:60 and $BaTiO_3$ photorefractive crystals. We expect that these properties will be substantially enhanced by adjusting the proper doping concentrations and improving the crystal quality. The improvements in photorefractive properties for BSTN are related to the higher optical figure-of-merit in this material.

A two-wave coupling gain of 25 cm^{-1} was measured for the same BSTN crystal. Preliminary measurements under an applied field of 5 kV/cm show a significant increase in coupling (>30 cm-

1). Similar measurements on SBN:60 and BSKNN-2 under applied field have shown that both the diffraction efficiency and the ratio of erasing time to writing time increase dramatically.[1] The sensitivity of gain with applied field in Ce-doped BSTN indicates that these key properties will also increase significantly in BSTN.

In order to maintain fast speed of response and low dark conductivity in BSTN and BSKNN-5, we are exploring the double doping schemes based on two different species such as Ce^{3+} + Fe^{3+}, Rh^{3+} + Fe^{3+} or Rh^{3+} + Mo^{4+}. Based on our previous work on SBN, we found that using such scheme it is possible to maintain fast speed of response and high coupling.
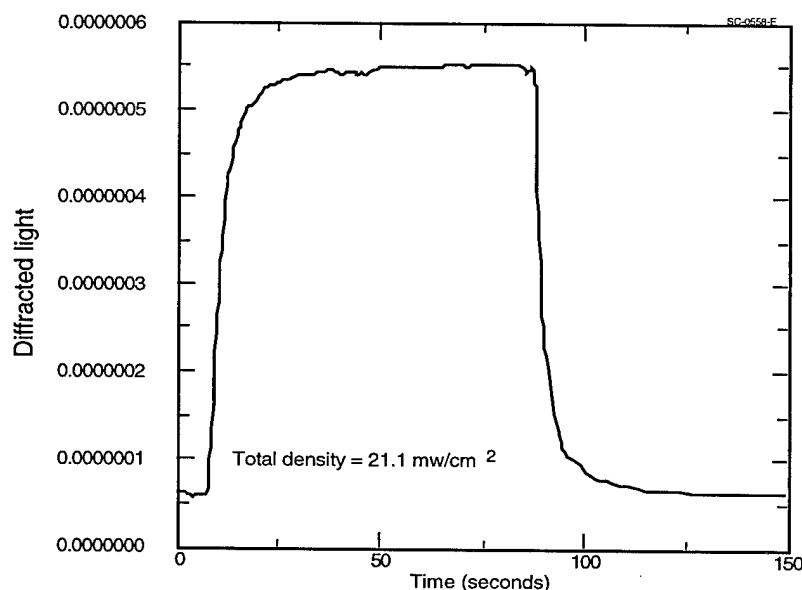
Figure 3.5 -- Intensity of the diffracted light as a function of time.

3.2.2   Holograms Fixing in Tungsten Bronze Crystals

In order to use these photorefractive tungsten bronze crystals for data storage, optical pattern recognition and other applications, it is important to establish a technique by which information can be stored for a long period of time. Currently, holograms are being successfully stored in $LiNbO_3$ by the use thermal processes and information can be stored over the period of a year. At Caltech and Rockwell attempts are being made to fix hologram in these tungsten bronze crystals using two different methods: a) Use of external field and b) thermal process used for $LiNbO_3$. Fixing with

an external electric field has been successful in SBN:75 and SBN:60, and these holograms have persisted for over a year. It was observed that higher fields were required to fix holograms in SBN:60 than in SBN:75 because the ferroelectric phase transition temperature (T_c) is higher for SBN:60, and fixing was done room temperature.

Our first attempts at hologram fixing in photorefractive BSTN at room temperature show the same problem, namely, incomplete or weak storage at moderate fields (< 5 kV/cm). BSTN has T_c over 100°C, so it is not surprising that it is even more difficult to achieve fixing than SBN:60. To overcome this problem, we are exploring the use of both high fields and elevated temperatures during fixing. Currently, both these approaches are being evaluated for the high T_c tungsten bronze crystals. Since T_c for BSKNN is even higher (> 180°C), we may need to fix holograms at temperatures ~ 100°C.

The reason that it is worthwhile to develop fixing methods for the high T_c materials is that they have very low dark conductivity and fast response time, which will be a major factor in their use for large scale data storage applications.

3.2.3   Holographic Disk Development

A number of concepts for implementing 3-D memory storage using tungsten bronze crystals have been identified (Figure 3.4), and their storage capacities have been estimated. With a 5 cm diameter disk, and each hologram occupying 10 mm^2 of the disk and 1,000 holograms superimposed at each location, the total storage capacity approaches 2×10^{11} pixels.

Figure 3.5 shows the experimental curve of diffraction efficiency as a function of the disk rotation angle for LiNbO$_3$. Note that there is a 3-fold symmetry along the rotational axis. For crystals belonging to the 4mm symmetry such as BSTN, SBN or BaTiO$_3$, the diffraction efficiency should be independent of the rotational angle.

SC-2737-
T

Signal
beam

Reference beam
(reflection type)

SLM

Reference beam
(transmission type)

Detector/CCD
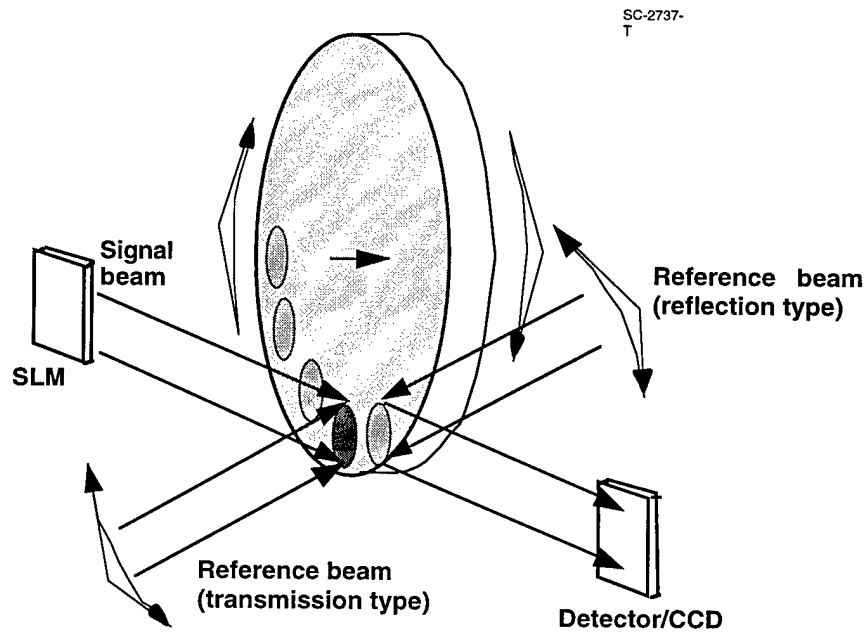
Figure 3.6 -- Schematic diagram of 3-D memory system.

SC-2739-T

Out-plane polarization
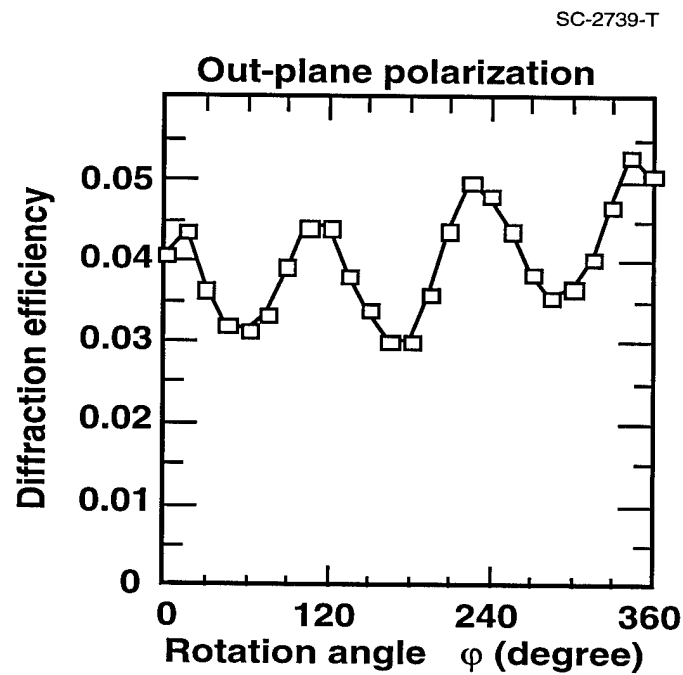
Figure 3.7 -- Diffraction efficiency η as a function of the disk rotation angle for LiNbO$_3$

Both BSTN and BSKNN offer significant advantages over $LiNbO_3$, SBN:60 and $BaTiO_3$ because of their superior photorefractive properties. In both of these crystals, holograms can be written much faster, while in BSKNN the storage capacity is greater because two large electro-optic coefficients are available for writing holograms. This is a unique crystal for holographic applications. Also, we anticipate that the dark conductivity should be low in these crystals and thus they should retain holograms for longer periods than SBN and $BaTiO_3$.

3.3 Accomplishments at Texas A&M University

Electro-optic modulators and switches are important elements in light-wave telecommunications that can be realized with the tungsten bronze materials, and the work at Texas A&M has focused on their development. For this work, we have used tungsten bronze SBN:60 and BSTN single crystal materials to take advantage of their large electro-optic coefficients and potential low cost. Table 3.2.summarizes the key optical properties of commercial ($LiNBO_3$ and $LiTaO_3$) and tungsten

Table 3.2
Selected Properties of Electro-Optic Crystals

Property	$LiNbO_3$	PZT/PLZT	SBN:60	BSTN
T_c (°C)	~ 1150	300	78	> 150
r_{33} (pm/V)	31	> 2000	420	200
Half-Wave Volt (V)	0.031	0.0003	0.002	0.004
Switching Energy	~ 3	.04	0.6	0.35
Optical Damage Threshold (W/cm^2)	40	---	---	---

Half Wave Voltage = $\lambda g/n^3 l \, (1/r_{33})$ Switching Energy = $\lambda^2 g^2/2n^6 l \, (\varepsilon/r^2)$

bronze crystals. This data shows that the tungsten bronze materials selected in this study have superior optical properties: specifically, half-wave voltage and switching energy are an order of magnitude better than $LiNbO_3$ and this will allow us to fabricate very efficient waveguide structures using tungsten bronze materials. A summary of our work is given below:

A previous disadvantage with the bronzes has been the relatively high optical losses found in waveguides formed by ion implantation or diffusion doping (Table 3.3). In this work, however, the channel waveguides were formed by a unique process which takes advantage of the static strain-optic (SSO) effect in ferroelectric crystals. The strain-induced waveguides were produced by depositing a thick SiO_2 film by e-beam evaporation on a crystal substrate at elevated temperature, typically around 300°C, and then patterning at room temperature. The difference in the thermal expansion coefficients of the film and substrate causes a strain in the substrate at the patterned regions which induces a localized index change in the crystal via the strain-optic effect. In z-cut crystal substrates, the channel waveguides are produced by the longitudinal strain component S_1 induced in the x-direction. In addition to the strain-optic effect, the net refractive index change also includes an electro-optic contribution due to electric fields produced by the piezoelectric effect and the redistribution of surface charges.

Besides its simplicity, a particular advantage of this process is that it does not require processing at high temperatures (e.g., above 500°C) and, as detailed below, results in the lowest-loss waveguides (less than 0.6 dB/cm at 1.3 µm wavelength) reported to date in tungsten bronze materials. We expect that these losses will reduce further with improved crystal quality (especially in the case of BSTN) and waveguide processing. Details of the waveguide fabrication and electro-optic characterization work performed at Texas A&M University on SBN:60 and BSTN crystals supplied by the Rockwell Science Center are detailed in the next two sections.

Table 3.3

Comparison of Losses in Waveguides for Different Materials

Crystal	Strain (dB/cm)	Diffused (dB/cm)
$LiTaO_3$	0.7 to 1.0	~ 4.0 (Vapor)
$LiNbO_3$	0.8 to 1.0	~ 0.5 (Vapor)
SBN:60	0.5 to 1.0	~ 5.0 (Vapor)
BSTN	0.6 to 1.0	-----

SBN:60

Guided mode propogation in z-cut SBN:60 was observed for both TM (extraordinary) and TE (ordinary) polarizations at 1.3 μm wavelength in 9.4 μm width channels etched in a 4.4 μm thick SiO2 film which was e-beam deposited at 320°C. These waveguides exhibited a single transverse mode for both TE and TM polarizations, and one depth mode for TE and two depth modes for TM. The power density full width at half maximum (RF) profiles for these waveguides were determined from near-field measurements on the fundamental modes; these are listed in Table 3.4 along with similar measurements on BSTN crystals discussed in the next section. Measurements on an SBN:60 sample with 7 μm wide, 8 mm length channel waveguide showed propogation losses of 0.7 dB/cm for TM polarized light, and 1.6 dB/cm for TE polarization. These are the lowest propogation loss values reported to date in SBN:60, and are evidently the result of the low-temperature process used to fabricate these waveguides.

Electro-optic modulation at frequencies up to 22 MHz was also demonstrated in the 9.4 μm width waveguides after poling at room temperature. The device structure utilized coplanar metal electrodes having a length of 5.5 mm and a width of 11 μm with an electrode separation of 0.4 mm; a schematic of the structure is shown in Figure 3.6 Polarization intensity modulation was achieved via the Pockels effect by coupling the light at 45° to the z-axis (crystallographic polar c-axis) and detecting the output through a crossed linear analyzer. Figure 3.7 shows an oscilloscope display of the modulator output at 200 kHz. The results show a 85% modulation depth at a half-wave voltage $v_\pi = 34$ volts.
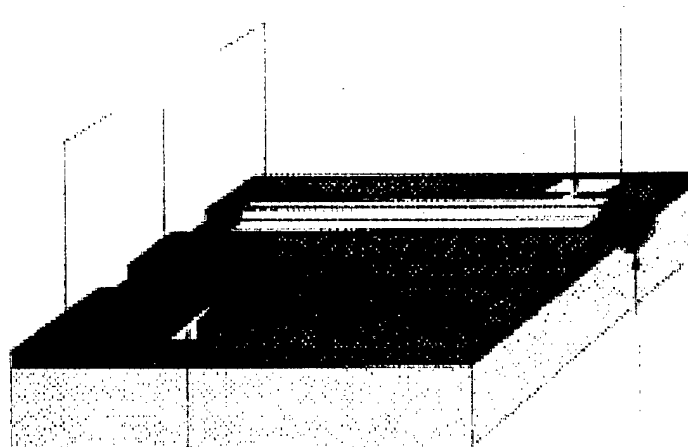

Figure 3.8 -- Schematic of device structure used for electro-optic modulation in SBN:60.
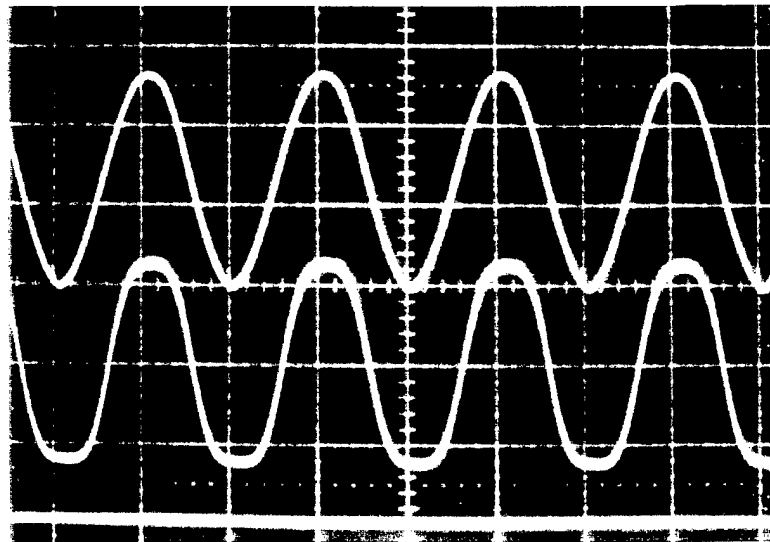
15

Figure 3.9 -- Modulation performance of a 9.4-μm wide SBN:60 strain waveguide at 1.3 μm wavelength. The upper trace is the applied electric signal at f = 200 kHz and 10 V/d. vertical scale. The middle trace is the optical response with zero light level indicated by the lower trace.

<u>BSTN</u>

BSTN crystals can be thought of as modified SBN crystals in that Ti replaces some of the Nb atoms, with the resulting distinction that BSTN has a "filled" lattice structure, with all of the A_1 and A_2 lattice sites filled by Ba and Sr, whereas in SBN only 5/6 of these sites are filled.

Since BSTN can now be grown in larger sizes with good optical quality, it is important to establish the fundamental optical properties of these crystals. The refractive index values were determined from Brewster angle measurements using a spectrometer. Horizontally-polarized TE light from a He-Ne laser at 0.6328 microns wavelength was used for the incident beam on an x-cut BSTN crystal sample. The angle for the null reflection was determined by monitoring the intensity of the reflected beam with a photodetector. The ordinary refractive index, no, was obtained by orienting the sample such that the crystallographic b-axis (or y-axis) was parallel to the incident light polarization. Similarly, the extraordinary refractive index, n_e, was obtained by orienting the sample with the polar c-axis (or z) parallel to the incident light polarization. The measured values were $n_o = n_1 = 2.301$ and $n_e = n_3 = 2.278$ at room temperature.

The linear electro-optic (Pockels) coefficients r_{33}, r_{13}, and $r_c = r_{33} - (n_1/n_3)_3 r_{13}$ were also measured at 0.6328 μm wavelength using a Mach-Zehnder interferometric. A z-cut BSTN crystal with dimensions 5 x 9 x 1.14 mm (x,y,z) was placed in one arm of the interferometric with optical propogation along the 9 mm long y-direction. DC voltage was applied along the z-direction (polar c-axis) using Cr/Au electrodes deposited on the z-cut faces. The electro-optic coefficients were determined by establishing the v_π voltage using increasing dc voltage. Measured values of $r33 = 218 \pm 12$ pm/V and $r13 = 51.2 \pm 6$ pm/V were obtained using TM and TE input polarizations, respectively. The measured value of $r33$ may be compared with the theoretical value from the relation

$$r_{33} = 2g_{33}P_3\varepsilon_{33}\varepsilon_0,$$

using measured values for the spontaneous polarization, $P_3 = 30.0$ μC/cm^2, the low-frequency dielectric constant, $\varepsilon_{33} = 560$, and the quadratic electro-optic constant $g_{33} = 0.10$ m^4/C^2, resulting in $r_{33} = 297$ pm/V. Some of the discrepancy between the measured and calculated values may be due to the value taken for g_{33} which is based on results from other tungsten bronze crystals. However, the roughly 4:1 ratio between r_{33} and r_{13} is consistent with past measurements on other crystal compositions. A measured value for $rc = 167 \pm 12$ pm/V was also obtained by coupling light polarized 45° to the z-axis; this is in very close agreement with with the calculated value of 165 pm/V using the measured n_1, n_3, r_{13} and r_{33} values.

Table 3.4

Measured FWHM of Mode Profiles for Strain-Induced Waveguides in SBN:60 and BSTN Crystals at 1.3 μm Wavelength

	SBN:60		BSTN	
	TM	TE	TM	TE
Vertical Scan	10.8 μm	21.6 μm	14.4 μm	25.4 μm
Horizontal Scan	13.0 μm	19.5 μm	12.7μm	15.2 μm

Strain-induced channel waveguides were fabricated on a z-cut BSTN crystal substrate in the same manner used for SBN:60 crystals, with a 3.4 μm thick SiO2 film deposited on the substrate at 300°C. Single mode propogation was observed for guided modes at 1.3 μm wavelength for 11 μm wide channels etched in the SiO2 film. Figure 3.8 shows the near-field mode profiles

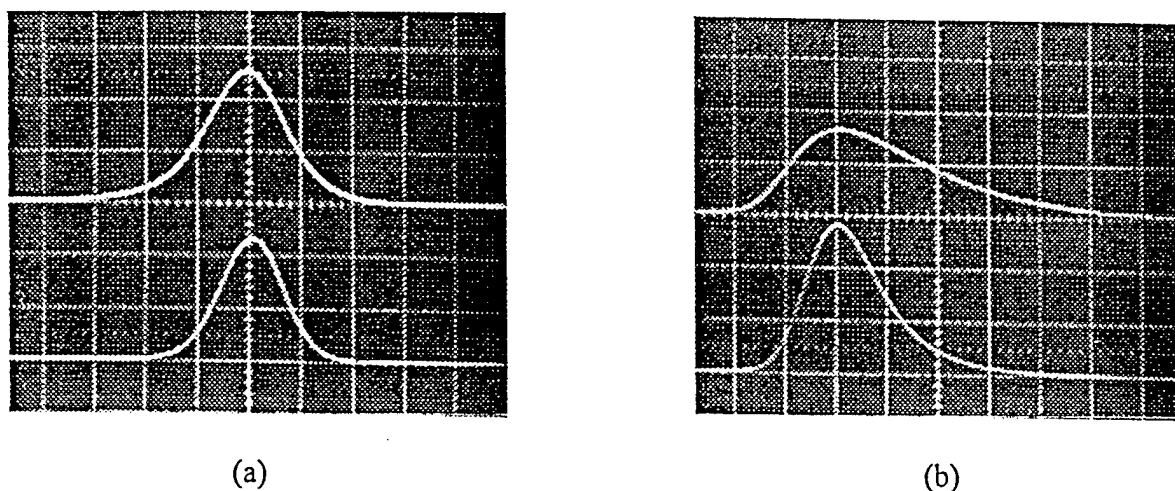obtained for both TM and TE polarizations at this wavelength. The measured

(a)   (b)

Figure 3.10: Near field mode profile of 11-μm wide BSTN strain waveguide at 1.3 μm wavelength. (a) Transverse scan. (b) vertical scan. In each photo, the upper trace is for TE and lower trace is for TM

FWHM values are listed in Table 3.4 in comparison with those for SBN:60. As in SBN:60, the propogation losses are quite low, being 0.6 dB/cm or less for the TM mode. Again, we expect these losses to reduce further with improved crystal quality and substrate/film processing. Since BSTN has a filled tungsten bronze crystal lattice, we expect that it will ultimately have substantially lower propogation losses in the visible and near-IR compared to unfilled structure materials such as SBN. Table 3.4 gives the summary on optical losses in different optical materials:

4.0   Recommendation

This program has successfully developed both superior tungsten bronze materials and device structures for various optical applications, including photorefractive pattern recognition and 3-D memory, and optical wave-guide for telecommunication and signal processing. The next step is to develop systems that exploit these unique materials and concepts. The lower operating voltages and smaller size achievable using these materials should enable much broader range of optical applications.

The three areas for future work are: (a) continuation of materials growth, including BSKNN and BSTN, and extending to higher from Pb^{2+}-containing materials, (b) design and development of new guided-wave structures for telecommunication and signal processing, and (c) establishment of feasibility of different concepts using these materials for pattern recognition and 3-D memory. BSKNN and BSTN are an order of magnitude better than $LiNbO_3$, while certain Pb^{2+}-containing tungsten bronzes exhibit another order of magnitude increase. The work to be pursued in this area is the optimization of growth techniques to grow these crystals on a large scale and determination of best crystal compositions for different applications.

A major target in optical guided-wave structures is high frequency operation (3 - 7 GHz). Pb^{2+}-containing compositions which are close to morphotropic phase boundary (MPB) regions offer high r_{ij}/ε (r = electro-optic coeff and ε = dielectric constant), which is most favorable for these applications.

Both pattern recognition and 3-D memory require long storage times and short writing times. Currently, $LiNbO_3$ provides long storage, but requires long writing times. BSTN and BSKNN have relatively low dark conductivity as compared to other other tungsten bronze crystals, and thus longer storage time, currently predicted at 1 month, while writing times are much faster than $LiNbO_3$. For this reason, we should continue to evaluate the feasibility of these materials for pattern recognition and 3-D memory applications.

5.0   REFERENCES

1. R. R. Neurgaonkar, W. W. Ho, W. K. Cory, W. F. Hall and L. E. Cross, Ferroelectrics 51, 185 (1984).

2. R. R. Neurgaonkar and W. K. Cory, J. Opt. Soc. Am. 3(B), 276 (1986).

3. R. R. Neurgaonkar, W. K. Cory, J. R. Oliver, M. D. Ewbank and H. F. Hall, J. Opt. Engineering 26(5), 392 (1987).

4. R. R. Neurgaonkar, W. K. Cory, J. R. Oliver, M. J. Miller, W. W. Clark III, G. L. Wood and E. J. Sharp, J. Cryst. Growth 84, 629 (1987).

5. R. R. Neurgaonkar, W. K. Cory, J. R. Oliver and L. E. Cross, Mat. Res. Bull. 24, 1025 (1989).

6. J. E. Ford, J Ma, Y. Feinman, S. H. Lee, D. Bize and R. R. Neurgaonkar, J. Opt. Soc. Am. 9, 1183 (1992).

7. Y. Qiao, S. Orlov, D. Psaltis, and R. R. Neurgaonkar, Opt. Lett. 18(12), 1004 (1993).

APPENDIX   6.1

FERROELECTRIC TUNGSTEN BRONZE CRYSTALS FOR

GUIDEDWAVE OPTICAL APPLICATIONS.

(J. Opt., Vol 24(3), 155-169, 1995)

FERROELECTRIC TUNGSTEN BRONZE CRYSTALS FOR GUIDED-WAVE OPTICAL APPLICATIONS

R. R. Neurgaonkar, W. K. Cory and J. R. Oliver

Rockwell Science Centre Thousand Oaks, CA 91360 USA
And

O. Eknoyan and H. F. Taylor

Texas A & M University, College Station, TX 77843-3128 USA

ABSTRACT

The state of the art in the Czochralski growth of various optical-quality ferroelectric tungsten bronze single crystals is reviewed with respect to crystal structure, phase transitions and cationic makeup. Based on our growth of over 25 single crystal bronzes, we have classified these bronzes into four categories having distinctly different ferroelectric and electro-optic characteristics. Currently, tungsten bronze $Sr_{0.6}Ba_{0.4}Nb_2O_6$ (SBN:60) and $Ba_{6-x} Sr_x (Nb,Ti)_{10}O_{30}$ (BSTN) single crystals with high electro-optic figures-of-merit have been optimized in guided-wave optical structures, in which the performance is superior to that of $LiNbO_3$ and $LiTaO_3$. We review the role of tungsten bronze materials for telecommunications, sensing and signal processing using these guided-wave structures.

1. INTRODUCTION

Tungsten bronze (T.B.) ferroelectrics are very useful for electro-optic, piezoelectric, pyroelectric and millimeter wave applications, and more recently for photorefractive applications [1-21]. Considerable work has been published on the development of this family of materials; however, initially these materials did not find widespread application due to the lack of crystals of adequate size and quality. At the Rockwell Science Centre, we have systematically studied the major growth problems, crystal habits and classification of these mateirals based on their ferroelectric and optical properties [22-37]. In this paper, we report our major findings on the growth of these crystals, their classification and potential applications.

2. BACKGROUND : FUNDAMENTAL PROPERTIES

A number of ferroelectrics of present or potential commercial importance have the tungsten bronze structure. This structure is typified by oxygen octahedra linked at the corners in a complex way to yield three types of openings, two of which normally contain the A_1 and A_2 cations as shown in Figure 1. The B

cations, typically niobium (Nb^{5+}) or tantalum (Ta^{5+}), are inside the oxygen octahedra. The tungsten bronze compositions are characterized by the chemical formulae $(A_1)_4(A_2)_2C_4B_{10}O_{30}$ or $(A_1)_4(A_2)_2B_{10}O_{30}$, in which the A_1 cations are in the 15-fold coordinated site, the A_2 cations are in the 12-fold coordiantes site, the C cations are in the 9-fold coordinated site and the B cations are in two different 6-folds coordinated sites. Detailed descriptions of this structure have been given in several articles [38-40]. Only two compositions, $K_3Li_2Nb_5O_{15}$ and $K_3Li_2Ta_5O_{15}$, can be represented by the first chemical formula where all five crystallographic sites are filled [41-42]. For this reason, these compositions are known as "stuffed" bronzes. All other tungsten bronzes are called either "filled" or "unfilled" bronzes with the 9-fold coordinated site vacant and the 15- and 12-fold coordinated sites either fully of partially occupied. For example, lead metaniobate and strontium barium niobate have unfilled unit cells containing $Pb_5Nb_{10}O_{30}$ and $(Sr,Ba)_5Nb_{10}O_{30}$ (usually simplified to $PbNb_2O_6$ and $(Sr,Ba)Nb_2O_6$) where the A sites are only 5/6 filled. Although the presumption is that the distribution among the 15-and 12-fold coordinated A sites is random, it is more likely that in SBN, Ba^{2+} predominantly occupies the 15-fold coordinated site since Ba^{2+}(1.74 Ľ) is substantially larger than Sr^{2+} (1.54Ľ).

Like the ferroelectric pervoskite family, the bronze family embraces more than 150 compounds and solid solutions including several morphotropic phase boundary systems [43-44]. Because of the structural complexity which accommodates a wide range of cationic substitutions, often the ferroelectric transition can be achieved in the desired temperature range with suitable ferroelectric and optical propeprties.

● CHEMICAL FORMULAE

$(A_1)_4(A_2)_2C_4B_{10}O_{30}$

$(A_1)_4(A_2)_2B_{10}O_{30}$

A_1 = 15-FOLD COORDINATED SITE

A_2 = 12-FOLD COORDINATED SITE

C = 9-FOLD COORDINATED SITE

B = 6-FOLD COORDINATED SITE

● CRYSTAL STRUCTURE

4/MMM TO 4MM (TETRAGONAL-TETRAGONAL)

4MMM TO MM2 (TETRAGONAL-ORTHORHOMBIC)

● CHEMICAL FORMULAE

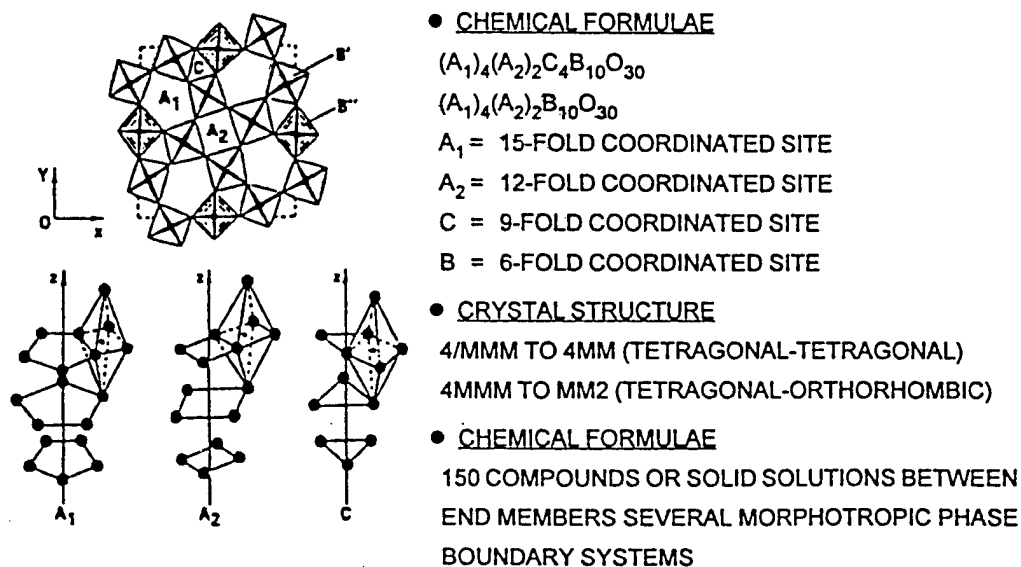150 COMPOUNDS OR SOLID SOLUTIONS BETWEEN END MEMBERS SEVERAL MORPHOTROPIC PHASE BOUNDARY SYSTEMS

Figure 1- Projection of the tungsten bronze structure parallel to (001)

3. CRYSTAL DEVELOPMENT

Table 1 lists a number of tungsten bronze single crystals grown in our work and their associated growth conditions. The Czochralski pulling technique was used for these growths, with the crystals pulled from 5x5 cm platinum crucibles in an oxygen atmosphere to minimize the the reduction of Nb^{5+} to Nb^{4+}. All of the crystals listed in Table 1 were grown along the (001) direction, except for $K_3Li_2Nb_5O_{15}$ crystals where the best growth direction was along the (110) direction. Crystal cracking during cool-down through the paraelectric/ferroelectric phase transition was initially a problem for most of these crystals, but this problem has now been minimized, particularly for SBN, BSKNN and BSTN.

Table 1
Ferroelectric Tungsten Bronze Crystals Grown at Rockwell

Composition	Growth Temp (^{0}C)	Pull Rate (mm/hr)	Sym	Diameter (cm)	Tc (^{0}C)	Phase Transitions
$Sr_{0.75}Ba_{0.25}N_2O_6$ (SBN:75)	1480	4-5	4mm	4.0	56	One
$Sr_{0.6}Ba_{0.4}Nb_2O_6$ (SBN:60)	1485	5-7	4mm	6.0	78	One
$Sr_{0.5}Ba_{0.5}Nb_2O_6$ (SBN:50)	1485	5-6	4mm	4.0	128	One
$BaSrK_{0.75}Na_{0.25}Nb_5O_{15}$	1475	3-4	4mm	3.0	178	One
$Ba_{0.5}Sr_{1.5}K_{0.75}Na_{0.25}Nb_5O_{15}$	1475	4-5	mm2	3.0	172	Two?
$Sr_{1.9}Ca_{0.1}Na\ Na_5O_{15}$	1500	2-3	mm2	1.0	270	Two
$K_3Li_2Nb_5O_{15}$	1100	1-2	4mm	1.0	370	One
$Sr_2KNb_5O_{15}$	1450	3-4	4mm	1.0	157	One
$Pb_{0.6}Ba_{0.4}Nb_2O_6$ (PBN:60)	1350	1-2	4mm	1.5	320	One

Sym = Symmetry.

Based on ferroelectric and optical studies of both tetragonal orthorhombic bronze crystals, we have classified this family into four different groups shown in Figure 2. These classifications are:

1. Crystals exhibiting strong transverse effects with 4mm symmetry (e.g. SBN, $Sr_2KNb_5O_{15}$): <001> polar axis.

2. Crystal exhibiting strong longitudinal effects with 4mm symmetry (e.g. BSKNN, $K_3Li_2Nb_5O_{15}$) : <001> polar axis.

3. Crystal exhibiting strong transverse and longitudinal effects with mm2 symmetry (e. g. $Sr_{2-x}Ca_xNaNb_5O_{15}$, $K_2BiN_5O_{15}$) : <001> polar axis.

4. Crystals exhibiting strong longitudinal effects with mm2 symmetry (e. g. $Pb_2KNb_5O_{15}$, $Pb_{1-x}Ba_xNb_2O_{15}$): <100> or <010> polar axis.
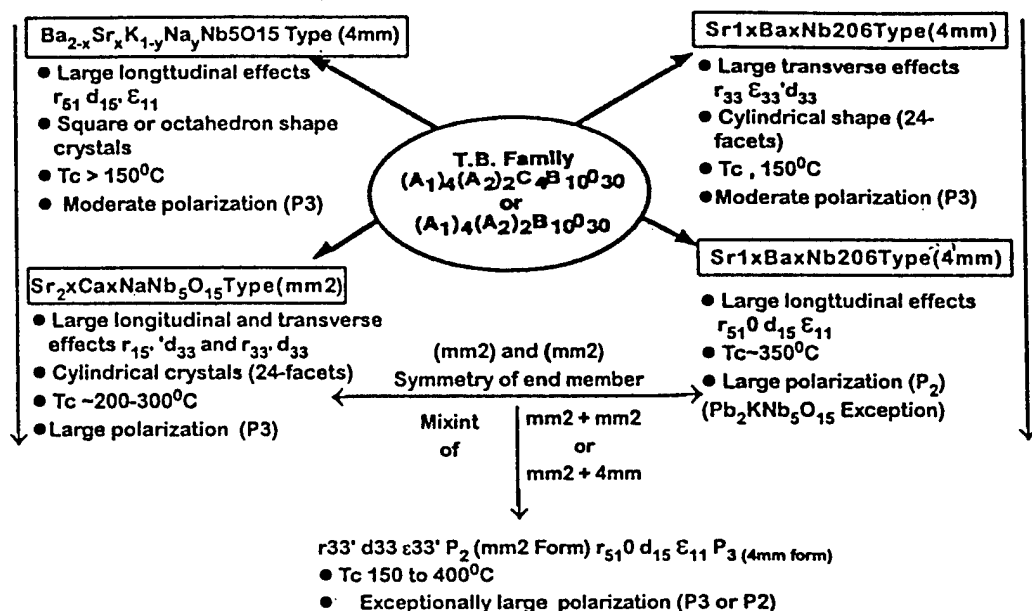

Figure 2 - Classification of tungsten bronze crystals.

Over 25 different bronze crystal compositions have been grown (partial list in Table 1) and in some cases they have been modified to meet the requirements for electro-optic and photorefractive applications. All of these crystals have been grown by the Czochralski technique [23-35]. Table 2 summarizes the key ferroelectric and optical properties of the selected T. B. crystals.

Table 2

Ferroelectric and electro-Optic Properties of Tungsten Bronze Single Crystals

Crystal	r_{ij} (10^{-12} m/v)		ε		r_{ij}/ε	Device Configuration
SBN : 75	r_{33} =	1400	ε_{33} =	300	0.47	- Transverse Mode
SBN : 60	r_{33} =	420	ε_{33} =	900	0.47	- Transverse Mode
SBN : 50	r_{33} =	210	ε_{33} =	430	0.48	- Transverse Mode
BSKNN-2	r_5 =	380	ε_{11} =	750	0.51	- Longitudinal Mode
BSKNN-3	r_5 =	400	ε_{11} =	800	0.50	- Longitudinal Mode
BSTN	r_3 =	250	ε_{33} =	350	0.72	- Transverse Mode
SCNN	r_{33} =	1250	ε_{33} =	1750	0.70	- Transverse Mode
	r_{51} =	1180	ε_{11} =	1700	0.69	- Longitudinal Mode

Tungsten bronze crystals are relatively easy to grow compared to most ferroelectric crystals based on perovskite, layered structure $Bi_4Ti_3O_{12}$, and lead germanate, phosphate and vanadate. This is due in part becuase the bronzes have simple phase transitions and are usually free of 90^0 and 180^0 twins which occur in perovskite single crystals. Among the growth problems associated with these crystals, we have found the following to be major contributors toward poor crystal quality:

1. Multicomponent solid solution systems make it difficult to control crystal homogeneity.

2. Exchange among crystallographic sites, specifically of the 15-and 12-fold coordinated ions such as Ba^{2+}, Sr^{2+}, K^+, La^{3+}, causes severe striation problems.

3. High temperature growths (up to 1500^0C) cause volatilization and oxidation-reduction (Nb^{5+} to Nb^{4+}) problems.

4. Cracking of crystals when thermally cycling through phase transitions. This is often aggravated by crystal imperfections.

Neverthless, several bronze compositions have been grown as large size, defect-free crystals, including SBN (6 cm diameter) and $Ba_{2-x}Sr_xK_{1-y}N_yNb_5O_{15}$ (> 4 cm diameter) which have excellent optical quality.

4. CRYSTALS EXHIBITING STRONG TRANSVERSE PROPERTIES (4MM)

The $Sr_{1-x}Ba_xNb_2O_6$ (SBN) solid solution is the best example of a bronze system with strong transverse properties, including the dielectric constant (ε_{33}), and the electro-optic (r_{33}) and piezoelectric (d_{33}) coefficients, with the polar axis being along $<001>$. The configuration for guided-wave optical applications for SBN is similar to $LiNbo_3$; however, the half-wave voltages in SBN solid solution system, three compositions, e.g. $Sr_{0.75}Ba_{0.25}Nb_2O_6$ (SBN:75), $Sr_{0.6}Ba_{0.4}Nb_2O_6$ (SBN:60) and $Sr_{0.5}Ba_{0.5}Nb_2O_6$ (SBN:50), are potentially useful for optical applications,
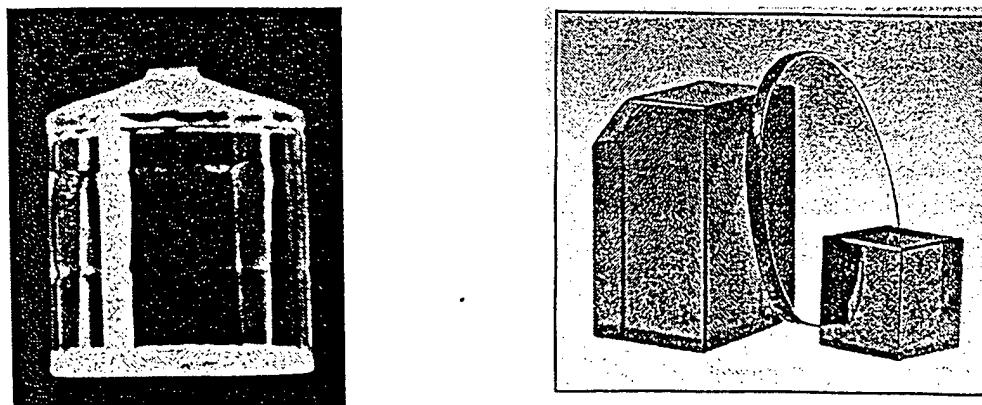

Figure 3: Large SBN:60 single crystal and products.

and these crystals are routinely grown in our laboratory. Other examples of bronze ferroelectrics with strong transverse optical properties are $Sr_2KNb_5O_{15}$, $Ba_2KNb_5O_{15}$ and $(Ba,Sr)_6(TiNb)_{10}O_{30}$ (BSTN). Crystal growth has been well-established for SBN, and these crystals are grown in sizes up to 6 cm diameter as shown in Figure3 [45-50]. These crystals have a distinct cylindrical growth habit with 24 well-defined facets, each facet corresponding to a definite crystallographic orientation. For this reason, precise orientation and cutting of these crystals is greatly simplified.

5. CRYSTALS EXHIBITING STRONG LONGITUDINAL PROPERTIES (4MM)

A prototypical member of this class is the $Ba_{2-x}Sr_xK_{1-y}Na_yNb_5O_{15}$ (BSKNN) solid solution, which has large longitudinal properties (r_{51}, ε_{11}). We have grown these crystals as large as 4 cm. diameter with excellent optical quality (Figure 4). BSKNN crystals resemble $BaTiO_3$ in many of their ferroelectric characteristics, and these crystals can be useful in the longitudinal configuration. A particualr advantage of BSKNN over $BaTiO_3$ is the absence of twins which makes growth to large sizes (4 cm diameter) and crystal poling much easier. Other examples of bronzes with strong longitudinal properties are $K_3Li_2Nb_5O_{15}$ and $K_3(Na,Li)_2Nb_5O_{15}$.
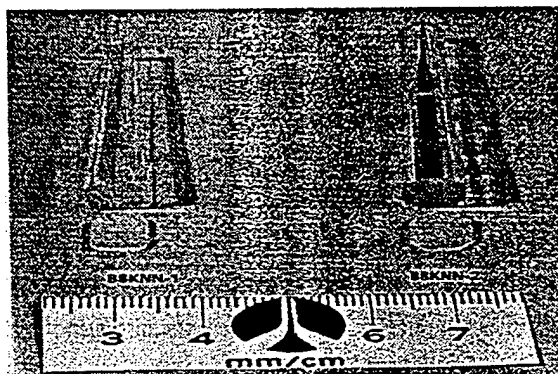

Figure 4 - Large size tungsten bronze BSKNN single crystal grown along <001>.

The striking differences between BSKNN and SBN crystals are in their growth habits and ferroelectric properties. BSKNN single crystals grow either with a square or octahedral cross section depending on the unit cell dimensions, with the bigger unit cell BSKNN crystals (a > 12.500 Ḷ, c > 3.955 Ḷ) being square in shape. Figure 5 shows the differences among BSKNN-1, BSKNN-2 and SBN-type crystals. We anticipate the presence of a 4mm to mm2 phase transition in BSKNN-1 (K^+-rich) single crystals, similar to $Ba_2NaNb_5O_{15}$, but this transition would occur below 100K.
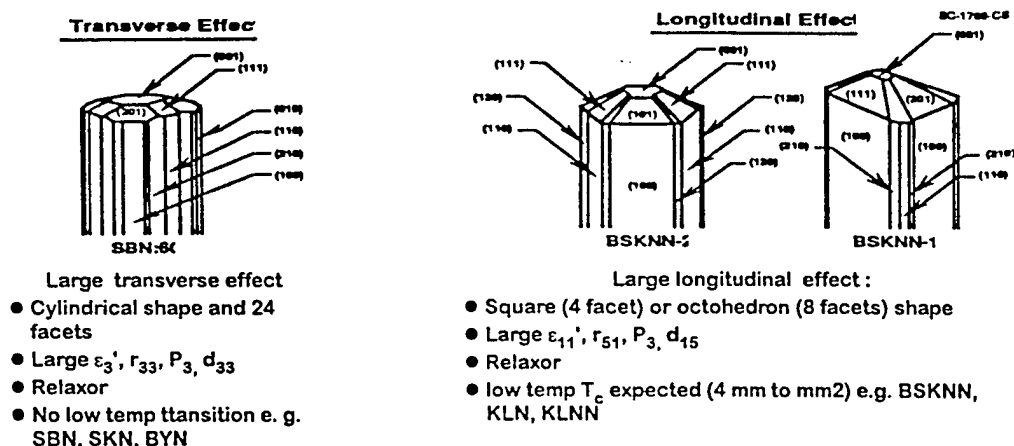
Figure 5 - Growth habits for tetragonal tungsten bronze crystals.

6. CRYSTAL EXHIBITING LARGE TRANSVERSE AND LONGITUDINAL PROPERTIES

A typical example of this class is found in the $Sr_{2-x}Ca_xNaNb_5O_{15}$ (SCNN) solid solution system in which both transverse (r_{33} and ε_{33}) and longitudinal (r_{51} and ε_{11}) electro-optic properties are large and nearly equal. These crystals can be used in both transverse and longitudinal configurations for guided-wave optical applications. Other interesting examples of orthorhombic bronzes in this category are $Ba_2NaNb_5O_{15}$ (BNN), $Sr_2NaNb_5O_{15}$ (SNN), and $Sr_2(Na,Li)Nb_5O_{15}$(SNL), although the electro-optic properties in these crystals are not as good as in SCNN.

These orthorhombic crystals have two phase transitions above room temperature [23]. one paraelectric (4/mmm) to ferroelectric (4mm), and the other ferroelectric (4mm) to ferroelastic (mm2). As shown in Figure 6, the dielectric constant along < 100 > increases with decreasing temperature, resulting in large transverse and longitudinal dielectric and optical properties at room temperature or below. In the case of SCNN, a reasonably high spontaneous polarization at room temperature (34 $\mu C/cm^2$) with large electro-optic coefficients r_{33} and r_{51}
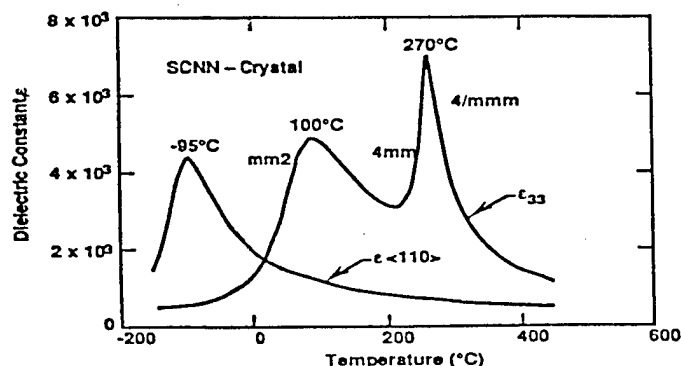

Figure 6 - Polar and nonpolar < 110 > dielectric constants for SCNN at 10 kHz. The low temperature peak along < 110 > is due to the freeze-out of the polarizibility in this direction.

comparable to SBN:75 ($r_{33} = 1400 \times 10^{-12}$ m/V) has been observed. Compared to SBN and BSKNN crystals,, these orthorhombic crystals are generally difficult to grow due to their two-phase transitions and lower crystal symmetry. Efforts are under way to modify our current growth techniques so we can grow reasonably large size crystals (~ 3 cm diameter).

7. Pb2+ -CONTAINING BRONZES

Pb^{2+} and Ta^{5+} or Nb^{5+} -containing bronze compositions are strongly orthorhombic at room temperature, and they are differentiated from other bronze crystals by their polar axis. These materials have only one pahse transition from 4/mmm to mm2, with the polar axis oriented along $<100>$ or $<010>$. The compositions most studied in this category are $PbNb_2O_6$ (PN), $(Pb,Ba)Nb_2O_6$(PBN) and $Pb_2KNb_5O_{15}$(PKN) for surface acoustic wave (SAW) and piezoelectric applications [51-52] becuase of their excellent electromechanical coupling and piezoelectric properties. The polarization in these materials can exceed 40µC/cm^2, and their optical figures of merit are estimated to be 2 to 3 times better than the current best-known ferroelectrics such as SBN and $BaTiO_3$. Because of these properties, single crystals and thin film growths of PBN and PKN compositions have been actively pursued in our laboratory and at Penn State University [53-54]. However, bulk crystal grwoth is extremely difficult due to cracking when passing through the paraelectric/ferroelectric phase transition as a result of the large strain developed in the plane orthogonal to the $<001>$ growth direction. These materials are potentially important for optical applications, if suitable quality and size crystals become available.

8. GUIDED-WAVE OPTICAL STUDIES IN T.B. CRYSTALS

We are conducting a systematic study of tungsten bronze crystals for electro-optic applications becuase of their large electro-optic coefficients and the availability of large size crystals. In the present paper we are discussing guided-wave optical properties in tungsten bronze crystals. Table 3 summarizes relevant electro-optic and optical properties for SBN:60 and BSTN compared to those for $LiNbO_3$ and $LiTaO_3$. The figure of merit $M = (\varepsilon/n^6r^2)$ is a measure of the switching energy required for a π- radian pahse shift in a modulator or switch.

T. B. crystals are of interest for guided-wave optics because their very large electro-optic coefficients makes it possible to produce compact, low-voltage modulation amd switching devices for applications in communications, signal processing and sensing. The operations of these devices is based on the Pockels effect, and the realization of low-loss single-mode optical waveguides in the substrate material is critical for their practical implementation. The Pockels effect refers to refractive index changes Δn_i that are induced in a crystal by an applied electric field of components E_j given by:

$$\Delta(1/n^2_i) = r_{ij}E_j \qquad (i = 1,2, \text{------} 6, j = 1,2,3) \tag{1}$$

where r_{ij} represents the elements of the third rank linear electro-optics coefficient tensor in reduced notation. The electric field in the crystal is established by applying a voltage across electrodes placed on the surface. The resultant values in the refractive index changes, Δn_i, can be written as the elements of a symmetric 3 x 3 matrix which is referred to as the perturbed refractive index matrix. Utilization of the diagonal elements of the resultant matrix leads to a chang in phase for an incident optical wave polarized along a major crystallographic axis as it transverses the crystal. This is useful for the design of modulators and switches. Changes in the off-diagonal elements, however, induce conversion (or mixing) between orthogonal polarization states of an optical wave propagating in the crystal. This is utilized in the design of polarization control devices and optical filters.

Table 3

Relevant Properties of Some Ferroelectrics (at 0.633 mm wavelength)

Crystal	Tc (^{0}C)	r_{33} (pm/V)	ε_{33}	n	M ($10^{20}V^2/m^2$)
LiNbO$_3$	1195	31	28	$n_1 = 2.2866$	
				n_2-n_1	2.55
				$n_3 = 2.2028$	
LiTaO$_3$	620	30	43	$n_1 = 2.1786$	4.41
				$n_2 = n_1$	
				$n_3 = 2.1833$	
SBN:60	78	420	900	$n_1 = 2.3103$	
				$n_2 = n_1$	0.40
				$n_3 = 2.2817$	
BSTN	116	218	440	$n_1 = 2.3012$	
				$n_2 = n_1$	0.66
				$n_3 = 2.2778$	

In any of these applications, the crystal orientation and device design should be arranged to achieve the index change with the least possible applied voltage through the use of the largest r_{ij} coefficient. Comparing the listed valueds of r_{33} in Table 3, tungsten bronze crystals have a clear advantage in this regard. A Mach-Zehnder interferometer fabricated in SBN:60 has in fact produced a p-radian phase shift voltage-length (VL) product of 0.48 V-cm at a wavelength of 0.83 μm, which is the lowest reported for any electro-optic modulator[55] and more than an order of magnitude lower than a comparable device of similar dimensions in LiNbO$_3$.

Optical waveguides are formed by producing a localized high index region in

a substrate of lower refractive index. In ferroelectric crystals, this has often been accomplished by changing the composition or stoichiometry by processes such as out-diffusion [56], ion exchange [57,58], or indiffusion from a metal film [59] as well as vapor phase [60]. A simple method for making waveguides has been developed recently using the strain induced by a surface film deposited at an elevated temperature to adjust the index in ferroelectric substrates through the static strain-optic (SSO) effect [61]. In this technique, waveguides are produced without altering the compositions of the substrate. In tungsten bronze crystals, neither metal diffusion nor ion exchange has been successful for making waveguides, and elements that have been used for vapor diffused waveguides in SBN:60 have resulted in losses which are unfortunately rather high (>10 dB/cm). This drawback has been overcome, however, by the use of the recently developed SSO effect for waveguide fabrication. The low propogation loss values are evidently a result of the absence of surface damage from the low temperature process used in making the waveguides, and the absence of diffused impurities which may introduce scattering centes.

To produce strain-induced waveguides, a thick SiO_2 film ($\sim 3\mu m$) is deposited on a substrate at an elevated temperature ($\sim 300^\circ C$), then cooled down to room temperature. This induces a compressive strain in the film because of the large thermal expansion mismatch between the substrate and film. By selective etch patterning, straight channels are next delineated in the SiO_2 by reactive ion etching. Formaton of a channel makes it possible for the edges of the film to expand towards the center, as shown by the inward arrows in Figure 7. The process of strain relief in the film results in a localized compressive strain in the substrate in the vicinity of the channel. This induces an index increase in the crystal via the strain-optic effect. Channel waveguides have been produced by this method in Z-cut (c-plate) SBN:60 BSTN substrates using the longitudinal S_1 strain component. The refractive index changes form the strain-optic effect, Δn_i^{so}, with $i = 1,3$ are given by [61],

$$\Delta n_i^{so} = -(n_i^3/2)p_{ij}S_j \qquad (2)$$

where $j = 1$ for z-cut substrates, and p_{ij} is the relevant strain-induced coefficient. In addition to the strain-optic effect, the net refractive index change also includes an electro-optic contribution due to electric field in the strained region produced by the piezoelectric effect and by surface charge redistribution. A finite element relaxation method was used to determine the strain profiles illustrated in Figure 7. The constant strain contours are drawn normalized relative to the strain value at the surface of the substrate in the center of the channel. As indicated in the figure, the maximum strain occurs near the edges of the channel and is compressive in the channel but tensile beneath the film. Propagation losses <1 dB/cm in SBN:60 and 1.8 dB/cm in BSTN have been measured in strain induced waveguides

at 1.3 μm wavelength [62]. These are considerably lower than in SBN waveguides produced by vapor diffusion [55,63] and approach those attainable in $LiNbO_3$.
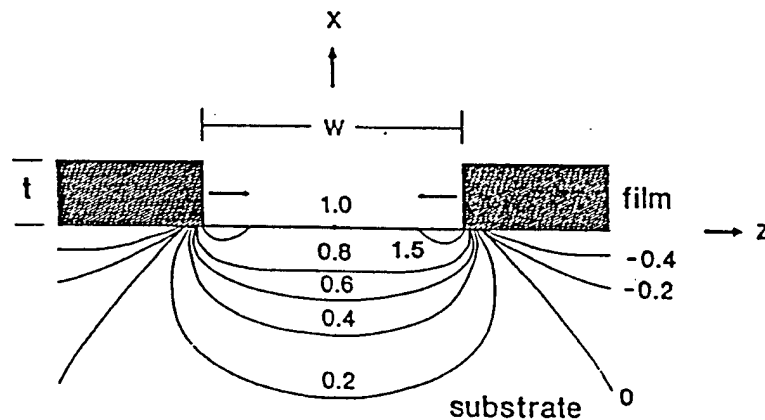

Figure 7- Normalized constant contours for the longitudinal S_3 strain component.

Polarization intensity modulation has been realized via the linear Pockels effect on strain-induced waveguides in SBN:60 and BSTN substrates [63]. To impress an electric field, planar electrodes are delineated on the surface using photolithography. Figure 8 is a schematic of a final device configuration produced on a z-cut SBN:60. The strain inducing film was formed by depositing a 4.4 μm thick SiO_2 film at 320°C. The crystal was repoled before dilineation of the final electrode pattern. Propagation losses of 0.7 dB/cm and 1.6 dB/cm were measured for the extraordinary and ordinary polarizations, respectively, at 1.3 μm wavelength. Electro-optic modulation was realized through the use of the effective electro-optic coefficient $r_c = r_{33} - (n_1/n_3)^3 r_{13}$. A half-wave voltage $V_\pi = 34$ V was obtained for an electrode separation of 400 μm, an interaction length of 5.5 mm, and a waveguide width of 9.4 μm. Electro-optic modulation at frequencies > 700 MHz has been observed in SBN:60 as well as in BSTN. On a similar SBN
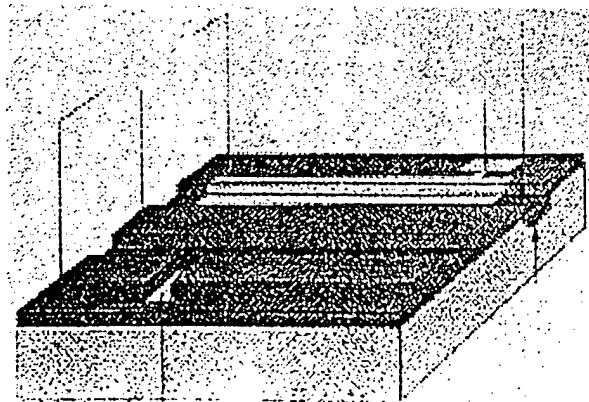

Figure 8 - Strain-induced channel waveguide electro-optic modulator in SBN:60

modular structure but with a reduced gap separation of 70 μm, a value of $V_\pi = 9.5$ V was observed using a coplanar surface electrode arrangement. Lower values can be expected with further reductions in the gap. The record low voltage-length product of 0.48 V-cm in SBN:60 was achieved with a 7.5 μm gap, using waveguides produced by Zn diffused from vapor phase.

The SSO effect has also been used to induce polarization conversion in birefringent $LiTaO_3$ of the ilmenite family [64]. For a wave propagating in a diffused channel waveguide, phase-matched coupling between TE and TM modes may be induced by static shear strain from a spatially periodic surface film. The phase match condition imposed by the crystal birefringence is highly wavelength selective. Wavelength tuning for maximum conversion can be realized by adjusting the birefringence in the wavelength electro-optically via the linear Pockels effect. A schematic for an electro-optically tunable polarization converter produced LiTaO3 is shown in Figure 9. Polarization conversion in the waveguide is caused by the off-diagonal element n_5 of the refractive index, which is produced by the shear-strain component S_6, and is given by

$$\Delta n_5 = -(n^3/2)P_{41}S_6 \tag{3}$$

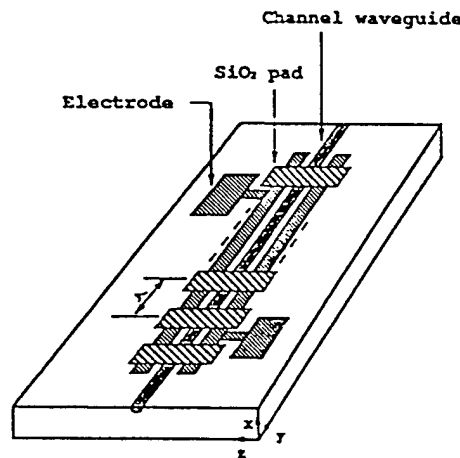with $n = (n_1 n_2)^{1/2}$ and p_{41} is the relevant strain-optic coefficient.

Figure 9 - Electro-optically tunable strain induced polarization converter.

The use of polarization coupling by the SSO effect can be extended to produced a channel-dropping electro-optic tunable filter (EOTF) using a four-port interferometer configuration. A schematic diagram of a four-port polarization-independent (EOTF) using a four-port interferometer configuration. A schematic diagram of a four-port polarization-independent EOTF[65] is shown in Figure 10. It consists of two polarization splitters (PS) near the input and output ends that are joined by a pair of tunable SSO converters in the center. If the wavelength of a light beam entering at one of the input ports (e.g#1) satisfies the phase matching condition of the converter section, the TE and TM components which get separated by the PS undergo polarization rotation then recombine and emerge

·from the port #4 at the putput. The induced off-diagonal index Δn_5 responsible for coupling is given by equation(3), as before. Wavelength tuning can be accomplished by adjusting the birefringence electro-optically in the converter section through the r_c coefficent.
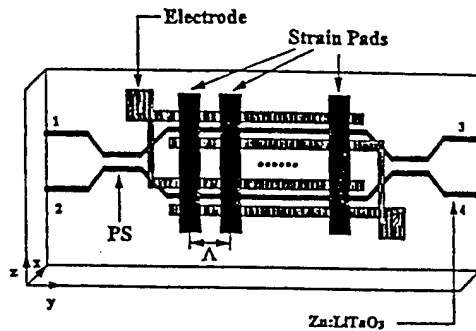

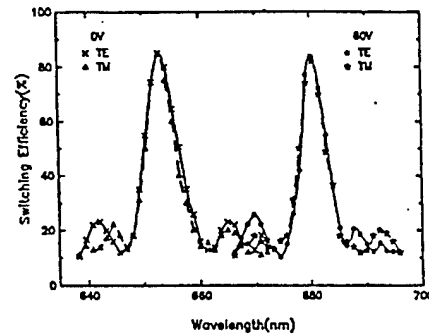Figure 10 - Polarization independent electro-optically tunable channel-dropping filter.

Figure 11 - Spectral response of EOTF at V = 0 and 60 volts.

Optical test results for an EOTF produced in $LiTaO_3$ are shown in Figure 11. The waveguides are fabricated by zinc ion vapor diffusion. The strain-inducing pads were produced from a 1.0 µm thick SiO_2 film deposited at 300^0C and patterned at room temperature with a spatial periodic separation of 100 µm. The spectral response is shown for the untuned (O V) and tuned (60 V) filter conditions. A total shift of 37 nm for the peak wavelength with an applied voltage of 90V was achieved. The incomplete extinction is due to the splitters providing only 95% separation between TE and TM polarizations, and the TE-TM polarization conversion being limited to 96%. Narrower wavelength passbands could be realized in $LiTaO_3$ through an increase in the conversion section, or by the use of substrates with larger birefringence (e.g. BSTN with $\Delta n = 0.0235$ in contrast to $LiTaO_3$ of $\Delta n = 0.0035$). The use of tungsten bronze crystals with a larger r_{33} coefficient, such as SBN:60 or BSTN, could also provide a means for increasing the tunable bandwidth.

In conclusion, although $LiNbO_3$ - based devices are now commercially available, interest in producing guided-wave devices in materials with higher linear electro-optics coefficients is great. The tungsten bronze family of ferroelectrics as summarized in Table 3 offers several attractive choices for such devices with exceptionally large r_{33} coefficient values. Advances in growing large diameter optical-quality tungsten bronze crystals of various compositions, coupled with the recent development of low loss optical waveguides in several of these crystals, make it feasible to consider their use for commerical applications. Propagation losses < 1 dB/cm in SBN, < 2dB/cm in BSTN, and electro-optic modulation in both crystals at frequencies > 700 MHz at 1.3 mm wavelength have been demonstrated. A value of $V_\pi < V$ has been achieved in SBN:60 at 0.81 µm

wavelength, which is a record low for guided-wave modulators in ferroelectric materials. The SSO effect from shear strain has been used in Zn-diffused $LiTaO_3$ waveguide to produce an electro-optically tunable polarization converter and channel-dropping filter. The use of SBN and BSTN crystals for such devices is an attractive possibility, as the larger r_{33} coefficients in these substrates will make it possible to access a large number of channels through birefringence tunning.

ACKNOWLEDGEMENT

REFERENCES

1.   R.B.Maciolek and S.T. Liu, J. Electron. Mater. **2**, 191 (1973).
2.   R. B. Maciolek T.L Schuller and S.T. Liu, J. Electron. Mater. **5**, 415 (1976).
3.   S. Kuroda and, K. Kubota, J. Phys. Chem. Solids **44**, 527 (1983).
4.   E.G. spencer, P.V. Lenzo, and A.A, Ballman, Proc. IEE **52**, 2074 (1976).
5.   A. M. Glass, J. Appl. Phys. **40**, 4699 (1969).
6.   P.V. Lenzo, E.G. spencer and A.A. Ballman, Appl. Phys. Lett. **11**, 23 (1967).
7.   R. L. Townsend and J.T. LaMacchia, J. Appl. Phys. **51**, 88 (1970).
8.   J. J. Amodei, D. L. Staebler and A.W. Stephens, Appl. Phys. Lett. **18**, 507 (1971).
10.   W.W. Ho, W.F. Hall, R. R. Neurgaonkar, R.E. DeWames and T.C. Lim, Ferroeletrics **38**, 63 (1981).
11.   G. Rakuljic, A. Yariv and R. R. Neurgaonkar, Opt. Eng. **25**, 1212 (1986).
12.   O. Eknoyan, C. H. Bulmer, H. F. Taylor, W. K. Burns and A.S. Greenblatt, L.A. Beach and R. R. Neurgaonkar, Appl. Phys. Lett. **48**, 13(1986).
13.   M. D. Ewbank, R. R. Neurgaonkar, W. K. Cory and J. Feinberg, Appl. Phys. Lett, **62**(2), 373 (1987).
14.   B. Bobbs, M. Matloubian, H.R. Fetterman, R.R. Neurgaonkar and W.K., Cory, Appl. Phys. Lett. **48**, 1642 (1986).
15.   E.J. Sharp, M. J. Miller, G. L. Wood W. W. Clark III, G. Salamo and R. R. Neurgaonkar, Appl. Phys. Lett. **52**, 765 (1987).
16.   G. L. Wood, W. W. Clark III, M. J. Miller, E. J. Sharp, G. Salamo and R. R. Neurgaonkar, J. Quantum Electronics **23**(12), 2126(1987).
17.   J. F. Jelsma, R. R. Neurgaonkar and W. K. cory, Proc. SPIE **832**, 198(1987).

18.   G. J. Salamo, M. J. Miller, W. W. Clark III, G. L. Wood, E. J. Sharp and R. R. Neurgaonkar, Appl. Optics **27**(21), 4356(1988).
19.   E. J. Sharp, M. J. Miller, G. J. Salamo, W. W. Clark III, G. L. Wood, and R. R. Neurgaonkar, Ferroelectrics **87**, 335 (1988).
20.   K. Sayano, G.A. Rakuljic, A. Agranat, A. Yariv and R. R. Neurgaonkar, Optics. Lett. **14**(9). 459 (1989).
21.   A. S. Kewitch, T. W. Towe, G. J. Salamo, A. Yariv, M. Shang, M. Segev, E. J. Sharp and R. R. neurgaonkar" Appl. phys Lett. **66**(15), 1865, (1995)
22.   J. Ford Y. Taketomi, S. Lee. D. Bize, S, Feinman and R. R, Neurgaonkar, Proc. SPIE **1148**, 12 (1989).
23.   R. R, Neurgaonkar, W. K. Cory, J. R. Oliver, E. J. Sharp, G. L. Wood, M.S. Miller, W. W. Clark III and G. Salamo, Mat. Res. Buul. **23**, 1459(1988).
24.   R. R. Neurgaonkar, J.G. Nelson, J.R. Oliver and L.E. Cross, Mat. Res. Bull. **25**, 959 (1990).
25.   R. R. Neurgaonkar, J. R. Oliver and J. G. Nelson, private communication.
26.   R. R. Neurgaonkar, M. H. Kalisher, T.C. Lim, E.J. Staples and K.L. Keester, Mat. Res. Bull. **15**, 1305 (1980).

27. R. R. Neurgaonkar, W.K. Cory, W.W. Ho, W.F. Hall, and L.E. Cross, Ferroelectrics 38, 857 (1981).
28. R. R. Neurgaonkar, W. K. Cory, Ferroelectrics 35, 301 (1983).
29. R. R. Neurgaonkar, W. K. cory, W.F. Hall, and L. E. Cross, Ferroelectrics 51, 185 (1984).
30. R. R. Neurgaonkar, Proc. SPIE 465, 97 (1984).
31. R. R. Neurgaonkar and L.E. Cross, Mat. Res. Bull. 21, 893(1986).
32. R. R. Neurgaonkar and W. K. Cory, J. Opt. Soc. Am.3(B), 276(1986).
33. R. R. Neurgaonkar and W. K. Cory, J. R. Oliver and L.E. Cross, Proc. SPIE 567, 11 (1985).
34. R. R. Neurgaonkar, W. K. Cory, J. R. Oliver, and L.E. Cross, Mat. Res. Bull. 24, 1025 (1989).
35. R. R. Neurgaonkar, W. K. Cory, J. R. Oliver, M.J. Miller, W.W. Clark III, G.L. Wood, and E.J. Sharp, J. Cryst. Growth 84, 629 (1987).
36. R. R. Neurgaonkar, W.K. Cory and J. R. Oliver, Proc. Spie 739, 91 (1987).
37. R. R. Neurgaonkar, W.K. Cory, J.R. Oliver, M.D. Ewbank and W.F. Hall, Opt. Eng. 26(5), 392 (1987).
38. M.H. Francombe and B. Lewis, Acta Cryst, 11, 696 (1958).
39. L.G. Van Uitert, H.J. Levinstein, J.J. Rubin, C.D. Capio, E.F. Dearborn and W.A. Bonner, Mat. Res. Bull. 3, 47 (1968).
40. P.B. Jamieson, S.C. Abrahams, J.L. Bernstein, J. Chem. Phys. 48, 5048 (1968).
41. T. Fukuda, Jap. J. Appl. Phys. 9, 599 (1970).
42. T.V. Tiaou, N. N. Krainnik, I.H. Ismailzade, V.A. Isupov, and F.A. Ageve, Izv. Acad. Nauk. SSSR, Ser. Phys, 35, 1825 (1971).
43. M. H. Framcombe, Acta Cryst. 13, 131 (1960).
44. V.A. Isupov and V.I. Kosiakov, Zh. Tekh. Fiz. 28, 2175 (1958).
45. J.R. Oliver, R.R. Neurgaonkar and L,E. Cross, J. Am. Ceram. Soc. 72, 202 (1989).
46. A.A. Ballman, S.K. Kurtz, and H. Brown, J. Cryst. Growth 10, 185 (1971).
47. A. A. Ballman and H. Brown, J. Cryst. Growth 1, 311 (1967).
48. K. Megumi, N. Nagatsuma, K. Kashiwada and Y. Furuhata, Mater. Sci. 11, 1583(1976).
49. H.C. Chen and Y. Xu, J. of Chinese Silicate Soc. 10, 406(1982).
50. R. R. Neurgaonkar, W.K. Cory, J. R. Oliver, M. Khoshnevisan and E. J, Sharp, Ferroelectrics 102, 3 (1990).
51. I. Katahiro, T. Yano and A. Watanbe, Jap. J. Appl. Phys. 54, 2355 (1971).
52. J.E.Geusic, Appl. Phys. Lett. 11(9), 269(1967).
53. J.E.Geusic, Appl. Phys. Lett. 12(9), 306(1968).
54. R.R. rice, J. Electrochem. Soc. 116(6), 839 (1969).
55. O. Eknoyan, V. P. Swenson, J.D. Quinn and R.R, Neurgaonkar, Appl. Phys. Lett., 59, 28 (1991).
56. I.P. Kaminow and J.R. carruthers, Appl. Phys. Lett, 23 326 (1974).
57. M.L. Sah, Appl. Phys. Lett., 26, 652(1975).
58. J. L. Jackel, Appl. Opt., 19, 1966(1980)
59. R.V. Smith and I.P. Kaminow, Appl. Phys. Lett, 25 458(1974).
60. D.W. Yoon and O. Eknoyan, J. Lightwave Technol, 6, 877(1988).
61. O. Eknoyan, C.H. Bulmer, H.F. Taylor, W.K. Burns, A.S. Greenblatt, L.A. beach and R.R. Neurgaonkar, Appl. Phys. Lett,. 48. 13 (1986).
62. O. Eknoysn, C. H. Bulmer, H. F. Taylor, W. K. Burns, A. S. Greenblatt, L. A. Beach and R. R. Neurgaonkar, Appl. Phys. Lett., 48, 13 (2986).
63. J. M. Marx, Z. Tang, O. Eknoyan, H.F. Taylor, and V.P. Swenson, Electron. Lett., 28, 2248(1992).
64. Z. Tang, O. Eknoyan, II. F. Taylor, and V. P. Swenson, Electron. Lett., 28, 2248 (1992).
65. Z. Tang, O. Eknoyan and H.F. Tayoor, Electron. Lett, 30, 1758(1994).

APPENDIX 6.2

Growth and Optical Properties of Ferroelectric Tungsten Bronze Crystals

(Ferroelectrics, Vol 142, 167-188, 1993)

GROWTH AND OPTICAL PROPERTIES OF FERROELECTRIC TUNGSTEN BRONZE CRYSTALS

R. R. NEURGAONKAR, W. K. CORY and J. R. OLIVER

Rockwell International Science Center, Thousand Oaks, CA 91360 USA

and

E. J. SHARP, G. L. WOOD and G. J. SALAMO

Center for Night Vision and Electro-Optic, Fort Belvoir, VA 22060-5677 USA

The state of the art in the Czochralski growth of various optical-quality ferroelectric tungsten bronze single crystals is reviewed with respect to crystal structure, phase transitions and cationic make-up. Based on our growth of over 25 single crystal bronzes, we have classified these bronzes into four categories having distinctly different ferroelectric and optical characteristics. With the use of this classification, optimal bronzes can be chosen for specific electro-optic and photorefractive applications.

Keywords: ferroelectrics, dielectrics, crystal growth, electro-optic, piezoelectric, pyroelectric, photorefractive, tungsten bronze crystals

INTRODUCTION

Tungsten bronze (T.B.) ferroelectrics are very useful for electro-optic, piezoelectric, pyroelectric and millimeter wave applications, and more recently for photorefractive applications.[1-21] Considerable work has been published on the development of this family of materials; however, initially these materials did not find widespread application due to the lack of availability of crystals of adequate size and quality. At the Rockwell International Science Center, we have systematically studied the major growth problems, crystal habits and classification of these materials based on their ferroelectric and optical properties.[22-37] In this paper, we report our major findings on the growth of these crystals, their classification and potential applications.

BACKGROUND: FUNDAMENTAL PROPERTIES

A number of ferroelectrics of present or potential commercial importance have the tungsten bronze structure. This structure is typified by oxygen octahedra linked at the corners in a complex way to yield three types of openings, two of which normally contain the A_1 and A_2 cations as shown in Figure 1. The B cations, typically niobium (Nb^{5+}) or tantalum (Ta^{5+}), are inside the oxygen octahedra. The tungsten bronze compositions are characterized by the chemical formulae $(A_1)_4(A_2)_2C_4B_{10}O_{30}$ or $(A_1)_4(A_2)_2B_{10}O_{30}$, in which the A_1 cations are in the 15-

167
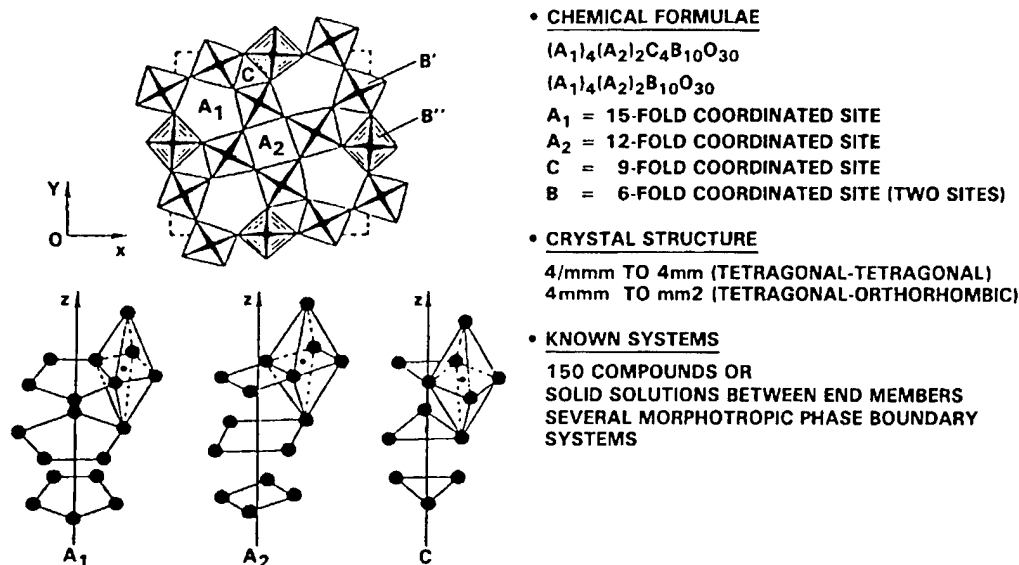
FIGURE 1　Projection of tungsten bronze structure parallel to ⟨001⟩.

fold coordinated site, the A_2 cations are in the 12-fold coordinated site, the C cations are in the 9-fold coordinated site and the B cations are in two different 6-fold coordinated sites. Detailed descriptions of this structure have been given in several articles.[38–40] Only two compositions, $K_3Li_2Nb_5O_{15}$ and $K_3Li_2Ta_5O_{15}$, can be represented by the first chemical formula where all five crystallographic sites are filled.[41–42] For this reason, these compositions are known as "stuffed" bronzes. All other tungsten bronzes are called either "filled" or "unfilled" bronzes with the 9-fold coordinated site vacant and the 15- and 12-fold coordinated sites either fully or partially occupied. For example, lead metaniobate and strontium barium niobate have unfilled unit cells containing $Pb_5Nb_{10}O_{30}$ and $(Sr, Ba)_5Nb_{10}O_{30}$ (usually simplified to $PbNb_2O_6$ and $(Sr, Ba)Nb_2O_6$) where the A sites are only 5/6 filled. Although the presumption is that the distribution among the 15- and 12-fold coordinated A sites is random, more likely in SBN, Ba^{2+} predominantly occupies the 15-fold coordinated site since Ba^{2+} (1.74 Å) is substantially larger than Sr^{2+} (1.54 Å).

Like the ferroelectric perovskite family, the bronze family embraces more than 150 compounds and solid solutions including several morphotropic phase boundary systems.[43–44] Because of the structural complexity which accommodates a wide range of cationic substitutions, often the ferroelectric transition can be achieved in the desired temperature range with suitable ferroelectric and optical properties.

POLARIZATION STATES IN TUNGSTEN BRONZES

Bronze crystals are in the prototypic point group 4/mmm. Customarily the 4-fold symmetry axis is oriented along the (3), or z axis.
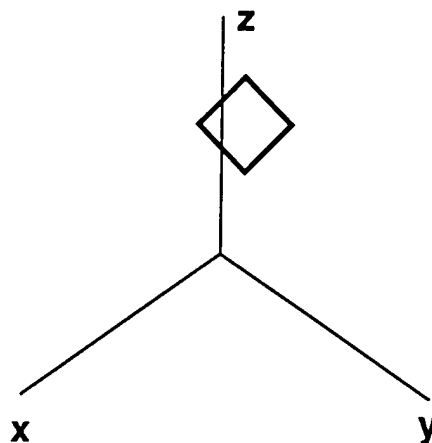
In the Aizo/Shuvalov classification, permitted ferroelectric species for 4/mmm in descending order of symmetry are:

1. 4/mmm (1) D 4 F 4 mm
2. 4/mmm (2) D 2 F mm2
3. 4/mmm (4) A 2 F m
4. 4/mmm (4) A 4 F m
5. 4/mmm (8) A 1 F 1

Only solutions (1) and (2) have been found so far in the macrosymmetry of any known bronze (Figure 2a). For these two states:

1. $P_z^2 \neq 0$, $Ps = \pm P_z(s)$ Two domain states oriented along the 4-fold axis.

2. $P_x^2 = P_y^2 \neq 0$, $P_z^2 = 0$ Four states oriented along the
$\langle 110 \rangle$ + Ps: + Ps: 0 $\langle 110 \rangle$ family, i.e., along the
$\langle 110 \rangle$ − Ps: + Ps: 0   2-fold axes.
$\langle 110 \rangle$ − Ps: − Ps: 0
$\langle 110 \rangle$ + Ps: − Ps: 0

For the point group 4/mmm, the permitted ferroelastic states are:

1. 4/mmm (2) D 2 F mmm
2. 4/mmm (4) A 2 F 2/m
3. 4/mmm (4) A 2 F 2/m
4. 4/mmm (8) A 1 F 1

Of these states, only (1) has been observed in any known bronze macrosymmetry. In mmm the square cross section of the section normal to 4 experiences a sheer $\pm X_{12}$.
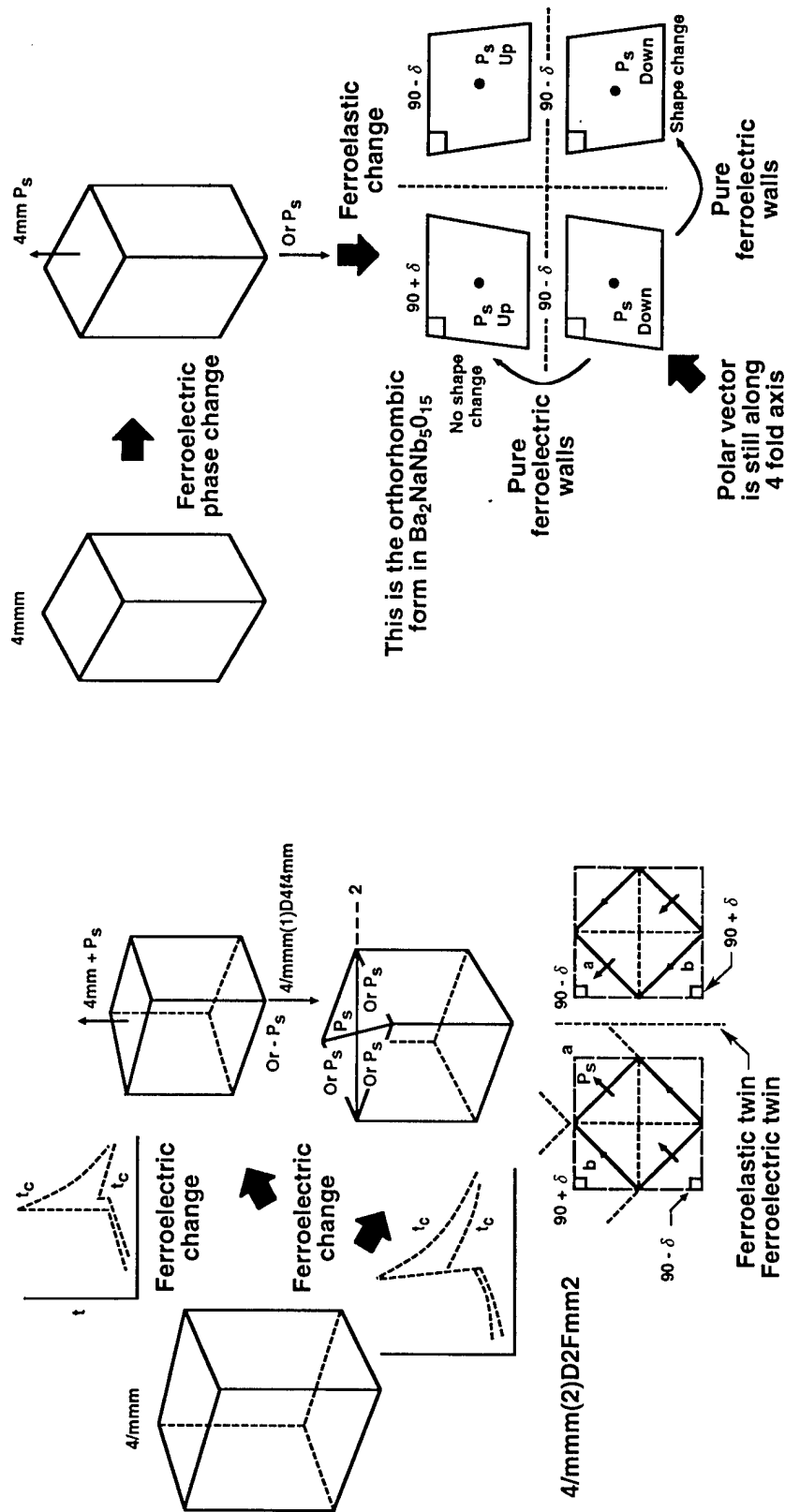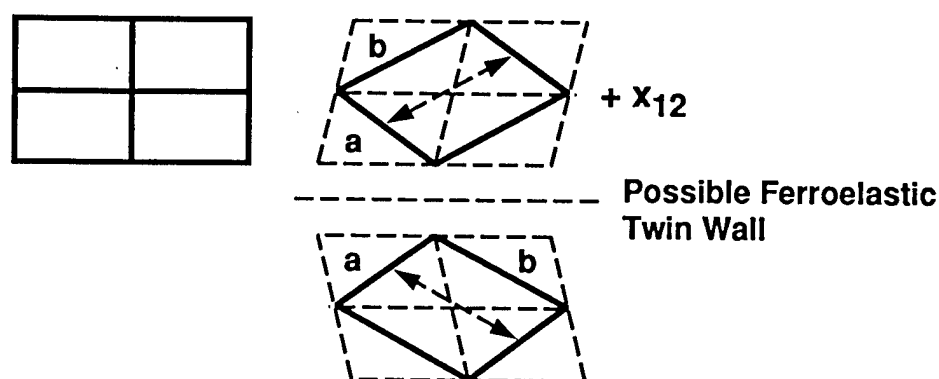
FIGURE 2   Ferroelectric/ferroelastic phase transitions and polar directions in tungsten bronze crystals.

+ x_{12}

Possible Ferroelastic Twin Wall

It is possible for the ferroelectric 4/mmm (1) DF 4 mm state to occur first on cooling, then the ferroelastic 4 mm (2) D 2 F mm2. This is depicted in Figure 2b. Note that the polar axis is $\pm P_z$ as in the original tetragonal term.

CRYSTAL DEVELOPMENT

Table I lists a number of tungsten bronze single crystals grown in our work and their associated growth conditions. The Czochralski pulling technique was used for

TABLE I

Ferroelectric tungsten bronze crystals grown at Rockwell

Composition	Growth Temp (°C)	Pull Rate (mm/hr)	Sym	Diameter (cm)	T_c (°C)	Phase Transitions
$Sr_{0.75}Ba_{0.25}N_2O_6$ (SBN:75)	1480	4-5	4mm	4.0	56	One
$Sr_{0.6}Ba_{0.4}Nb_2O_6$ (SBN:60)	1485	5-7	4mm	5.0	78	One
$Sr_{0.5}Ba_{0.5}Nb_2O_6$ (SBN:50)	1485	5-6	4mm	4.0	128	One
$Sr_{0.4}Ba_{0.6}Nb_2O_6$ (SBN:40)	1500	3-4	4mm	2.0	190	One
$Ba_{1.5}Sr_{0.5}K_{0.5}Na_{0.5}Nb_5O_{15}$	1470	3-4	4mm	1.5	209	One
$BaSrK_{0.75}Na_{0.25}Nb_5O_{15}$	1475	3-4	4mm	1.5	178	One
$Ba_{0.5}Sr_{1.5}K_{0.75}Na_{0.25}Nb_5O_{15}$	1475	4-5	mm2	2.0	172	Two?
$Sr_{1.9}Ca_{0.1}NaNb_5O_{15}$	1500	2-3	mm2	1.0	270	Two
$Sr_{1.8}Sr_{0.2}NaNb_5O_{15}$	1500	2-3	mm2	1.0	270	Two
$K_3Li_2Nb_5O_{15}$	1100	1-2	4mm	1.0	370	One
$K_3LiNaNb_5O_{15}$	1100	1-2	4mm	1.0	340	One
$Sr_2KNb_5O_{15}$	1450	3-4	4mm	1.5	157	One
$Pb_{0.6}Ba_{0.4}Nb_2O_6$ (PBN:60)	1350	1-2	4mm	1.5	320	One
$Pb_2KNb_5O_{15}$	1340	2-3	mm2	2.0	360	One
$K_2BiNb_5O_{15}$	1200	3-4	mm2	2.0	420	?
$Ba_2LiNb_5O_{15}$	1400	1-2	mm2	1.0	560	Two
$Ba_4Sr_2Ti_2Nb_8O_{30}$	1480	3-4	4mm	1.5	168	One
$Ba_3Sr_3Ti_2Nb_8O_{30}$	1480	2-3	4mm	1.5	140	One
$Ba_{2.5}Sr_{3.5}Ti_2Nb_8O_{30}$	1490	1-2	4mm	1.8	110	One
$Sr_4Ca_2Ti_2Nb_8O_{30}$	1500	2-3	mm2	1.0	200	Two
$Ba_4Ca_2Ti_2Nb_8O_{30}$	1460	1-2	mm2	1.0	175	Two

Sym = Symmetry.

these growths, with the crystals pulled from 5×5 cm platinum crucibles in an oxygen atmosphere to minimize the reduction of Nb^{5+} to Nb^{4+}. All of the crystals listed in Table I were grown along the $\langle 001 \rangle$ direction, except for the $K_3Li_2Nb_5O_{15}$ crystals where the best growth direction was found to be along the $\langle 110 \rangle$ direction. Crystal cracking during cool-down through the paraelectric/ferroelectric phase transition was initially a problem for most of these crystals, but this problem has now been minimized, particularly for SBN, BSKNN and BSTN.

Based on ferroelectric and optical studies of both tetragonal and orthorhombic bronze crystals, we have classified this family into four different groups shown in Figure 3.

1. Crystals exhibiting strong transverse effects with 4 mm symmetry (e.g. SBN. $Sr_2KNb_5O_{15}$, $Ba_6Ti_2Nb_8O_{30}$): $\langle 001 \rangle$ polar axis.
2. Crystal exhibiting strong longitudinal effects with 4 mm symmetry (e.g. BSKNN, $K_3Li_2Nb_5O_{15}$): $\langle 001 \rangle$ polar axis.
3. Crystal exhibiting strong transverse and longitudinal effects with mm2 symmetry (e.g. $Sr_{2-x}Ca_xNaNb_5O_{15}$): $\langle 001 \rangle$ polar axis.
4. Crystals exhibiting strong longitudinal effects with mm2 symmetry (e.g. $Pb_2KNb_5O_{15}$, $Pb_{1-x}Ba_xNb_2O_{15}$): $\langle 100 \rangle$ or $\langle 010 \rangle$ polar axis.

Over 25 different bronze crystal compositions have been grown (as listed in Table I) and in some cases they have been modified to meet the requirements for electro-optic, photorefractive and piezoelectric applications. All of these crystals have been grown by the Czochralski technique.[23-35]

Tungsten bronze crystals are relatively easy to grow compared to most ferroelectric crystals based on perovskite, layered structure $Bi_4Ti_3O_{12}$, and lead germanates, phosphates and vanadates. This is due in part because the bronzes have simple phase transitions and are usually free of 90° and 180° twins which occur in perovskite single crystals. Among the growth problems associated with these crystals, we have found major contributors toward poor crystal quality, as shown in Figure 4:

1. Multicomponent solid solution systems make if difficult to control crystal homogeneity.
2. Exchange among crystallographic sites, specifically of the 15- and 12-fold coordinated ions such as Ba^{2+}, Sr^{2+}, K^+, La^{3+}, causing severe striation problems.
3. High temperature growths (up to 1500°C) cause volatilization and oxidation-reduction (Nb^{5+} to Nb^{4+}) problems.
4. Cracking of crystals when thermally cycling through phase transitions. This is often aggravated by crystal imperfections.

Nevertheless, several bronze compositions have been grown as large size, defect-free crystals, including SBN (>4 cm diameter) and $Ba_{2-x}Sr_xK_{1-y}Na_yNb_5O_{15}$ (>1.5 cm diameter) which have excellent optical quality.

Crystals Exhibiting Strong Transverse Properties (4 mm)

The $Sr_{1-x}Ba_xNb_2O_6$ (SBN) solid solution is the best example of a bronze system with strong transverse properties, including the dielectric constant (ε_{33}) and the

Addition of Na+

Addition of K + and Na+

$Sr_{1-x}Ba_xNb_2O_6$ Type (4mm)
- Large transverse effects
  r_{33}, ε_{33}, d_{33}
- Cylindrical shape (24-facets)
- $T_c < 150°C$
- Moderate polarization (P_3)

$PbNb_2O_6$-Type (mm2)
- Large longitudinal effects
  r_{51}, d_{15} ε_{11}
- $T_c \sim 350°C$
- Large polarization (P_2)
  ($Pb_2KNb_5O_{15}$ Exception)

T.B. Family
$(A_1)_4(A_2)_2C_4B_{10}O_{30}$
or
$(A_1)_4(A_2)_2B_{10}O_{30}$

(mm2) and (mm2)
Symmetry of end member

Mixing
of

mm2 + mm2
or
mm2 + 4mm

Morphotropic phase boundary materials

r_{33}, d_{33} ε_{33}, P_2 (mm2 Form)
r_{51}, d_{15}, e_{11}, P_3 (4mm form)
- T_c 150 to 400°C
- Exceptionally large polarization (P3 or P2)

$Ba_{2-x}Sr_xK_{1-y}Na_yNb_5O_{15}$ Type (4mm)
- Large longitudinal effects
  r_{51}, d_{15}, ε_{11}
- Square or octahedron shape crystals
- $T_c > 150°C$
- Moderate polarization (P_3)

$Sr_{2-x}Ca_xNaNb_5O_{15}$ Type (mm2)
- Large longitudinal and transverse effects
  r_{15}, d_{15} and r_{33}, d_{33}
- Cylindrical crystals
- $T_c \sim 200-300°C$
- Large polarization (P_3)
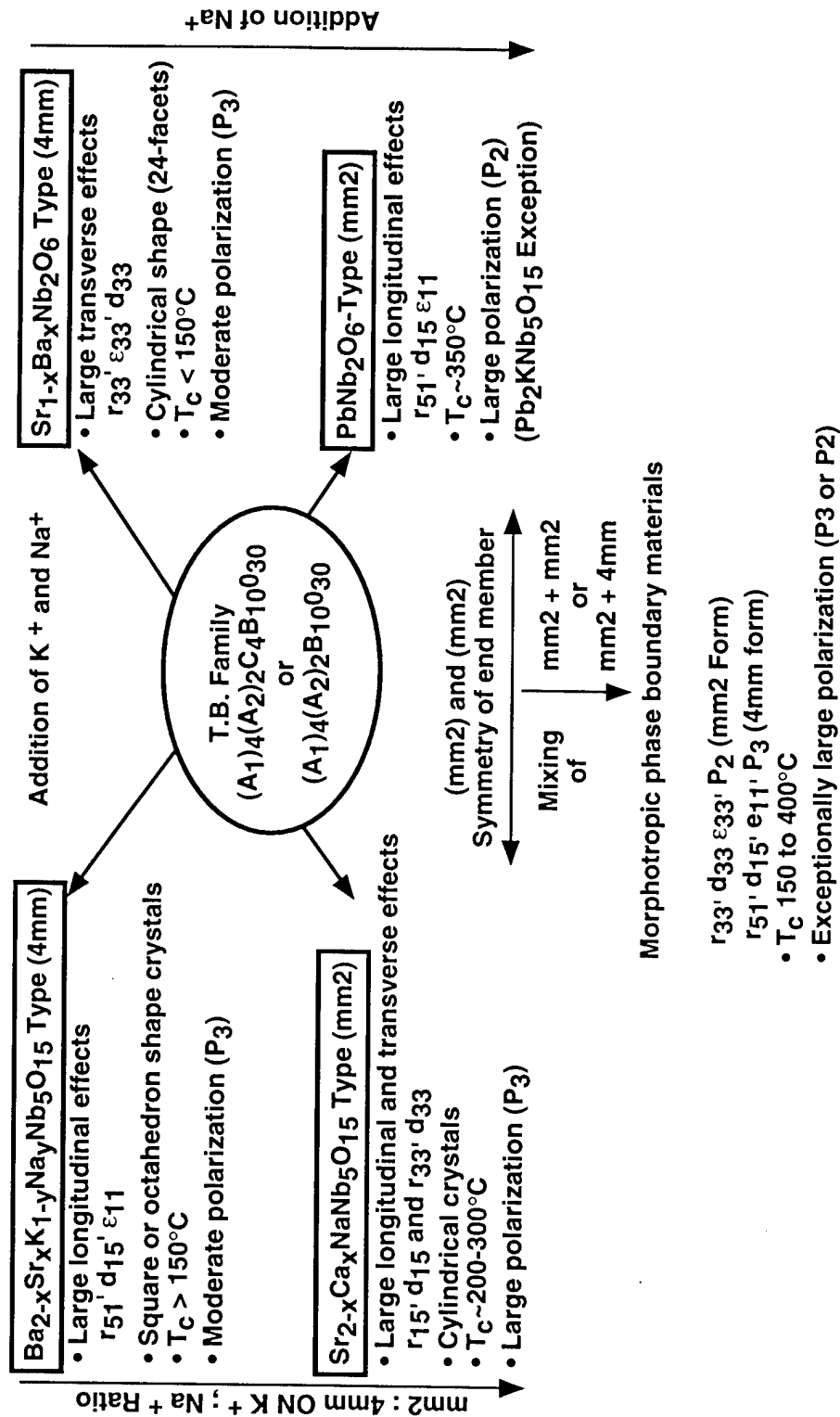
mm2 : 4mm ON K + ; Na + Ratio

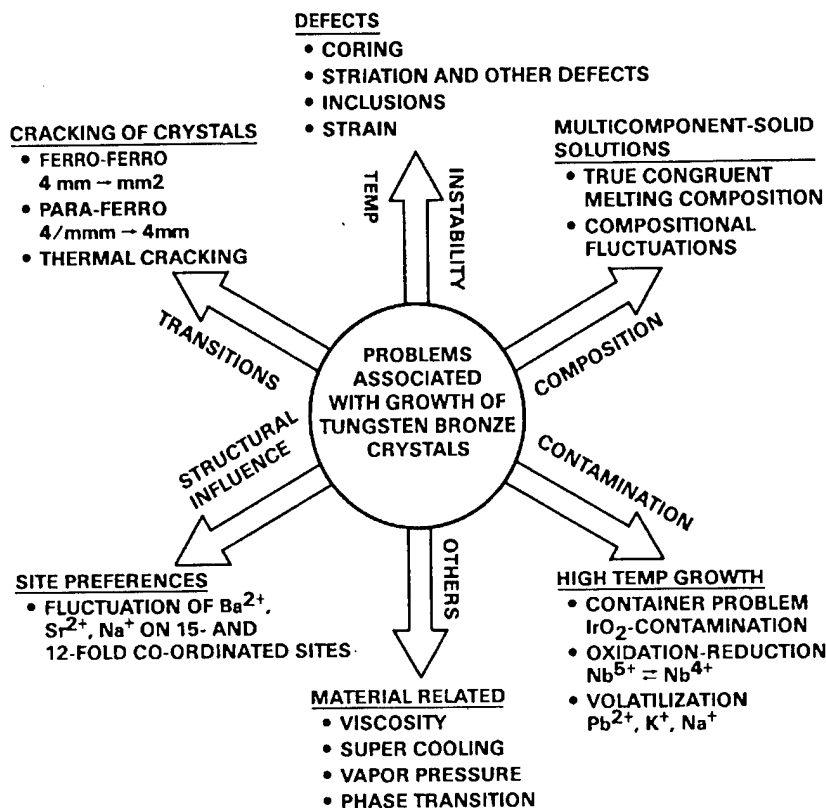FIGURE 3   Classification of tungsten bronze family crystals.

FIGURE 4   Problems associated with the growth of tungsten bronze crystals.

electro-optic (r_{33}) and piezoelectric (d_{33}) coefficients, with the polar axis along $\langle 001 \rangle$. SBN crystal growth has been studied extensively,[36-48] and for optical device applications, both large crystal size and high optical quality are needed. We have been able to grow 4 cm diameter optical-quality SBN crystals (Figure 5) for electro-optic, photorefractive and piezoelectric applications (10–21). The growth of such large crystals requires establishing of the details of the temperature-composition relationship and precise control of the growth conditions.

SBN crystals have a distinct cylindrical growth habit with 24 well-defined facets, each facet corresponding to a definite crystallographic orientation. For this reason, precise orientation and cutting of these crystals is a greatly simplified task. Although SBN crystals are relaxor (frequency-dependent) ferroelectrics with second-order phase transitions,[74] the relaxor behavior becomes even more pronounced as La^{3+} is added (Figure 6). Also of interest is that La^{3+}-doped SBN:60 crystals become square in cross section with increasing La^{3+} concentration up to 1.0 wt%. Optical-quality SBN:50, SBN:60 and SBN:75 crystals have excellent electro-optic, photorefractive and piezoelectric properties and they are currently being used in a number of laboratories for various device studies.

Other examples of bronze ferroelectrics with strong transverse optical properties are $Sr_2KNb_5O_{15}$, $Ba_2KNb_5O_{15}$ and $(Ba, Sr)_6Ti_2Nb_8O_{30}$ (BSTN). We have grown several tetragonal BSTN compositions within the $Ba_6Ti_2Nb_8O_{30}$-$Sr_6Ti_2Nb_8O_{30}$ system which exhibit optical and piezoelectric figures-of-merit about two times

cm 0   1   2   3   4   5

Rockwell International
Science Center
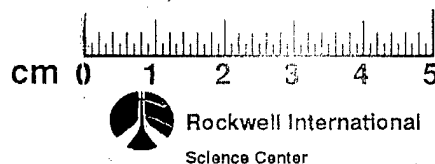
Wafer

AS grown crystal

FIGURE 5   Large size tungsten bronze SBN single crystal boule grown along ⟨001⟩ by the Czochralski method.
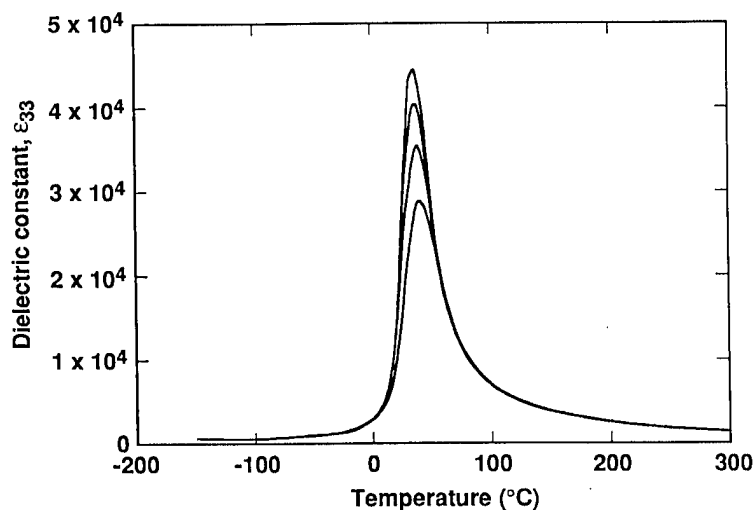

FIGURE 6   Temperature dependence of the polar axis dielectric constant for La^{3+}-doped SBN:60 at 0.1 kHz (upper), 1 kHz, 10 kHz, and 100 kHz (lower).

better than SBN:60. Figure 7 shows a typical BSTN crystal; growth up to 4 cm diameter is currently being attempted.

Crystals Exhibiting Strong Longitudinal Properties (4 mm)

A prototypical member of this class is the $Ba_{2-x}Sr_xK_{1-y}Na_yNb_5O_{15}$ (BSKNN) solid solution, which has large longitudinal properties for K^+-rich compositions. As
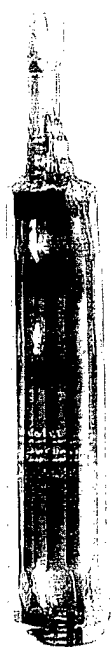
- **Crystal diameter:**   1.2 cm
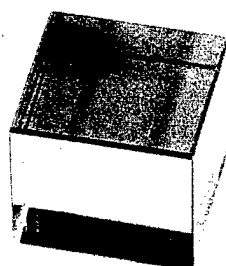
- **Crystal symmetry:** 4 mm

- **Large (r_{33}):**   400 x 10^{-12} m/V

- **Polarization:**   > 34 $\mu C/cm^2$

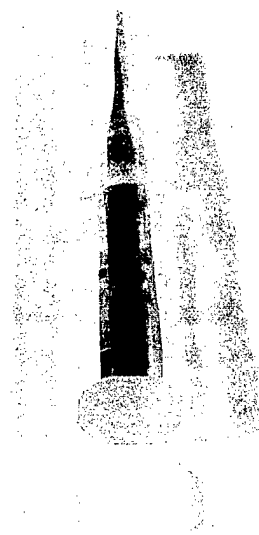FIGURE 7   Tungsten bronze BSTN crystal boule grown along the (001) direction.

BSKNN-1   **15 x 15 x 8mm**   **BSKNN-2**
                        Cube

FIGURE 8   Large size tungsten bronze BSKNN single crystal grown along (001).

shown in Figure 8, 1.5 cm diameter BSKNN crystals have been grown in optical quality.[35] The striking differences between BSKNN and SBN crystals are in their growth habits and ferroelectric properties. BSKNN single crystals grow either with a square or octahedral cross section depending on the unit cell dimensions, with the
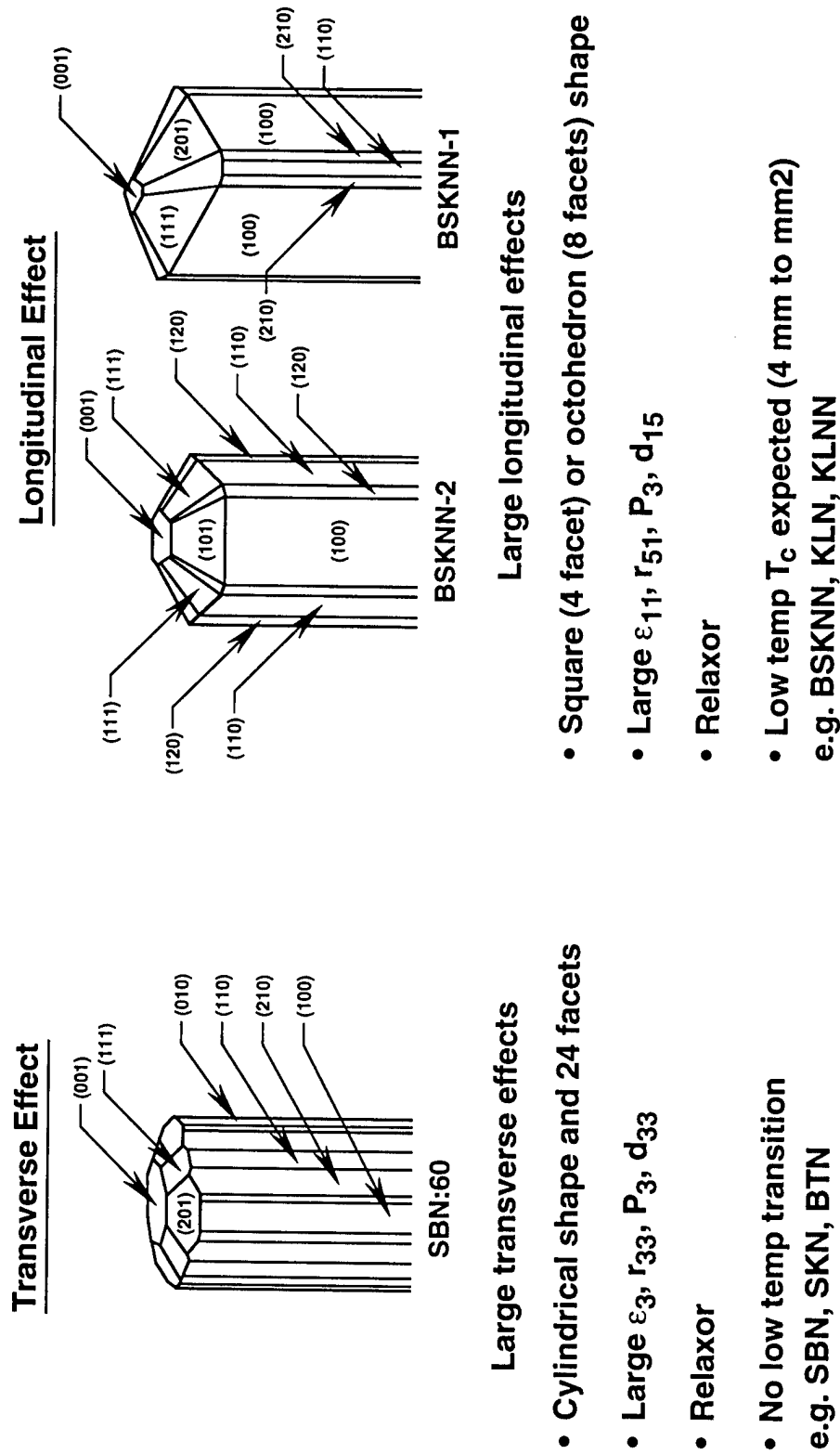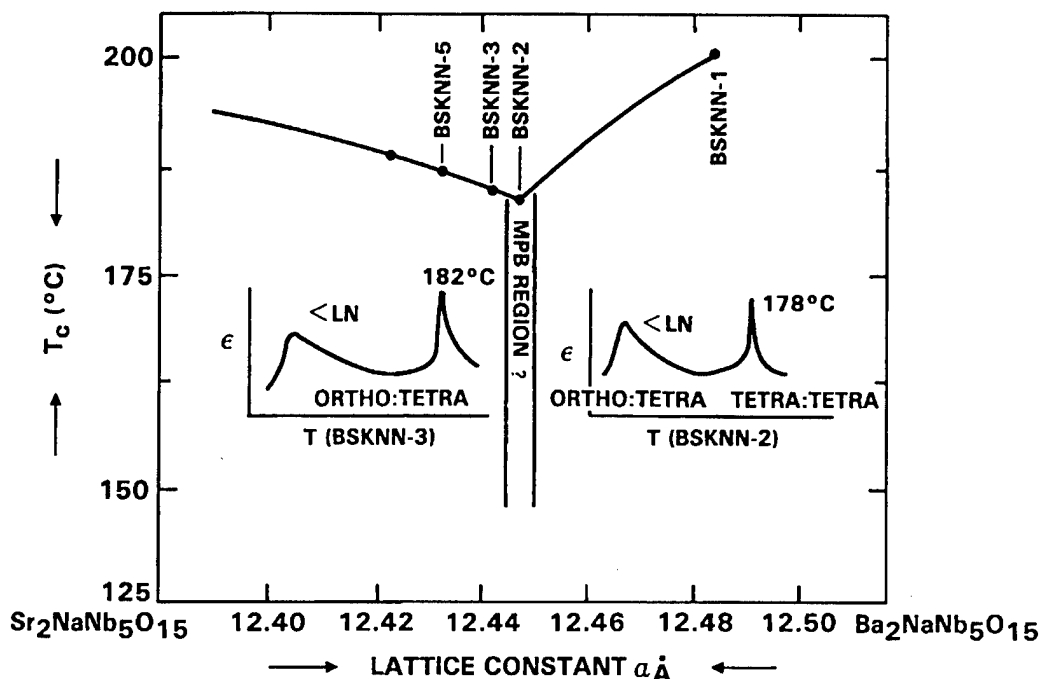
Longitudinal Effect

BSKNN-1

BSKNN-2

Large longitudinal effects

- Square (4 facet) or octohedron (8 facets) shape

- Large ε_{11}, r_{51}, P_3, d_{15}

- Relaxor

- Low temp T_c expected (4 mm to mm2)
  e.g. BSKNN, KLN, KLNN

Transverse Effect

SBN:60

Large transverse effects

- Cylindrical shape and 24 facets

- Large ε_3, r_{33}, P_3, d_{33}

- Relaxor

- No low temp transition
  e.g. SBN, SKN, BTN

FIGURE 9   Growth habits for tetragonal tungsten bronze crystals.

FIGURE 10   The ferroelectric $Sr_2NaNb_5O_{15}$-$Ba_2NaNb_5O_{15}$ system.

bigger unit cell BSKNN crystals ($a > 12.500$ Å, $c > 3.955$ Å) being square in shape. Figure 9 shows the differences among BSKNN-1, BSKNN-2 and SBN-type crystals. We anticipate the presence of a 4 mm to mm2 phase transition in BSKNN-1 (K^+-rich) single crystals, similar to $Ba_2NaNb_5O_{15}$, but this transition would occur below 100K. Xu et al.[49] have claimed such transition and it needs to be verified. The BSKNN compositions that are Na^+-rich (e.g. BSKNN-3, BSKNN-4) appear to be weakly orthorhombic at room temperature. As shown in Figure 10, a morphotropic phase boundary region seems to exist between BSKNN-2 and BSKNN-3, with transverse effects being larger in BSKNN-3.[50] Recently, we have successfully grown BSKNN-3 and BSKNN-5 crystals in excess of 1.5 cm diameter; and we believe we should be able to grow these crystals larger than 3 cm in diameter.

BSKNN crystals have a second-order phase transition with a much less pronounced relaxor character than in SBN. BSKNN crystals resemble $BaTiO_3$ in many of their ferroelectric characteristics, and for this reason we expect that they will replace this well-known material in many electro-optic and photorefractive applications. A particular advantage of BSKNN over $BaTiO_3$ is the absence of twins which makes growth to large sizes (>2 cm diameter) and crystal poling much easier. Other examples of bronzes with strong longitudinal properties are $K_3Li_2Nb_5O_{15}$ and $K_3(Na, Li)_2Nb_5O_{15}$.

Crystal Exhibiting Strong Transverse and Longitudinal Properties

Three types of orthorhombic tungsten bronzes are found in this category (Figure 11): (1) orthorhombic bronzes with the polar axis along ⟨001⟩ having two phase transitions; (2) bronzes with the polar axis along ⟨001⟩, but with only one phase

Classification of Orthorhombic Tungsten Bronze Materials

Polar Axis <100> or <010>

- Strongly Orthorhombic

- Second order phase transition with relaxor character

- Phase transition (Tc) is high, up to 500° C: 4/mmm to mm2

- No evidence of low temperature phase transition

- Strong longitudinal effects are prominent with exceptionally high polarization

- e.g. $Pb_2KNb_5O_{15}$
  $(Pb,Ba)Nb_2O_6$

Polar Axis <001>

- Weakly Orthorhombic (Pseudo Tetragonal)

- First order phase transition

- Phase transition varies from -200° to 400° C: 4/mm to mm2

- No evidence of low temperature transition

- Strong longitudinal and transverse effects, but low polarization

- e.g. $K_2BiNb_5O_{15}$
  $K_3Bi_3Ti_2Nb_5O_{15}$
  $Ba_2LiNb_5O_{15}$

- Weakly Orthorhombic (Pseudo Tetragonal)

- First order phase transition

- Two phase transitions, 4/mmm to 4mm & 4mm to mm2 (100° - 600° C)

- Possibility of low temperature transition below 77K

- Strong longitudinal and transverse effects, but moderately high polarization

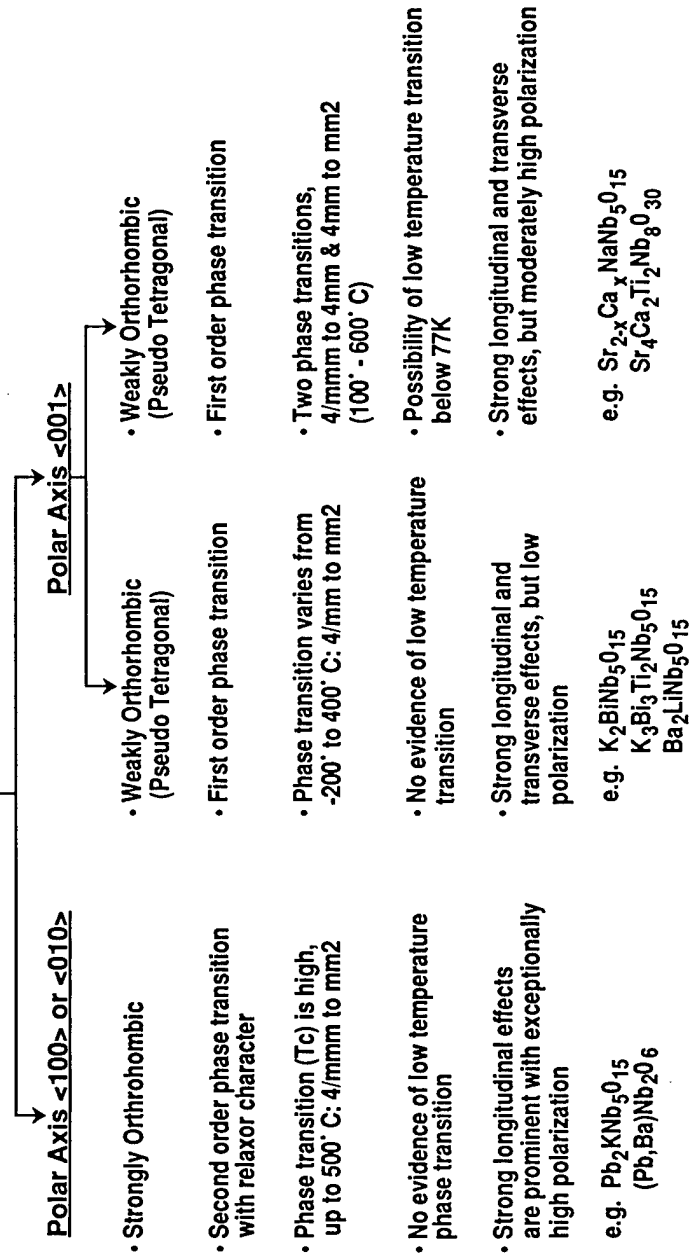- e.g. $Sr_{2-x}Ca_xNaNb_5O_{15}$
  $Sr_4Ca_2Ti_2Nb_8O_{30}$

FIGURE 11 Classification of orthorhombic tungsten bronze crystals.

transition; and (3) bronzes with the polar axis along $\langle 010 \rangle$ or $\langle 100 \rangle$ and only one phase transition. The latter will be discussed in the next section.

Typical examples of the first type of orthorhombic bronzes are found in the $Sr_{2-x}Ca_xNaNb_5O_{15}$ (SCNN) solid solution system. SCNN crystals have two phase transitions above room temperature,[23] one paraelectric (4/mmm) to ferroelectric (4 mm), and the other ferroelectric (4 mm) to ferroelastic (mm2). As shown in Figure 12, the dielectric constant along $\langle 100 \rangle$ increases with decreasing temperature, resulting in large transverse and longitudinal dielectric and optical properties at room temperature or below. SCNN has a reasonably high spontaneous polarization at room temperature (34 $\mu C/cm^2$) with electro-optic coefficients r_{33} and r_{51} comparable to SBN:75 (r_{33} = 1400 × 10^{-12} m/V). For this reason, SCNN is being considered for photorefractive applications such as double phase conjugation and optical computing. Other interesting examples of orthorhombic bronzes in this category are $Ba_2NaNb_5O_{15}$ (BNN), $Sr_2NaNb_5O_{15}$ (SNN) and $Sr_2(Na, Li)Nb_5O_{15}$ (SNLN).

$K_2BiNb_5O_{15}$ (KBN) is another crystal in which both longitudinal and transverse ferroelectric properties are large; however, this crystal has only one phase transition (4/mmm to mm2) with no ferroelastic contribution. Crystal growth of KBN is relatively easy compared to SCNN; as shown in Figure 13, approximately 2 cm diameter crystals can be grown with excellent optical quality. $Sr_2(K, Li)Nb_5O_{15}$ (SKLN) is also reported to possess only one phase transition from 4/mmm to mm2.[51] Based on our work on various bronze systems discussed earlier, we believe that this ferroelectric should possess two phase transitions above room temperature, similar to SCNN and BNN. A detailed investigation of SKLN single crystals is still needed to firmly establish the correct structure and transition sequences.

All of these tungsten bronzes are orthorhombic at room temperature and have first-order ferroelectric phase transitions with no relaxor character. BNN single crystals have been studied extensively and they possess excellent acoustical and nonlinear optical properties.[52-57] However, they have not been widely accepted
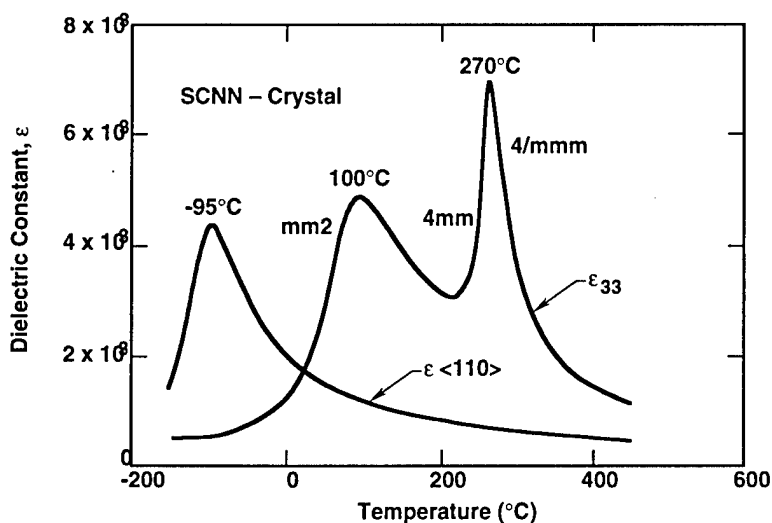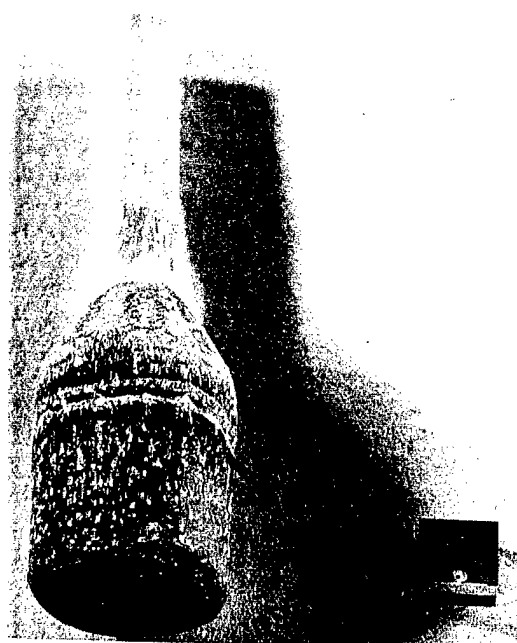

FIGURE 12   Polar and nonpolar $\langle 110 \rangle$ dielectric constants for SCNN at 10 kHz. Low temperature peak along $\langle 110 \rangle$ is due to the freezeout of the polarizability in this direction.

CRYSTAL DIMENSIONS
DIAMETER: 1.5 CM
HEIGHT: 5 CM
QUALITY: EXCELLENT

FIGURE 13   Tungsten bronze orthorhombic $K_2BiNb_5O_{15}$ crystal grown along $\langle 001 \rangle$.

for practical applications due to the difficulties in the growth of large size, adequate quality crystals. At Rockwell, we have also investigated other Bi^{3+}-containing compositions having potentially large r_{33} and r_{51} with photorefractive spectral responses extending into the near-IR (up to 1.0 μm). However, these compositions, except for KBN, are difficult to grow due to the formation of two-phase liquids at the growth temperature.

Pb^{2+}-Containing Bronzes

As summarized in Table II, many of the Pb^{2+} and Ta^{5+}-containing bronze compositions are strongly orthorhombic at room temperature. These materials have only one phase transition from 4/mmm to mm2, with the polar axis oriented along $\langle 100 \rangle$ or $\langle 010 \rangle$. The compositions most studied in this category are $PbNb_2O_6$ (PN), $(Pb, Ba)Nb_2O_6$ (PBN) and $Pb_2KNb_5O_{15}$ (PKN) for surface acoustic wave (SAW) and piezoelectric applications[58-59] because of their excellent electromechanical coupling and piezoelectric properties. The polarization in these materials can exceed 40 μC/cm^2, and their optical figures-of-merit are estimated to be better than the current best-known ferroelectrics such as SBN and $BaTiO_3$. Because of these properties, single crystal and thin film growths of PBN and PKN compositions have been actively pursued in our laboratory and at Penn State University.[60-61] However, bulk crystal growth is extremely difficult due to cracking when passing through the paraelectric/ferroelectric phase transition as a result of the large strain developed in the plane orthogonal to the $\langle 001 \rangle$ growth direction. Another problem with bulk crystal growth is the volatilization of Pb^{2+} at the growth temperature which causes severe compositional inhomogeneity. Hence, the sputtered or sol-gel growth

TABLE II

Symmetry and T_c trends in Nb^{5+} and Ta^{5+}-containing bronzes

Tetragonal bronzes 4/mmm to 4 mm		Orthorhombic bronzes 4/mmm to mm2	
• $Pb_2KTa_5O_{15}$	$(T_c = -41°C)$	• $Pb_2KNb_5O_{15}$	$(T_c = 460°C)$
• $Pb_2NaTa_5O_{15}$	$(T_c = 20°C)$	• $Pb_2NaNb_5O_{15}$	$(T_c = 560°C)$
		• $PbNb_2O_6$	$(T_c = 560°C)$
• $Sr_2NaTa_5O_{15}$	$(T_c = 153°C)$	• $Sr_2NaNb_5O_{15}$	$(T_c = 270°C)$
• $Ba_2NaTa_5O_{15}$	$(T_c = 120°C)$	• $Ba_2NaNb_5O_{15}$	$(T_c = 560°C)$
		• $PbTa_2O_6$	$(T_c = 265°C)$
• $Ba_2KNb_5O_{15}$	$(T_c = 373°C)$	• $Ba_2KTa_5O_{15}$	$(T_c = 10°C)$
• $Sr_2KNb_5O_{15}$	$(T_c = 156°C)$	• $Sr_2KTa_5O_{15}$	$(T_c = 110°C)$
• $K_3Li_2Nb_5O_{15}$	$(T_c = 450°C)$	• $K_3Li_2Ta_5O_{15}$	$(T_c = -266°C)$

of epitaxial thin films appears to be the best growth method for these ferroelectrics, especially for electronic memory and optical applications.

Table II shows that when Pb^{2+} is combined with Nb^{5+}, the compounds crystallize with an orthorhombic symmetry; however, a tetragonal (4 mm) structure can be stabilized when Pb^{2+} is combined with Ta^{5+}, with the exception of $PbTa_2O_6$ (PT) which is orthorhombic at room temperature with a Curie point of 260°C. The situation is reversed for non-Pb^{2+}-containing bronzes, however. For example, when Ba^{2+} and Sr^{2+} are combined with K^+ and Nb^{5+}, the phases are tetragonal, and when they are combined with K^+ and Ta^{5+}, the phases are orthorhombic. Since only a few of the Ta^{5+}-containing bronzes are ferroelectric above room temperature, and these compositions melt at very high temperatures (>1600°C), very few Ta^{5+}-containing bronze crystals have been grown to date. As a result, the Ta^{5+}-containing bronzes are not yet well understood.

Photorefractive Applications of T. B. Crystals

We are exploring tungsten bronze family materials in single crystal and thin film forms for various applications, including photorefractive, electro-optic, piezoelectric, pyroelectric devices. The unusually strong linear and nonlinear effects in these materials make them excellent candidates for such applications. Photorefractive applications are of current great interest, and we have grown several optical-quality bronzes that possess high photorefractive figures-of-merit. Table III lists some of the photorefractive bronze crystals with their key optical figures of merit.

The improved sensitivity and photorefractive response time exhibited in large-size, high optical quality single crystals of SBN and BSKNN have made possible the demonstration of a number of applications. Beam fanning[62] is a well-known photorefractive phenomenon in which scattered light from a laser beam is asymmetrically amplified as it passes through high-gain crystals such as SBN and BSKNN. Beam fanning gives rise to a number of possible applications and plays an auxiliary

TABLE III

Electro-optic coefficients and figures of merit for tungsten bronzes

Crystal	Electro-Optic Coeff. ($r_{ij} \times 10^{-12}$ m/V)	ε_{ij}	$n^3 r_{ij}/\varepsilon$	Crystal Size (cm.)
SBN:60	$r_{33} = 240$	$\varepsilon_{33} = 1000$	5.01	> 5.0
BSTN	$r_{33} = 200$	$\varepsilon_{33} = 345$	8.05	> 1.5
BSKNN-2	$r_{51} = 380$	$\varepsilon_{11} = 800$	6.2	> 1.8
BSKNN-3	$r_{51} = 420$	$\varepsilon_{11} = 800$	6.4	> 1.5
SCNN	$r_{33} = 1200$	$\varepsilon_{33} = 1740$	8.63	~ 1.0
	$r_{51} = 1150$	$\varepsilon_{11} = 1700$	8.32	

role in the formation of self-pumped phase conjugators[63] and double phase conjugators.[64] In particular, the photorefractive processes of beam-fanning, self-pumped phase conjugation and double phase conjugation have been used to demonstrate several important beam control and image processing applications. For example, techniques for using tungsten bronze materials to perform optical limiting,[65,66] imaging restoration (beam clean-up),[67] incoherent-to-coherent conversion,[68] real-time volume storage of color images,[69] addition/subtraction,[70] and correlation-convolution operations[71] have been developed. We also recently demonstrated that beam fanning, self-pumped phase conjugation and double phase conjugation can be performed in color (i.e., using many mutually incoherent laser wavelengths), thereby expanding the range and variety of applications possible in these crystals.[69,71]

In addition to high gain and fast response, a photorefractive crystal must have good optical quality (free of index variations), and in many cases, must be of a large size to be used successfully. For example, when two-wave mixing is used to amplify images, severe phase aberrations may be introduced by the photorefractive gain medium unless the medium is free from all index variations and the surfaces are prepared very carefully. High optical quality crystals will allow image amplification without having to resort to phase conjugation to clean-up the images.

We recently demonstrated the principle of incoherent-to-coherent conversion using a self-pumped phase conjugator based on SBN:60 crystals.[68] The self-pumped phase conjugator[63] used in these experiments required only one input wave. In this geometry the incident input wave is reflected from self-generated gratings in the crystal to form the pumping beams. The experimental set up is shown in Figure 14 where an extraordinary polarized beam at 514 nm from an argon-ion laser was used to generate a phase conjugate replica of the input wave. A counterpropagating beam, consisting of a white light source, was passed through a binary transparency and imaged into the crystal to form image-modulated volume phase gratings. The selective erasure of the self-organized gratings written by the self-pumping beam encoded the amplitude information from the incoherent beam onto the phase conjugate signal. The inverted-contrast coherent output image is compared with the input image in Figure 15. The resolution for this set of images is 28 lines/mm.
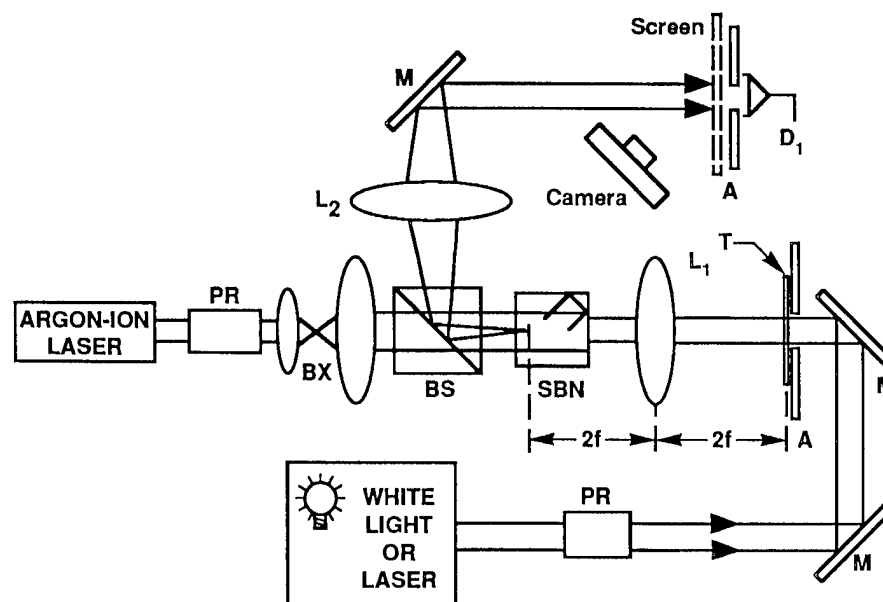
FIGURE 14   Experimental arrangement used to demonstrate the principles of incoherent-to-coherent conversion in a self-pumped phase conjugator.

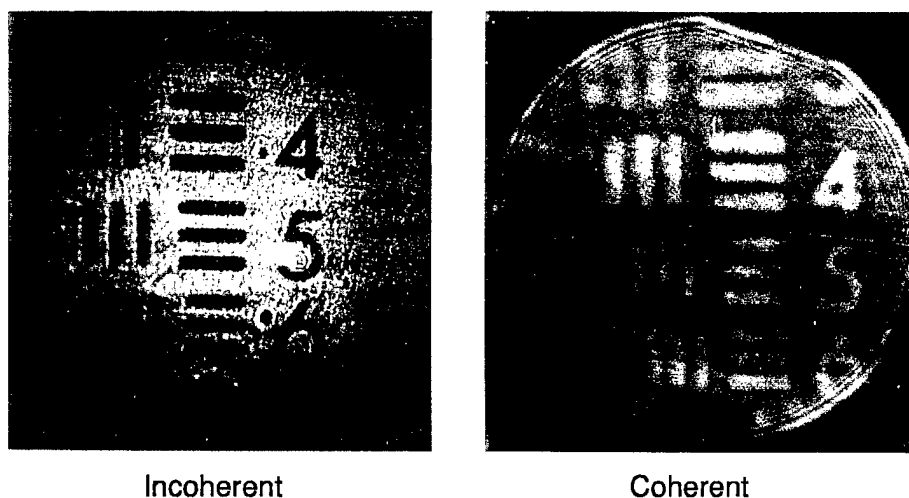Incoherent   Coherent

FIGURE 15   Comparison of the reversed contrast incoherent input image and the coherent output image.

We note that, since any aberration introduced on the writing beam by the crystal would also be transferred to the signal beam, this high resolution is due in part to the high optical quality of the crystal used.

A recent development in phase conjugation techniques has been the double phase conjugate mirror (DPCM),[64,70,73] where the photorefractive crystal acts as a simultaneous conjugate mirror for two incoming waves. When the output of two independent lasers with incident optical electromagnetic fields E_1 and E_2 are directed into a photorefractive medium, a phase conjugate replica of each beam appears under appropriate conditions. Both beams are required for either conjugate
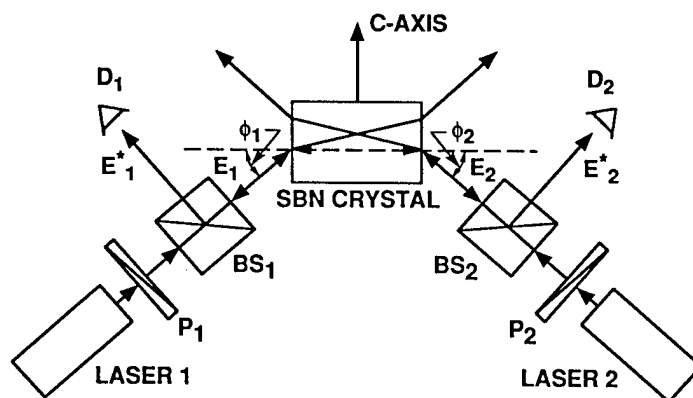
FIGURE 16 Experimental apparatus used to observe the phase conjugate signals from a double phase conjugate mirror based on a single crystal of SBN:60.

beam (E_1^* or E_2^*) to exist, and the energy for the conjugate of one beam is supplied by the other beam. Although DCPMs have many different configurations, significant benefits can be derived from specific geometric arrangements. For example, both the time response and magnitude of the conjugate signal will vary significantly depending on which geometry is employed for a particular crystal. Recently, we reported[70] on a new method for double phase conjugation which is particularly suited to tungsten bronze SBN, although the method has also been applied to BaTiO$_3$ and BSKNN. This new arrangement is highly insensitive to the alignment of the incident beams, quick to form a conjugate image with high reflectivity and fidelity, and free from instabilities due to frequency shifts or competition with self-pumping. The geometry for this new DPCM is depicted in Figure 16 where the two input beams have "fanned" into one another to form the coupling region observed in the crystal after the conjugate waves appear. Since the two beams bridge to overlap in the crystal without reflecting off a crystal face, this arrangement is called the "bridge conjugator." The bridge conjugator shown in Figure 16 was used to demonstrate image addition/subtraction[70] and more recently correlation-convolution.[71]

When the output of a linearly polarized argon-ion laser oscillating at eight discrete lines simultaneously is directed onto an SBN or BSKNN crystal at an angle Θ with the normal to the entrance crystal face, a broad fan of linearly polarized light appears on the negative c-axis side of the transmitted beam. This fan appears independent of whether Θ is positive or negative as defined by the c direction. For negative Θ values, however, an intense multicolored ring or rainbow pattern also appears.[72] Examination of the rainbow pattern using a spectrometer indicates that all eight lines are present, although only four or five of them are discernible to the eye. In fact, reflection of the multicolored ring back into the crystal using a curved mirror produced the phase conjugate of all eight lines in a time very near to the crystal beam-fanning response time.[69] In this sense, the crystal acts as a broadband "self-pumping" device.[74] Tungsten bronze crystals are particularly suited for broadband applications because their open crystal structure makes possible multi-dopant concepts which broaden the photorefractive absorption spectrum without degrading the optical quality. We have used the effect of multicolor beam fanning to overcome

the earlier difficulty of erasure between colors when a multi-wavelength source is used to demonstrate real-time volume storage of color images.

In addition to those applications discussed here, other important image processing applications will continue to be improved and developed as the quality of photorefractive crystals continues to improve.

CONCLUSIONS AND REMARKS

A variety of ferroelectric tungsten bronze crystals have been successfully grown, and using their ferroelectric and electro-optic properties, this family of materials can be classified into four different groups. The doped tungsten bronze crystals specifically SBN and BSKNN, exhibit interesting photorefractive properties and have a wide range of applications in incoherent-to-coherent conversion, double phase conjugate mirrors, image processing, data storage and optical computing.

REFERENCES

1. R. B. Maciolek and S. T. Liu, *J. Electron. Mater.*, **2**, 191 (1973).
2. R. B. Maciolek, T. L. Schuller and S. T. Liu, *J. Electron. Mater.*, **5**, 415 (1976).
3. S. Kuroda and K. Kubota, *J. Phys. Chem. Solids*, **44**, 527 (1983).
4. E. G. Spencer, P. V. Lenzo, and A. A. Ballman, *Proc. IIIE*, **52**, 2074 (1967).
5. A. M. Glass, *J. Appl. Phys.*, **40**, 4699 (1969).
6. P. V. Lenzo, E. G. Spencer and A. A. Ballman, *Appl. Phys. Lett.*, **11**, 23 (1967).
7. R. L. Townsend and J. T. LaMacchia, *J. Appl. Phys.*, **51**, 88 (1970).
8. J. J. Amodei, D. L. Staebler and A. W. Stephens, *Appl. Phys. Lett.*, **18**, 507 (1971).
9. J. B. Thaxter, *Appl. Phys. Lett.*, **15**, 210 (1969).
10. W. W. Ho, W. F. Hall, R. R. Neurgaonkar, R. E. DeWames and T. C. Lim, *Ferroelectrics*, **38**, 63 (1981).
11. G. Rakuljic, A. Yariv and R. R. Neurgaonkar, *J. Opt. Eng.*, **25**, 1212 (1986).
12. O. Eknoyan, C. H. Bulmer, H. F. Taylor, W. K. Burns, A. S. Greenblatt, L. A. Beach and R. R. Neurgaonkar, *Appl. Phys. Lett.*, **48**, 13 (1986).
13. M. D. Ewbank, R. R. Neurgaonkar, W. K. Cory and J. Feinberg, *Appl. Phys. Lett.*, **62**(2), 373 (1987).
14. B. Bobbs, M. Matloubian, H. R. Fetterman, R. R. Neurgaonkar and W. K. Cory, *Appl. Phys. Lett.*, **48**, 1642 (1986).
15. E. J. Sharp, M. J. Miller, G. L. Wood, W. W. Clark III, G. Salamo and R. R. Neurgaonkar, *Appl. Phys. Lett.*, **52**, 765 (1987).
16. G. L. Wood, W. W. Clark III, M. J. Miller, E. J. Sharp, G. Salamo and R. R. Neurgaonkar, *J. Quantum Electronics*, **23**(12), 2126 (1987).
17. J. F. Jelsma, R. R. Neurgaonkar and W. K. Cory, *Proc. SPIE*, **832**, 198 (1987).
18. G. J. Salamo, M. J. Miller, W. W. Clark III, G. L. Wood, E. J. Sharp and R. R. Neurgaonkar, *Appl. Optics*, **27**(21), 4356 (1988).
19. E. J. Sharp, M. J. Miller, G. J. Salamo, W. W. Clark III, G. L. Wood and R. R. Neurgaonkar, *Ferroelectrics*, **87**, 335 (1988).

20. K. Sayano, G. A. Rakuljic, A. Agranat, A. Yariv and R. R. Neurgaonkar, *Optics. Lett.*, **14**(9), 459 (1989).
22. J. Ford, Y. Taketomi, S. Lee, D. Bize, S. Feinman and R. R. Neurgaonkar, *Proc. SPIE*, **1148**, 12 (1989).
23. R. R. Neurgeonkar, W. K. Cory, J. R. Oliver, E. J. Sharp, G. L. Wood, M. S. Miller, W. W. Clark III and G. Salamo, *Mat. Res. Bull.*, **23**, 1459 (1988).
24. R. R. Neurgaonkar, J. G. Nelson, J. R. Oliver and L. E. Cross, *Mat. Res. Bull.*, **25**, 959 (1990).
25. R. R. Neurgaonkar, J. R. Oliver and J. G. Nelson, private communication.
26. R. R. Neurgaonkar, M. H. Kalisher, T. C. Lim, E. J. Staples and K. L. Keester, *Mat. Res. Bull.*, **15**, 1305 (1980).
27. R. R. Neurgaonkar, W. K. Cory, W. W. Ho, W. F. Hall and L. E. Cross, *Ferroelectrics*, **38**, 857 (1981).
28. R. R. Neurgaonkar and W. K. Cory, *Ferroelectrics*, **35**, 301 (1983).
29. R. R. Neurgaonkar, W. W. Ho, W. K. Cory, W. F. Hall and L. E. Cross, *Ferroelectrics*, **51**, 185 (1984).
30. R. R. Neurgaonkar, *Proc. SPIE*, **465**, 97 (1984).
31. R. R. Neurgaonkar and L. E. Cross, *Mat. Res. Bull.*, **21**, 893 (1986).
32. R. R. Neurgaonkar and W. K. Cory, *J. Opt. Soc. Am.*, **3**(B), 276 (1986).
33. R. R. Neurgaonkar, W. K. Cory, J. R. Oliver and L. E. Cross, *Proc. SPIE*, **567**, 11 (1985).
34. R. R. Neurgaonkar, W. K. Cory, J. R. Oliver and L. E. Cross, *Mat. Res. Bull.*, **24**, 1025 (1989).
35. R. R. Neurgaonkar, W. K. Cory, J. R. Oliver, M. J. Miller, W. W. Clark III, G. L. Wood and E. J. Sharp, *J. Cryst. Growth*, **84**, 629 (1987).
36. R. R. Neurgaonkar, W. K. Cory and J. R. Oliver, *Proc. SPIE*, **739**, 91 (1987).
37. R. R. Neurgaonkar, W. K. Cory, J. R. Oliver, M. D. Ewbank and W. F. Hall, *J. Opt. Eng.*, **26**(5), 392 (1987).
38. M. H. Francombe and B. Lewis, *Acta Cryst.*, **11**, 696 (1958).
39. L. G. Van Uitert, H. J. Levinstein, J. J. Rubin, C. D. Capio, E. F. Dearborn and W. A. Bonner, *Mat. Res. Bull.*, **3**, 47 (1968).
40. P. B. Jamieson, S. C. Abrahams and J. L. Bernstein, *J. Chem. Phys.*, **48**, 5048 (1968).
41. T. Fukuda, *Jap. J. Appl. Phys.*, **9**, 599 (1970).
42. T. V. Tiaou, N. N. Krainnik, I. H. Ismailzade, V. A. Isupov and F. A. Ageve, Izv. Acad. Nauk. SSSR, *Ser. Phys.*, **35**, 1825 (1971).
43. M. H. Framcombe, *Acta Cryst.*, **13**, 131 (1960).
44. V. A. Isupov and V. I. Kosiakov, *Zh. Tekh. Fiz.*, **28**, 2175 (1958).
45. J. R. Oliver, R. R. Neurgaonkar and L. E. Cross, *J. Am. Ceram. Soc.*, **72**, 202 (1989).
46. A. A. Ballman, S. K. Kurtz and H. Brown, *J. Cryst. Growth*, **10**, 185 (1971).
47. A. A. Ballman and H. Brown, *J. Cryst. Growth*, **1**, 311 (1967).
48. K. Megumi, N. Nagatsuma, K. Kashiwada and Y. Furuhata, *Mater. Sci.* **11**, 1583 (1976).
49. H. C. Chen and Y. Xu, *J. of Chinese Silicate Soc.*, **10**, 406 (1982).
50. R. R. Neurgaonkar, W. K. Cory, J. R. Oliver, M. Khoshnevisan and E. J. Sharp, *Ferroelectrics*, **102**, 3 (1990).
51. I. Katahiro, T. Yano and A. Watanabe, *Jap. J. Appl. Phys.*, **54**, 2355 (1971).
52. J. E. Geusic, *Appl. Phys. Lett.*, **11**(9), 269 (1967).
53. J. E. Geusic, *Appl. Phys. Lett.*, **12**(9), 306 (1968).
54. R. R. Rice, *J. Electrochem. Soc.*, **116**(6), 839 (1969).
55. R. G. Smith, *Appl. Phys. Lett.*, **39**(8), 4030 (1968).
56. A. W. Warner, *Appl. Phys. Lett.*, **14**(1), 34 (1969).
57. B. Jaffe, W. R. Cook and H. Jaffe, *Piezoelectric Ceramics*, (Academic, New York), 1971.
58. M. Yokosuka, *Jap. J. Appl. Phys.*, **16**, 379 (1977).
59. K. Nagata and K. Okazaki, *Jap. J. Appl. Phys.*, **24**, 812 (1985).
60. T. R. Shrout, H. Chen and L. E. Cross, *Ferroelectrics*, **56**, 45 (1983).
61. T. R. Shrout, L. E. Cross and D. A. Hukin, *Ferroelectrics Lett.*, **44**, 325 (1983).
62. J. Feinberg, *J. Opt. Soc. Am.*, **72**, 46 (1982).
63. J. Feinberg, *Opt. Lett.*, **7**, 486 (1982).
64. S. Weiss, S. Sternkler and B. Fischer, *Opt. Lett.*, **12**, 114 (1987).
65. G. L. Wood, W. W. Clark III, M. J. Miller, G. J. Salamo and E. J. Sharp, Mat. For Opt. Switches, Isolators and Limiters, M. J. Soileau, ed., *SPIE*, **1105**, 154 (1989).
66. G. L. Wood, W. W. Clark III, G. J. Salamo, A. Mott and E. J. Sharp, *J. Appl. Phys.*, **71**, 37 (1992).
67. E. J. Sharp, M. J. Miller, G. J. Salamo, W. W. Clark III, G. L. Wood and R. R. Neurgaonkar, *Ferroelectrics*, **87**, 335 (1988).
68. E. J. Sharp, G. L. Wood, W. W. Clark III, G. J. Salamo and R. R. Neurgaonkar, *Opt. Lett.*, **17**, 207 (1992).

69. S. G. Rabbani, J. L. Shultz, G. J. Salamo, E. J. Sharp, W. W. Clark III, M. J. Miller, G. L. Wood and R. R. Neurgaonkar, *Appl. Phys.*, **B53,** 323 (1991).
70. E. J. Sharp, W. W. Clark III, M. J. Miller, G. L. Wood, B. Monson, G. J. Salamo and R. R. Neurgaonkar, *Appl. Opt.*, **29,** 743 (1990).
71. R. J. Anderson, E. J. Sharp, G. L. Wood, W. W. Clark III, G. J. Salamo and R. R. Neurgaonkar, Paper ThC2, 1992 Annual OSA Meeting, Sept. 24, 1992.
72. G. J. Salamo, M. J. Miller, W. W. Clark III, G. L. Wood, E. J. Sharp and R. R. Neurgaonkar, *Appl. Opt.*, **27,** 4356 (1988).
73. P. Yeh, T. Y. Chang and M. D. Ewbank, *J. Opt. Soc. Am*, **B5,** 1743 (1988).
74. M. Cronin-Golamb, S. Kwong and A. Yariv, *Appl. Phys. Lett.*, **44,** 727 (1984).

Rockwell

Appendix 6.3

GHZ- BANDWIDTH OPTICAL INTENSITY MODULATION IN SELF- POLED WAVEGUIDES IN SBN.

GHz-Bandwidth Optical Intensity Modulation in Self-Poled Waveguides in Strontium Barium Niobate (SBN)

J. M. Marx, *Member, IEEE*, O. Eknoyan, *Member, IEEE*, H. F. Taylor, *Fellow, IEEE*, and R. R. Neurgaonkar

Abstract— Wide-band electrooptic intensity modulation at a wavelength of 1.3 μm has been demonstrated in single mode channel waveguides in SBN:60 without repoling the substrates after processing at elevated temperatures. Waveguide losses were $\leq$0.7 dB/cm for both polarizations.

Fig. 1. Schematic diagram of the modulator configuration.

THE FABRICATION of low-loss optical waveguides in ferroelectric substrates in the tungsten bronze family was recently reported [1], [2]. Tungsten bronze substrates such as $Sr_{0.6}Ba_{0.4}Nb_2O_6$ (SBN:60) and $Ba_{1-x}Sr_xTi_yNb_{2-y}O_6$ (BSTN) are of interest for guided wave optical devices because of their large r_{33} electro-optic coefficients, which makes it possible to produce compact, low-voltage electro-optic modulators [3] and switches. In SBN:60, for example r_{33} = 4.2 × 10^{-10} m/V [4], a factor of 13.5 greater than in LiNbO$_3$. This letter reports a 1 GHz bandwidth electrooptic intensity modulator produced in SBN:60 using a strain waveguide without repoling the substrate after processing at temperatures far above T_c. The results reported here represent the widest modulation bandwidth and the lowest waveguide losses in a tungsten bronze substrate as well as the first observation of self-poling in SBN.

A schematic diagram of the modulator structure is shown in Fig. 1. First, the substrate edges were polished and the crystal was annealed at 900 °C in O$_2$ ambient. The channel waveguide was next produced using the static-strain optic (SSO) effect [1]. The procedure involved the deposition of a 4.4-μm-thick SiO$_2$ film on a 1-mm-thick Z-cut substrate at T = 320 °C, annealing at 350 °C in oxygen ambient, then delineating 7.0-μm-wide straight channels in the film at room temperature. The strain resulting from thermal expansion mismatch between the substrate and film combined with related induced electric fields contribute to localized refractive index changes in the crystal via the strain-optic and electro-optic effects. This leads to the formation of the optical waveguide in the substrate along the patterned oxide region. After delineation of the channel in the film a buffer layer of SiO$_2$ was deposited over the surface, and asymmetric coplanar electrodes 4.8 mm in length
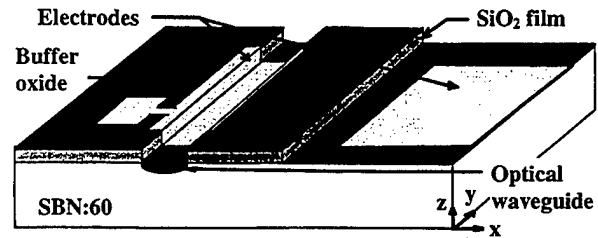
with a separation gap of 95 μm were defined by liftoff using a combination of Cr–Al–Au metal layers ~8000 Å in total thickness. The narrow electrode over the oxide channel is 20 μm wide with an oxide overlay of 2 μm toward the other electrode and had a measured resistance of 25 Ω/mm. The ground electrode is 1.2 mm in width and had a resistance of 1.5 Ω/mm. The strain film appearing between electrodes on the surface is 60 μm wide. The measured capacitance across the electrodes was 5 pF at 1 MHz.

Optical characterization at 1.3-μm wavelength revealed single mode propagation for both TE and TM polarizations. Measurements on the 8.38-mm long sample showed propagation losses of 0.5 dB/cm for the extraordinary (TM) polarization, and 0.7 dB/cm for the ordinary (TE) polarization.

Electrooptic modulation was demonstrated on the strain induced channel waveguide without repoling the crystal even though the substrate was processed at temperatures as high as 900 °C, far above the Curie temperature of 73 °C. Testing was carried out by coupling light from a 1.3-μm wavelength DFB diode laser with linear polarization oriented at an angle of 45° relative to the Z-axis of the crystal and detecting the output through a crossed linear analyzer. A half-wave voltage V_π = 20.6 V was measured at a frequency of 200 kHz. The large value of V_π is due to the wide gap between electrodes (95 μm) and some potential drop across the oxide layer. For frequencies above 10 MHz, a small signal microwave synthesizer was utilized to drive the modulator and a 50-Ω chip resistor was shunted at the input side. The modulator frequency response was displayed on a spectrum analyzer using a pigtailed germanium APD. The measurement results are shown as data points in Fig. 2 and indicate a 3-dB rolloff at ~1.04 GHz. The results are compared with calculations (solid line in Fig. 2) obtained by modeling the electrodes as an open ended transmission line, that is connected to a 50-Ω source (synthesizer) through a 50-Ω shunt resistor (chip) at the input
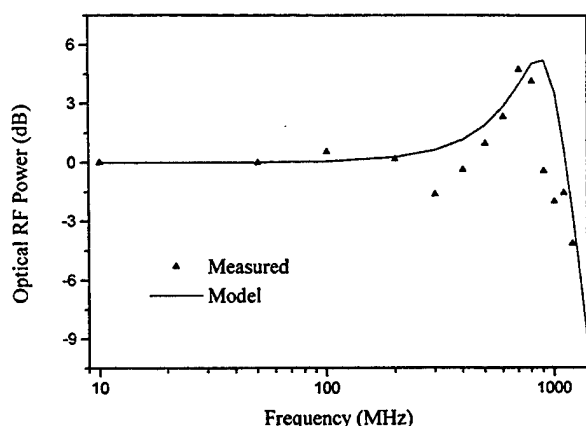
Fig. 2. Frequency response of the modulator (dots are measured data, solid line is model predictions).

of the electrodes [5]. The 2-dB dip near 300 MHz is likely caused by absorption in the material at this frequency.

The "self-poling" phenomenon is believed to be related to large localized strain gradients that are present near the etched channels. It appears to be confined to regions near the surface of the substrate only, since efforts to obtain electrooptic modulation in the bulk (interior) of unpoled samples containing strain waveguides produced a negative result. Self-poling seems to be complete, since the repoling of substrates containing modulators with a dc applied electric field did not yield an improvement in the value of V_π. All repoling tests were carried out under applied dc electric fields of 8 kV/cm and greater. The much smaller ac electric fields applied during modulation tests ($\sim$1 kV/cm peak) are not expected to impact repoling significantly, even though some resistive heating is present. Self-poling was also observed recently in ferroelectric BSTN, another crystal in the tungsten bronze family [2].

In conclusion, an optical intensity modulator at 1.3-μm wavelength with a small-signal electrical bandwidth near 1 GHz was observed in SBN:60 for the first time without repoling the crystal after processing far above its Curie temperature. The optical waveguide formed by the static strain-optic effect from a surface film exhibited the lowest propagation losses ever reported in this material. The "self-poling" is believed to result from strong localized strains near the surface. The half-wave voltage can be reduced substantially by using a narrower electrode gap. Higher frequency response can be achieved by reducing the resistance through the use of thicker electrodes and implementing a velocity-matched traveling wave structure utilizing the thick electrodes [6]. To overcome the low characteristic impedance ($<$10 Ω) imposed by the high dielectric constant of SBN:60 (ε_{33} = 880) [3], [4], an impedance matching electronic chip could be used for interfacing the modulator with 50-Ω microwave inputs.

REFERENCES

[1] J. M. Marx, Z. Tang, O. Eknoyan, H. F. Taylor, and R. R. Neurgaonkar, "Low-loss strain induced optical waveguides in strontium barium niobate (Sr$_{0.6}$Ba$_{0.4}$Nb$_2$O$_6$) at 1.3 μm wavelength," Appl. Phys. Lett., vol. 66, pp. 274–276, 1995.
[2] J. M. Marx, O. Eknoyan, H. F. Taylor, Z. Tang, and R. R. Neurgaonkar, "Electrooptic modulation and self-poling in strain-induced waveguides in barium strontium titanate niobate waveguides (BSTN)," Appl. Phys. Lett., vol. 67, pp. 1381–1383, 1995.
[3] O. Eknoyan, V. P. Swenson, and J. D. Quinn, "Low-voltage interferometric modulator in zinc-diffused strontium barium niobate (SBN:60)," Appl. Phys. Lett., vol. 59, pp. 28–30, 1991.
[4] R. R. Neurgaonkar, W. F. Hall, J. R. Oliver, and W. K. Cory, "Ferroelectric tungsten bronze oxides: A case study of optoelectronic materials," in Chemistry of Advanced Materials, C.N.R. Rao, Ed. Boston, MA: Blackwell Scientific, 1992, pp. 81–105.
[5] F. Auracher and R. Keil, "Design considerations and performance of Mach-Zehnder waveguide modulator," Wave Electron. vol. 4, pp. 129–140, 1980.
[6] K. Noguchi, O. Mitomi, H. Miyazawa, and S. Seki, "A broadband Ti:LiNbO$_3$ optical modulator with a ridge structure," J. Lightwave Technol., vol. 13, pp. 1164–1168, 1995.

APPENDIX 6.4

ELECTRO-OPTIC MODULATION AND SELF-POLING IN STRAIN-INDUNCED WAVEGUIDES IN BSTN

(Appl. Phys. Lett., 67(10) 1381-1381, 1995)

Electro-optic modulation and self-poling in strain-induced waveguides in barium strontium titanate niobate

J. M. Marx, O. Eknoyan, H. F. Taylor, and Z. Tang
Department of Electrical Engineering, Texas A&M University, College Station, Texas 77843

R. R. Neurgaonkar
Rockwell International Science Center, Thousand Oaks, California 91360

Characterization of bulk single crystals and optical waveguides in $Ba_{1-x}Sr_xTi_yNb_{2-y}O_6$ (BSTN) indicate it to be a promising new ferroelectric material for electrooptic devices. The electro-optic coefficient r_{33} is measured to be 218 ± 12 pm/V, a factor of 7 greater than $LiNbO_3$. Data on refractive indices, dielectric constant, and Curie temperature T_c in bulk samples are also presented. Strain-induced waveguides in Z-cut samples exhibited low losses (1.8 dB/cm for TM polarization and 2.5 dB/cm for TE polarization) at a wavelength of 1.3 μm. Electro-optic modulation was demonstrated in these waveguides to frequencies >100 MHz. A "self-poling" effect was found, whereby strong electro-optic modulation is observed in the strain waveguides without repoling the crystal after processing at temperatures far above T_c. © *1995 American Institute of Physics.*

Ferroelectric crystals have for decades been sought for electro-optic applications because they have the largest r_{ij} coefficients of available materials. Among the most useful have been $LiNbO_3$ and $LiTaO_3$ of the ilmenite family of ferroelectrics. However, it has long been known that some ferroelectrics in the tungsten bronze family, such as $Sr_{1-x}Ba_xNb_2O_6$ (SBN), have much larger r_{ij} coefficients than do $LiNbO_3$ and $LiTaO_3$. The technology for growing large optical quality crystals of several of the tungsten bronzes has been developed,[1] and recently low-loss optical waveguides and electro-optic modulators were reported in $Sr_{0.6}Ba_{0.4}Nb_2O_6$ (SBN:60).[2]

The first studies of the optical and dielectric properties of a new tungsten bronze material $Ba_{1-x}Sr_xTi_yNb_{2-y}O_6$ (BSTN) are reported in this letter. Electro-optic coefficients, refractive indices, dielectric constant, and Curie temperature are measured. Waveguides are produced using the static strain-optic (SSO) effect, and modulation experiments are carried out. Results on self-poled strain waveguides are presented. Potential advantages of BSTN for guided-wave devices are discussed.

Boules of BSTN used in these studies were pulled from the melt by the Czochralski technique, using a procedure similar to that developed for SBN. In fact, the BSTN composition is obtained by substituting a fraction $y/2$ of Ti atoms for Nb atoms in the original SBN. Both X-cut and Z-cut substrates ~ 1 cm$\times$1 cm$\times$1 mm in dimensions with surface polish were utilized.

The material properties were characterized from measurements performed on single crystal bulk samples. The dielectric behavior was examined over a frequency ranging from 100 Hz to 50 MHz using a 1.14 mm thick Z-cut substrate with metallized surfaces normal to the z axis. Values for the dielectric constant ϵ_{33} were determined by modeling the sample as an ideal dielectric capacitor and monitoring its response as a function of frequency. The measured values for ϵ_{33} were 690 for $f < 10^5$ Hz and 440 for $f > 10^7$ Hz. The observed dispersion is a characteristic of dielectric relaxation

associated with polarizability transitions in ferroelectrics.[3] The Curie temperature T_c of BSTN was determined by measuring the capacitance of a sample that is heated while submerged in oil. The results for two Z-cut samples of different surface areas indicated a value of 116 °C for T_c. The refractive indices of BSTN were evaluated from Brewster angle measurements using a spectrometer. Horizontally polarized (TE) light at 0.633 μm wavelength was used as the incident beam on an X-cut sample. The angle for null reflection was determined by monitoring the intensity of the reflected beam with a photodetector. The ordinary refractive index n_0 was obtained by orienting the sample such that the b (or Y) axis of the crystal was parallel to the polarization of the incident light. The extraordinary index n_e was measured by reorienting the crystal such that its optical c axis was parallel to the incident polarization. The obtained values are $n_0 \equiv n_1 = 2.3012 \pm 0.006$ and $n_e \equiv n_3 = 2.2778 \pm 0.004$. The linear electro-optic (Pockels) coefficients r_{33} and r_{13} were evaluated from measurements carried out on a poled bulk crystal using a Mach–Zehnder interferometer arrangement at 0.633 μm wavelength. A Z-cut BSTN substrate with optical propagation along the y direction was placed in one arm of the interferometer. The sample dimensions were 5 mm$\times$9 mm$\times$1.14 mm along the x, y, and z directions, respectively. In order to use a z-directed electric field, voltage was applied across metallized opposite end faces normal to the Z axis. The electro-optic coefficients were determined from measured half-wave voltage v_π values observed under an applied saw-tooth voltage at 0.1 Hz. The coefficients r_{i3}, with $i = 1$ or 3 corresponding to light polarized parallel to X or Z, respectively, were evaluated using the relation

$$|r_{i3}| = \frac{\lambda d}{2 n_i^3 L v_\pi},\tag{1}$$

where λ is the operating wavelength, d is the separation between electrodes, n_i is the relevant refractive index, and L is the interaction region length. Values of $|r_{33}| = 218 \pm 12$ pm/V and $|r_{13}| = 51.2 \pm 6$ pm/V were obtained. To determine the

TABLE I. Selected electro-optic properties of some ferroelectric crystals at 0.633 μm wavelength.

Crystal	T_c (°C)	r_{33} ($\times 10^{-12}$ m/V)	ϵ_{33}	n (@λ=0.633 μm)	$\epsilon_{33}/n_3^6 r_{33}^2$ ($\times 10^{20}$ V^2/m^2)
LiNbO$_3$	1195	31	28	n_1=2.2866 n_3=2.2028	2.55
LiTaO$_3$	620	30	43	n_1=2.1786 n_3=2.1833	4.41
SBN:60	78	420	900	n_1=2.3103 n_3=2.2817	0.37
BSTN	116	218	440	n_1=2.3028 n_3=2.2793	0.66

relative sign of the two coefficients, the effective electro-optic coefficient $r_c \equiv |r_{33} - (n_1/n_3)^3 r_{13}|$ was measured by coupling light polarized at 45° to the Z axis into the bulk crystal, and detecting the output through a crossed linear analyzer. Using Eq. (1) with $n_i = n_1$, a value of $r_c = 167 \pm 12$ pm/V was obtained from the measured v_π voltage. The measured r_c is in close agreement with a 165 pm/V figure calculated by using the measured r_{13}, r_{33}, n_1, and n_3 values, assuring that the electro-optic coefficients have like signs.

Table I compares relevant material properties of some electro-optic substrates. The figure of merit ($\epsilon_{33}/n_3^6 r_{33}^2$) is a measure of the switching energy required for π-radian phase shift in a modulator or switch. In comparison to SBN:60, the new BSTN material is also uniaxial ($n_1 = n_2$) and has a 4 mm symmetry; however, its relative dielectric constant ϵ_{33} is smaller by approximately a factor of 2 and its Curie temperature, T_c, is 38 °C greater. These features make BSTN an alternative to SBN:60 for guided-wave electro-optic device applications in so far as device stability at elevated temperatures and capacitance limitations are involved. In addition, the r_{33} coefficient of BSTN is a factor of ~7 greater than in LiNbO$_3$ or LiTaO$_3$, which makes it a desirable substrate material for low-voltage, compact electro-optic modulators and switches.

Optical channel waveguides have been produced in BSTN using the static strain-optic (SSO) effect.[4] The procedure involved the deposition of a 4.3 μm thick SiO$_2$ film on a 1 mm thick Z-cut substrate at T=320 °C, then delineating 7.5 μm wide straight channels in the film at room temperature. The strain resulting from thermal expansion mismatch between the substrate and film combined with related induced electric fields contribute to localized refractive index changes in the crystal via the strain-optic and electro-optic effects. This leads to the formation of the optical waveguide in the substrate along the patterned oxide region.

Guided mode propagation was observed for both TE and TM polarizations at 1.3 μm wavelength. Characterization of the channel waveguides at this wavelength revealed a single transverse mode in both TE and TM polarizations, and one depth mode for TE but two depth modes for TM. Near field mode profiles for a waveguide output are shown in Fig. 1. Measurements on the 8.9 mm long sample showed propagation losses of 1.8 and 2.5 dB/cm for the extraordinary (TM) and ordinary (TE) polarizations, respectively. These were obtained from total insertion loss measurements after applying

corrections for spatial mode mismatch and Fresnel reflection losses.

Electro-optic modulation was demonstrated on strain induced channel waveguides without repoling the crystal even though the substrate was processed at temperatures far above the Curie temperature. The modulator configuration that was used is shown in Fig. 2. The coplanar electrodes were formed by centering 11 μm wide 6.5 mm long Cr/Au patterns on the 7.5 μm wide oxide channels after the deposition of a buffer layer of SiO$_2$. The gap separation between channels is 400 μm. Electro-optic modulation was realized by coupling light from a 1.3 μm wavelength DFB diode laser at 45° to the Z

(a)

(b)
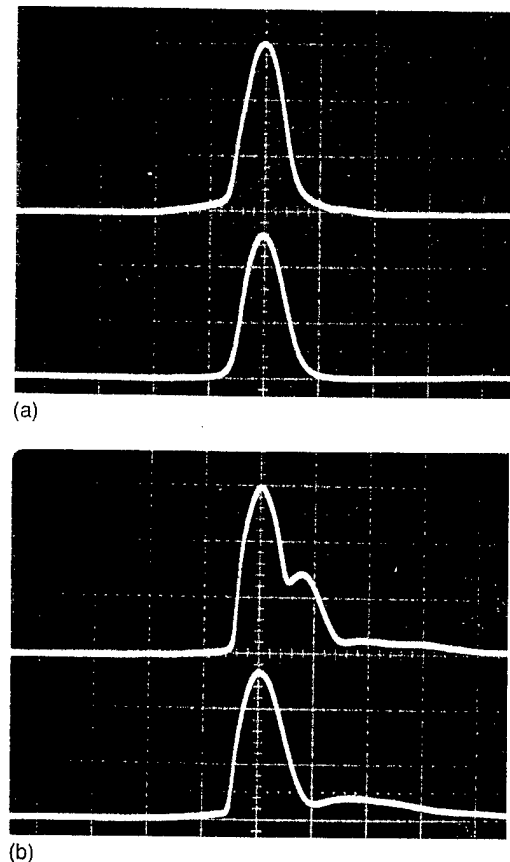
FIG. 1. Near field mode profiles for a 7.5 μm wide waveguide at 1.3 μm wavelength. (a) Horizontal scan with horizontal scale=13 μm/div and (b) vertical scan with horizontal scale=10 μm/div. In both frames, upper traces are for TM and lower trace for TE with vertical scale=50 mV/div for all cases.
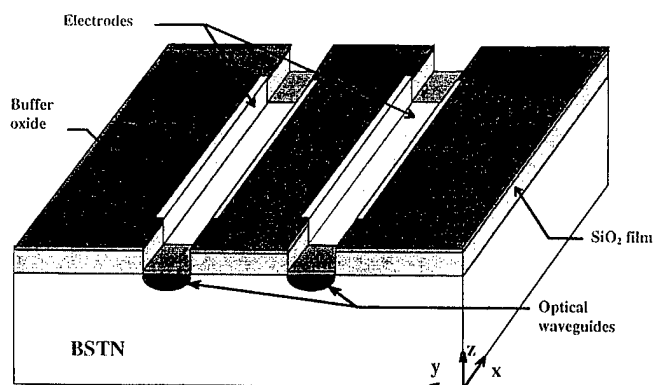
FIG. 2. Configuration of strain channel waveguide modulator in BSTN.

axis of the crystal and detecting the output through a crossed linear analyzer. Figure 3 shows an oscilloscope display of a modulator output at 100 kHz frequency, from which a half-wave voltage $v_\pi = 27$ V and a modulation depth of 75% are determined. Using the measured values of r_c and n_1, an electrical-optical overlap factor of 0.73 is calculated. Complete modulation was not realized due to the presence of the
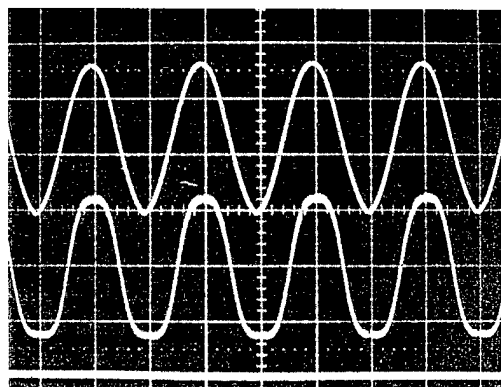

FIG. 3. Modulation response of 7.5 μm wide BSTN strain waveguide. Upper trace is the applied electrical signal at frequency=100 kHz and 10 V/div. Lower trace is the optical response with zero level shown at the bottom.

second order depth mode in the TM polarization. Modulation to frequencies beyond 100 MHz was observed in these initial devices.

To the best of our knowledge, the "self-poling" phenomenon has not been previously observed in optical waveguides on ferroelectric substrates when processed at temperatures above the T_c value of the crystal. It is believed to be related to large localized strains that are present near the etched channels. The self-poling appears to be confined to regions near the surface of the substrate only, since efforts to obtain electro-optic modulation in the bulk (interior) of unpoled samples containing strain waveguides produced a negative result. This further supports the presumption that the self-poling results from the presence of large strains that are spatially concentrated near the surface.

In conclusion, bulk dielectric and optical properties of the tungsten bronze BSTN material have been measured. The lower dielectric constant and higher Curie temperature of BSTN relative to SBN:60 combined with its large electro-optic coefficient makes this material an attractive alternative for low-voltage guided-wave electro-optic device applications. Guided mode propagation and electro-optic modulation at a wavelength of 1.3 μm have been realized in BSTN. The channel waveguides are produced by the static strain-optic effect from a surface film of SiO$_2$ deposited at 320 °C and patterned at room temperature. Electro-optic modulation to frequencies beyond 100 MHz was demonstrated without repoling the crystal after processing far above its Curie temperature. The "self-poling" is believed to result from strong localized strains near the surface. Higher modulation frequencies can be expected by optimization of the electrode geometry.

[1] R. R. Neurgaonkar, W. F. Hall, J. R. Oliver, and W. K. Cory, in *Chemistry of Advanced Materials*, edited by C. N. R. Rao (Blackwell, 1992), p. 81.
[2] J. M. Marx, Z. Tang, O. Eknoyan, H. F. Taylor, and R. R. Neurgaonkar, Appl. Phys. Lett. **66**, 274 (1995).
[3] M. E. Lines and A. M. Glass, *Principles and Applications of Ferroelectrics and Related Materials* (Clarendon, Oxford, 1977), p. 288.
[4] O. Eknoyan, H. F. Taylor, Z. Tang, V. P. Swenson, and J. M. Marx, Appl. Phys. Lett. **60**, 407 (1992).

APPENDIX 6.5

Low-Loss Strain Induced Optical Waveguides in SBN:60

at 1.3 μm wavelength.

(Appl. Phys. Lett., 66(3), 274-276 ,1995).

Low-loss strain induced optical waveguides in strontium barium niobate (Sr$_{0.6}$Ba$_{0.4}$Nb$_2$O$_6$) at 1.3 μm wavelength

J. M. Marx, Z. Tang, O. Eknoyan, and H. F. Taylor
Department of Electrical Engineering, Texas A&M University, College Station, Texas 77843

R. R. Neurgaonkar
Rockwell International Science Center, Thousand Oaks, California 91360

Low-loss optical waveguides have been produced in z-cut Sr$_{0.6}$Ba$_{0.4}$Nb$_2$O$_6$ (SBN:60) and electro-optic modulation has been demonstrated at a wavelength of 1.3 μm. The refractive index increase responsible for waveguiding results from a strain produced by a SiO$_2$ film which has been deposited on the surface of the substrate at 320 °C. The waveguides are formed in the crystal by dry etching of channels in the strain film. The resulting optical waveguides support both polarizations. Propagation loss values of 0.7 dB/cm for TM polarization and 1.6 dB/cm for TE polarization were measured. Electro-optic modulation up to 22 MHz was performed on repoled samples using coplanar electrodes. © *1995 American Institute of Physics.*

The tungsten bronze crystal Sr$_{0.6}$Ba$_{0.4}$Nb$_2$O$_6$ (SBN-60) is an attractive material for the fabrication of integrated optic devices due to its large r_{33} ($\sim$420$\times$10^{-12} m/V) electro-optic coefficient,[1] which is about 14 times larger than for the conventional substrate materials LiNbO$_3$ and LiTaO$_3$.[2] Compact, low-voltage modulators and tunable filters as well as highly sensitive electro-optic field sensors are thus feasible in such SBN substrates.

Advances in techniques for growing large diameter SBN:60 single crystals of excellent optical quality[3] have made it possible to produce substrates suitable for optical waveguide fabrication. Optical waveguiding in SBN has been produced by sulfur indiffusion at λ=0.633 μm optical wavelength[4] and by zinc indiffusion at λ=0.83 μm.[5] Results in both cases have demonstrated the effect of the large r_{33} electro-optic coefficient, but propagation losses were greater then 10 dB/cm for both TE and TM polarizations.

Recently, it has been shown that optical waveguides can be formed in ferroelectrics via the static strain-optic effect without altering the composition of the substrate.[6] At a wavelength of 0.633 μm, such waveguides have demonstrated propagation losses of less than 1dB/cm for TE and TM polarizations in LiNbO$_3$. This letter reports the first low-loss optical waveguides in SBN:60, and the demonstration of electro-optic modulation at 1.3 μm in such waveguides.

To produce channel waveguides, a strain film was formed by depositing a 4.4 μm thick SiO$_2$ film on a z-cut substrate at T=320 °C. Substrate dimensions were 1 cm$\times$0.5 cm$\times$1 mm along the x,y, and z directions, respectively. Samples were subsequently allowed to cool to room temperature, creating a strain along the SiO$_2$/SBN interface due to the difference in their thermal expansion coefficients. Selective etching of 9.4 μm wide channels in the oxide frees the film to expand near the edges of the etched pattern, concentrating the strain along the lower edges and causing a localized refractive index change in the crystal via the strain-optic effect. For the crystal orientation of Fig. 1, the resulting strain-optic index changes from a strain component S_1 in the x direction are given by

$$\Delta n_i = -(n_i^3/2)p_{i1}S_1, \tag{1}$$

with i=1,3 corresponding to TE and TM polarization, respectively, $p_{11}=p_{31}=0.10$,[7] are the magnitudes of the relevant strain-optic index coefficients, and n_1=2.239, n_3=2.216[8] are the refractive index values at 1.3 μm wavelength. The given p_{i1} coefficient values are estimated from a linear interpolation of SBN:50 and SBN:75 figures at 0.633 μm wavelength.[7] In addition to the strain-optic effect, the net refractive index change will also include an electro-optic contribution due to the electric field in the strained region produced by the piezoelectric effect and field produced by any surface charge distributions.[6]

Since the oxide deposition temperature (320 °C) was much higher than the 78 °C Curie temperature of SBN:60,[1] samples required repoling to restore single domain behavior and recover their electro-optic properties. Poling was carried out after the waveguides were formed but before delineation of the final electrode pattern of Fig. 1. The poling was conducted at room temperature by applying a dc electric field along the optical axis of the crystal (z direction). Samples containing the strain induced waveguides were prepared for poling by sputtering Pt onto the back side, then evaporating consecutively a buffer layer of SiO$_2$, a patterned Mo film,
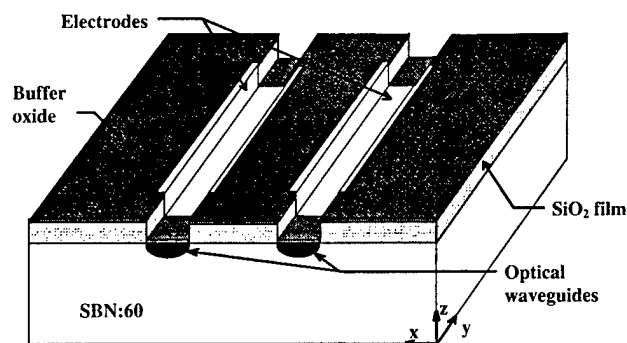

FIG. 1. Schematic of device configuration showing crystal orientation, strain inducing patterned SiO$_2$ film, and electrode geometry.
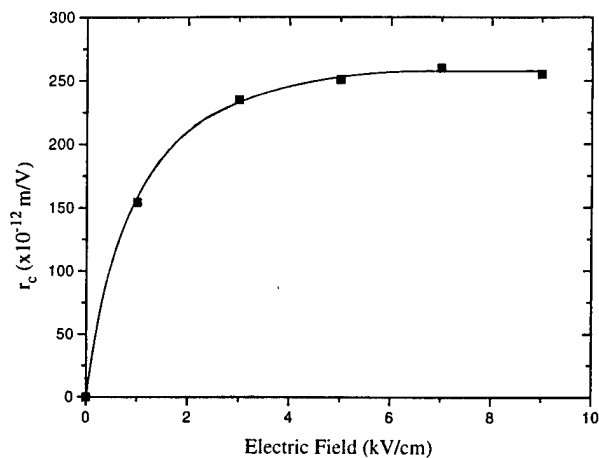
FIG. 2. Measured effective electro-optic coefficient values as a function of applied electric field used in poling of SBN:60 substrates at room temperature. The light propagates normal to the optic axis and modulation voltage is applied in the z direction across the sample 1-mm thickness.

and a combination of Cr/Au onto the upper side over the patterned thick strain oxide film. By measuring the half-wave voltage, V_π at 0.633 μm wavelength for polarization intensity modulation on bulk SBN:60 crystals that were repoled at various values of electric field, it was found that a minimum of 7 kV/cm electric field is required for repoling. Figure 2 shows the behavior of obtained effective electro-optic coefficient, $r_c \equiv r_{33} - (n_1/n_3)^3 r_{13}$, as a function of applied poling electric field strength E_z. The measured saturation value of 260×10^{-12} m/V agrees with reported bulk modulation results in SBN:60.[9]

The final step in producing the device of Fig. 1 was to delineate the upper Cr/Au electrode by liftoff of the molybdenum. The coplanar electrodes are 11 μm wide, 5.5 mm in length and centered on the 9.4 μm wide oxide channels. The gap separation between waveguides is 400 μm.

Optical characterization was carried out at 1.3 μm wavelength by coupling light from a laser diode into the waveguides with a polarization maintaining fiber. Guiding was observed for both TE and TM polarizations. The 9.4 μm wide waveguides exhibited a single transverse mode in both TE and TM polarizations, and one depth mode for TE but two depth modes for TM. Near-field patterns of the fundamental modes are shown in Fig. 3. Best values for the losses were obtained on 7 μm wide waveguides that supported a single mode in the transverse and depth directions for both TE and TM polarizations. Measurements on an 8-mm long sample showed a propagation loss of 0.7 dB/cm for the extraordinary (TM) polarization and 1.6 dB/cm for the ordinary (TE) polarization. These were obtained from total insertion loss measurements of 3.6 dB for TM and 10.6 dB for TE after applying correction factors for spatial mode mismatch losses of 2.1 and 8.4 dB for the former and latter polarization cases, respectively, and 0.9 dB for Fresnel losses in each case, leaving 0.6 dB for the TM and 1.3 dB for the TE propagation losses along the waveguide length. The mismatch loss values were estimated by comparing measured output intensity from a strain waveguide coupled to a photo-
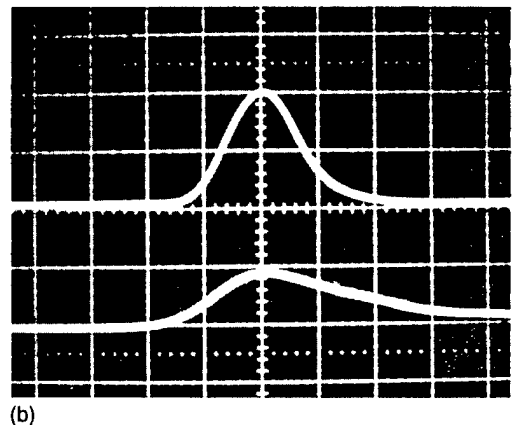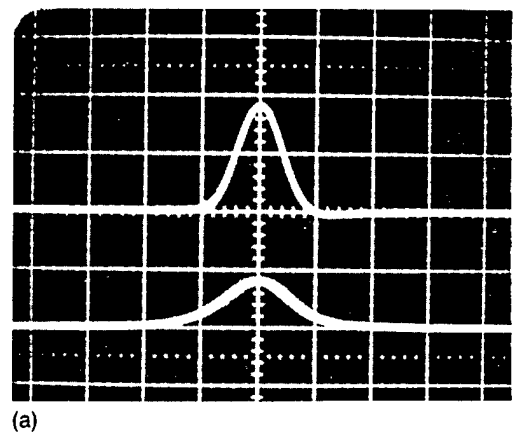

(a)

(b)

FIG. 3. Near-field mode profiles for 9.4 μm wide waveguide. (a) Horizontal scan with horiz. scale=13.9 μm/div. and (b) vertical scan with horiz. scale =7.7 μm/div. In both frames, upper traces are for TM with 200 mV/div. vertical scale, and lower traces are for TE with 50 mV/div. vertical scale.

detector through an objective lens with that obtained by coupling through a fiber identical to the one used for input coupling. The higher losses for the ordinary (TE) polarization are a result of the weaker optical confinement due to smaller index change as evidenced from the mode profiles. Propagation losses were also measured at 0.633 μm wavelength by sampling the intensity of scattered light from the surface of similar waveguides through a fiber that was translated along the propagation direction. Values of 0.6 and 4.1 dB/cm were obtained for the TM and TE polarizations, respectively. These propagation loss values are the lowest reported in SBN:60. This is possibly because the low-temperature process for making the waveguides produces very little damage, in contrast to higher-temperature processes used to make waveguides by diffusion.

Polarization intensity modulation was realized via the Pockels effect by coupling light polarized at 45° to the z axis, and detecting the output through a crossed linear analyzer. The voltage required for π-radian phase shift V_π and the resulting modulation depth were measured as a function of frequency from 200 Hz to 22 MHz. It was found that V_π increased significantly from 200 Hz to 200 kHz, above which it remained constant. The change in V_π was not observed in the bulk modulation tests performed at a wave-
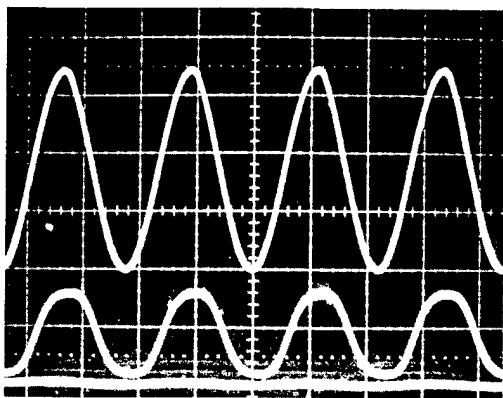
Appl. Phys. Lett., Vol. 66, No. 3, 16 January 1995

Marx et al.   275

FIG. 4. Modulation response of 9.4 μm wide SBN:60 strain waveguide. Upper trace is the applied electrical signal at frequency=200 kHz and 10 V/div. Lower trace is the optical response with zero level shown at the bottom.

length of 0.633 μm. Figure 4 shows an oscilloscope display of a modulator output at 200 kHz frequency, from which a half wave voltage V_π=34 V is determined. Using the previously reported value of r_c=330$\times$10^{-12} m/V for the effective electro-optic coefficient,[4] an electrical-optical overlap factor of 0.77 is calculated. The modulation depth in Fig. 4 is 85%. Complete modulation was not realized because the spatial field profiles for TE and TM modes differ significantly. This leads to a reduced value for the TE-TM overlap integral as compared with the case of polarization independent mode fields where 100% modulation is achievable.

In conclusion, low-loss optical waveguides and electro-optic modulation at 1.3 μm wavelength have been realized in SBN:60. The waveguides are formed by a refractive index increase due to the static strain-optic effect. The strain was produced by depositing a 4.4 μm thick layer of SiO$_2$ at an elevated temperature and patterning after cooling the substrates to room temperature. Electro-optic modulation up to 22 MHz was demonstrated after repoling the samples at room temperature. Lower half-wave voltage values can be anticipated by reducing the gap width between electrodes. The realization of large diameter optical quality SBN:60 single crystals and low-loss optical waveguides have made this material a candidate for guided-wave electro-optic device applications.

[1] R. R. Neurgaonkar, W. F. Hall, J. R. Oliver, W. W. Ho, and W. K. Cory, Ferroelectrics **87**, 167 (1988).

[2] I. P. Kaminow, in *Handbook of Lasers*, edited by R. J. Pressley (CRC, Cleveland, OH, 1971), p. 447.

[3] R. R. Neurgaonkar, Ferroelectrics **91**, 209 (1989).

[4] O. Eknoyan, C. H. Bulmer, H. F. Taylor, W. K. Burns, A. S. Greenblatt, L. A. Beach, and R. R. Neurgaonkar, Appl. Phys. Lett. **48**, 13 (1986).

[5] O. Eknoyan, V. P. Swenson, J. D. Quinn, and R. R. Neurgaonkar, Appl. Phys. Lett. **59**, 28 (1991).

[6] O. Eknoyan, H. F. Taylor, Z. Tang, V. P. Swenson, and J. M. Marx, Appl. Phys. Lett. **60**, 407 (1992)

[7] D. A. Pinnow, in *Handbook of Lasers*, edited by R. J. Pressley (CRC, Cleveland, OH, 1971), p. 478.

[8] E. L. Venturini, E. G. Spencer, P. V. Lenzo, and A. A. Ballman, J. Appl. Phys. **39**, 343 (1968).

[9] S. Nomura, H. Kojima, Y. Hattori, and H. Kotsuka, Jpn. J. Appl. Phys. **13**, 1185 (1974).

APPENDIX 6.6

Guided-Wave Electro-Optic Applications for Tungsten Bronze Ferroelectrics

(Submitted for Publications, 1996)

GUIDED-WAVE ELECTROOPTIC APPLICATIONS FOR TUNGSTEN BRONZE FERROELECTRICS

O. Eknoyan and H.F. Taylor
Department of Electrical Engineering
Texas A&M University
College Station, Texas 77843

R.R. Neurgaonkar
Rockwell International Science Center
Thousand Oaks, California 91320

ABSTRACT

Tungsten bronze ferroelectric materials have very large electrooptic coefficients which makes it possible to produce compact, low-voltage modulation and switching devices for applications in communications, signal processing and sensing. Waveguides produced using the static strain-optic effect have demonstrated much lower optical losses than those fabricated by diffusion techniques. Results on waveguides and modulators in strontium barium niobate (SBN) and barium strontium titanate niobate (BSTN) are described.

INTRODUCTION

Guided-wave electrooptic devices are widely used with optical fibers for applications in communications, signal processing and sensing [1,2]. The realization of low-loss single-mode optical waveguides is critical to the practical implementation of these devices, and it is desirable to use substrate materials with large electrooptic coefficients to achieve low voltage performance. Ferroelectric oxide crystals have generally been a popular material of choice for this technology. The most widely used among these have been $LiNbO_3$ and $LiTaO_3$ crystals in the ilmenite family, primarily because of their ready commercial availability, and established methods for fabricating optical waveguides in each [3-6]. Significant

interest, however, lies in producing optical waveguide devices in other ferroelectric materials with higher electrooptic coefficients which could be used for making compact low-voltage electrooptic modulators and switches, as well as tunable wide-band wavelength filters. The tungsten bronze family of ferroelectrics provides an attractive choice for such needs because their linear electrooptic coefficient r_{33} is generally much greater in magnitude than that in $LiNbO_3$ or $LiTaO_3$ [7]. Advances in growing large diameter tungsten bronze crystals of optical quality [8] combined with the recent development of low-loss optical waveguides in these materials [9], make the realization of a variety of practical devices in tungsten bronzes a feasible possibility. This overview gives a summary of the performance of guided-wave devices that have been demonstrated in these materials. Pertinent material properties are highlighted. The use of the static strain-optic (SSO) effect in producing low-loss channel waveguides in tungsten bronze $Sr_{1-x}Ba_xNb_2O_6$ (SBN) and $Ba_{1-x}Sr_xTi_yNb_{2-y}O_6$ (BSTN) crystals, as well as in the conventional $LiNbO_3$ and $LiTaO_3$ ilmenite materials is described. Results on electrooptic modulators in SBN and BSTN as well as a polarization converter and a tunable wavelength filter in $LiTaO_3$ are also presented.

MATERIAL CONSIDERATIONS

The interest in ferroelectric crystals for optical applications stems from the ability to change their refractive index by altering the spontaneous polarization in the material through various external means. In electro-optics, the external control signal is an electric field and its influence on a lightwave propagating in the crystal is exerted via the electro-optic effect. This makes it possible to control the behavior of a guided-wave light beam and has led to the realization of various practical commercial devices.

Because of the anisotropic nature of ferroelectrics, optical properties of a crystal are generally described in terms of its index ellipsoid (or indicatrix). In uniaxial crystals, $n_1 = n_2 \equiv n_0$ (ordinary index, for light polarized normal to the optic axis), and $n_3 \equiv n_e$ (extraordinary index, for light polarized along the optic axis). The electro-optic effect is closely connected with the optical anisotropy of the material and strongly depends upon its crystalline structure. The change in refractive indices that is caused by the application of an electric field is characterized by changes in the coefficients of the index ellipsoid. They include terms that vary with the applied field in a linear fashion (Pockels effect), or quadratically (Kerr effect). The Pockels effect exists only in noncentrosymmetric crystals, i.e., that do not posses inversion symmetry [10], and is the basis for nearly all guided-wave electro-optic devices. There is no restriction, however, on the non-linear Kerr

effect. The linear term in the index changes, due to an arbitrary applied electric field **E** of components E_1, E_2, E_3 (or E_x, E_y, E_z) along the principal axes of the crystal, is expressed as:

$$\Delta\left(\frac{1}{n_i^2}\right) = \sum_{j=1}^{3} r_{ij}\, E_j \qquad (i = 1,2,...6) \tag{1}$$

where r_{ij} represents the 6x3 elements of the third rank linear electro-optic coefficient tensor in reduced notation. The direction of the applied electric field determines whether an index increases or decreases. The electric field in the crystal is established by applying a voltage across electrodes placed on the surface. Upon substitution of the electro-optic tensor r_{ij} of a crystal in the above equation, the resultant six values in the refractive index changes, Δn_i, can be written as the elements of a symmetric 3x3 matrix which is referred to as the perturbed refractive index matrix. Utilization of the diagonal elements of the resultant matrix leads to a change in phase for an incident optical wave polarized along a major crystallographic axis as it traverses the crystal. This is useful for the design of modulators and switches. Changes in the off-diagonal elements, however, induce conversion (or mixing) between orthogonal polarization states of an optical wave propagating in the crystal. This is utilized in the design of polarization control devices and optical filters. In any of these applications, it is desirable to use materials of large r coefficient values, and to arrange the crystal orientation and device design to achieve the index change with the least possible applied electric voltage. Values of r_{ij} for many useful electrooptic crystals are available in the literature [11]. Because of piezoelectricity in such crystals, the values are customarily listed as "clamped" or "unclamped", relative to frequencies above or below the natural resonances of the crystal, respectively.

The inherent response time of the electrooptic effect is typically in the range of 10^{-13} s. In practice, however, the response of a device is limited by circuit delays that result from the capacitance across the electrodes through which the modulating voltage is applied. This limitation can be overcome to some extent by using a properly designed "traveling-wave" electrode geometry. But other factors such as uncompensated phase-velocity mismatch between electrical and optical signals, as well as dispersion and losses in the microwave transmission line eventually impose an upper limit on the frequency response in practical devices. For wide rf-band needs, preference is therefore given to choosing materials of relatively low dielectric constant.

Guided-wave devices based on the linear electro-optic effect have been developed in various ferroelectric crystals including $LiNbO_3$, $LiTaO_3$, $Sr_{0.6}Ba_{0.4}Nb_2O_6$ (SBN:60), $Ba_{1-x}Sr_xTi_yNb_{2-y}O_6$ (BSTN), and $KTiOPO_4$ (KTP). In all of these, the linear component of the electro-optic effect dominates and the largest coefficient is r_{33}. Table I lists relevant properties of these materials. Only KTP is a biaxial crystal, all the others are uniaxial. A figure of merit useful for comparison is $M = (\varepsilon/n^6r^2)$, which is a measure of the switching energy required for a π-radian phase shift in a modulator or switch. The tungsten bronzes SBN and BSTN are distinguishable by their relatively low values which are about a factor of 5 smaller in comparison to all the others. Other factors that must also be considered in the

Table I. Relevant Properties of Some Ferroelectrics (at 0.633 μm wavelength)

Crystal	T_c (°C)	r_{33} (pm/V)	ε_{33}	n	M (10^{20} V^2/m^2)
$LiNbO_3$	1195	31	28	$n_1 = 2.2866$ $n_2 = n_1$ $n_3 = 2.2028$	2.55
$LiTaO_3$	620	30	43	$n_1 = 2.1786$ $n_2 = n_1$ $n_3 = 2.1833$	4.41
KTP	965	35	15	$n_1 = 1.7634$ $n_2 = 1.7717$ $n_3 = 1.8639$	2.90
SBN:60	78	420	900	$n_1 = 2.3103$ $n_2 = n_1$ $n_3 = 2.2817$	0.40
BSTN	116	218	440	$n_1 = 2.3012$ $n_2 = n_1$ $n_3 = 2.2778$	0.66

course of selecting the substrate material for making a guided-wave device include low susceptibility to photorefractive effects - "optical damage", and low sensitivity to pyroelectric effects. Both of these effects produce undesirable index changes that could lead to instabilities in device operation. Optical damage is attributed to the presence of photoionizable impurity centers and crystal defects [12], and means to minimize its effects in $LiNbO_3$ have been suggested [13,14]. Fortunately, optical damage is much smaller in the infrared, where most interest for guided-wave devices lies, than at visible wavelengths [12].

Crystal Growth of Novel Electronic Materials

At the Rockwell International Science Center, efforts have been concentrated on the development of optimal (r_{ij}, ε) performance tungsten materials, and several bronzes have been identified including SBN, BSKNN, BSTN, SCNN, and KLN. These crystals are being grown in large sizes and high optical quality for electro-optic and photorefractive application needs. Figure 1 illustrates such atypical tungsten bronze crystal based on SBN composition. This technology is developed to produce > 6 cm diameter crystals. As such they hold a good promise for various commercial applications.
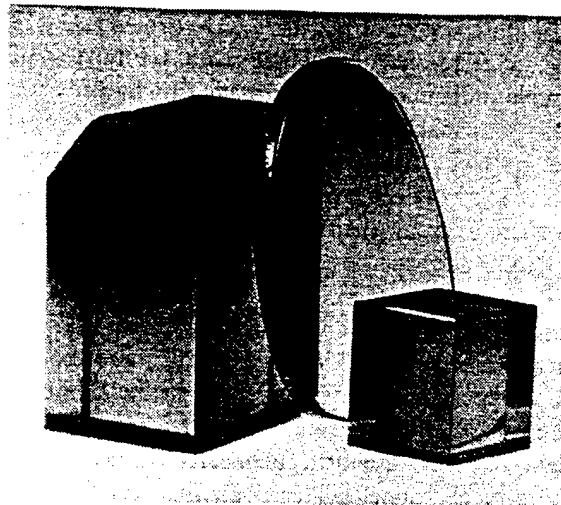

Fig. 1. SBN:60 single crystal grown by Czochralski technique.

OPTICAL WAVEGUIDES

Optical waveguides are formed by producing a localized high index region in a substrate of lower refractive index. In ferroelectric crystals, this has often been accomplished by changing the composition or stoichiometry by processes such as out-diffusion [15], ion exchange [4,5], or in-diffusion from a metal film [3] as well as vapor phase [6]. A simple method for making waveguides has been developed recently using strain induced from a surface film deposited at an elevated temperature [16]. In this technique, waveguides are produced without altering the composition of the substrate. The use of in-diffusion technique (film or vapor)

produces index increases, $\Delta n \sim 0.005 - 0.01$, for both the ordinary and extraordinary polarizations [17]. The most commonly used metal film for diffusion in LiNbO$_3$ and LiTaO$_3$ is Ti [18,19]. The diffusion is performed in an open tube furnace at temperatures ranging from 950 - 1200 °C. In the alternative vapor diffusion method, impurities are introduced into the substrate from gaseous phase in a sealed ampule, and the process is typically carried out near 800°C temperature. Elements that have been used for vapor diffusion in ferroelectrics are sulfur (S) in SBN [20], zinc (Zn) in LiTaO$_3$ [21] and also in SBN [22]. The ion exchange technique offers a low temperature approach which makes it attractive, however, the increase in refractive index is realized only for the extraordinary polarization. Molten benzoic acid has been a popular choice for the exchange of proton (H$^+$ ions) with Li$^+$ ions in LiNbO$_3$ [23] and LiTaO$_3$ [24]. The proton exchange process is carried out at temperatures in the range of 200 - 250 °C by immersing the sample in the melt. Neither metal film in-diffusion or ion exchange have been successful for making waveguides in tungsten bronze crystals, and the propagation losses of vapor diffused waveguides in SBN:60 are rather high (> 10 dB/cm). This drawback has been overcome, however, by the recent development of strain-induced method from a surface film to adjust the index in ferroelectric substrates through the static strain-optic (SSO) effect.

To produce strain-induced waveguides, a thick SiO$_2$ film (~ 3 μm) is deposited on a substrate at an elevated temperature (~ 300 °C), then cooled down to room temperature. This induces a compressive strain in the film because of the large thermal expansion mismatch between the substrate and film. By selective etch patterning, straight channels are next delineated in the SiO$_2$ by reactive ion etching. Formation of a channel makes it possible for the edges of the film to expand towards the center of the etched pattern, as shown by the inward pointing arrows in Fig. 2. The process of strain relief in the film results in a localized compressive strain in the substrate in the vicinity of the channel. This induces an index increase in the crystal via the strain-optic effect. Channel waveguides have been produced by this method in x-cut (a-plate) LiNbO$_3$, LiTaO$_3$, and BaTiO$_3$ substrates using the longitudinal S$_3$ strain component, and in z-cut (c-plate) SBN:60 and BSTN substrates using the longitudinal S$_1$ strain component. The refractive index changes from the strain-optic effect, Δn_i^{so}, with i = 1, 3 are given by [16]

$$\Delta n_i^{so} = -\left(n_i/2\right) p_{ij} \ S_j \qquad (2)$$

where j = 1 or 3 for z- or x-cut substrates, respectively, and p$_{ij}$ is the relevant strain-optic coefficient. In addition to the strain-optic effect, the net refractive

index change also includes an electrooptic contribution due to electric fields in the strained region produced by the piezoelectric effect and by surface charge redistribution. A finite element relaxation model was used to determine the strain profiles illustrated in Fig. 2. The constant strain contours are drawn normalized relative to the strain value at the surface of the substrate in the center of the channel. As indicated in the figure, the maximum strain occurs near the edges of the channel and is compressive in the channel but tensile beneath the film.
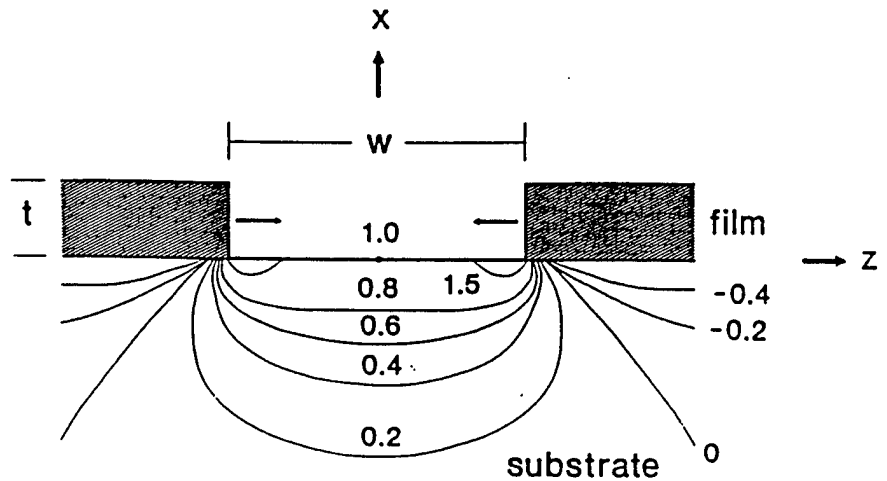

Fig. 2. Normalized constant contours for the longitudinal S_3 strain component.

Propagation losses < 1dB/cm have been measured in strain-induced waveguides on SBN:60 at 1.3 μm wavelength [9]. These are considerably lower than in SBN waveguides produced by vapor diffusion [20, 22], and approaching those attainable in LiNbO$_3$ technology. Losses for strain induced waveguides in the other materials are comparable. The low propagation loss values are evidently a result of the low temperature process used in making the waveguides, and the absence of diffused impurities which may introduce scattering centers.

GUIDED-WAVE DEVICES

A large number of guided-wave devices have been produced in birefringent ferroelectric crystals using various external control means. Only electro-optic devices that utilize the SSO effect will be described.

Polarization intensity modulation has been realized via the linear Pockels effect on strain induced waveguides in SBN:60, BSTN, and LiNbO$_3$ substrates [16,9]. To impress an electric field, planar electrodes are delineated on the surface using photolithography. Figure 3 is a schematic of a final device configuration produced on a z-cut SBN:60. The strain inducing film was formed by depositing 4.4 μm
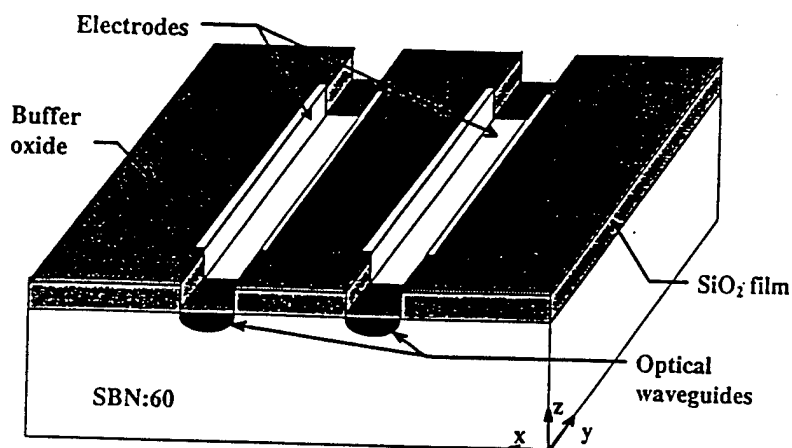

Fig. 3. Strain induced channel waveguide electrooptic modulator in SBN:60.

thick SiO$_2$ film at 320 °C. The crystal was repoled before delineation of the final electrode pattern. Propagation losses of 0.7 dB/cm and 1.6 dB/cm were measured, for the extraordinary and ordinary polarizations, respectively, at 1.3 μm wavelength. Electro-optic modulation was realized through the use of the effective electrooptic coefficient $r_c \equiv r_{33} - (n_1/n_3)^3 r_{13}$. A half-wave voltage $V_\pi = 34$ V was obtained for electrodes separation of 400 μm, interaction length of 5.5 mm, and a waveguide of 9.4 μm width. Using $r_c = 330 \times 10^{-12}$ m/V [9], a value of 0.77 is calculated for the electrical-optical overlap factor. Electro-optic modulation at frequencies greater than 100 MHz has been observed in SBN:60 as well as BSTN. On a similar SBN modulator structure but with a reduced gap separation of 70 μm, a value of $V_\pi = 9.5$ V was obtained. Lower values can be expected with further reductions in the gap. A record low voltage-length product of 0.48 V-cm was achieved by this group, with a push-pull interferometric modulator of 7.5 μm electrodes gap on vapor diffused waveguides in SBN:60

through the use of the large r_{33} (420×10^{-12} m/V) linear electrooptic coefficient [22].

Electro-optically Tunable Polarization Converter

The SSO effect has also been used to induce polarization conversion in birefringent ferroelectric crystals [25,26]. For a wave propagating in a diffused channel waveguide, phase matched coupling between TE (horizontally polarized) and TM (vertically polarized) modes may be induced by static shear strain from a spatially periodic surface film. The phase match condition imposed by the crystal birefringence is highly wavelength selective. Wavelength tuning for maximum conversion can be realized by adjusting the birefringence in the waveguide electro-optically via the linear Pockels effect.

A schematic for an electro-optically tunable polarization converter is shown in Fig 4. The strain inducing SiO_2 surface pads are patterned with a spatial period Λ along the waveguide, where Λ is the polarization beat length for the waveguide.
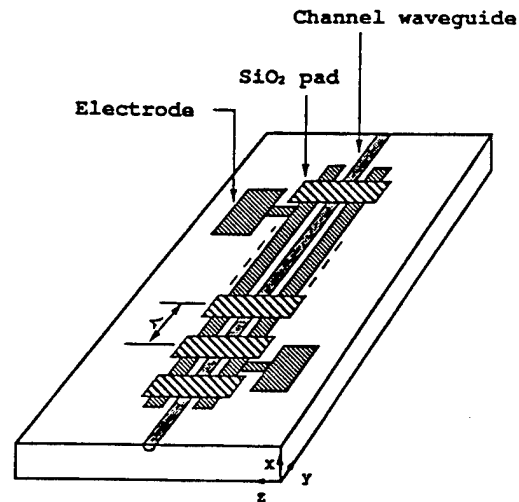

Fig. 4. Electrooptically tunable strain induced polarization converter.

Polarization conversion in the waveguide is caused by the off-diagonal element n_5 of the refractive index, which is produced by the shear-strain component S_6, and is given by

$$n_5 = -\left(n^3/2\right) p_{41} S_6 \tag{3}$$

with $n = (n_1 n_2)^{1/2}$ and p_{41} is the relevant strain-optic coefficient. This contrasts with the previously described strain-induced channel waveguide modulator where changes in the diagonal elements of the refractive index tensor were produced by the principal strain component S_1 in the substrate.

Spectral data for an electro-optically tunable polarization converter in LiTaO$_3$ are shown in Fig. 5. The channel waveguide was formed by Zn vapor diffusion, and the strain produced from a 1.75 μm thick SiO$_2$ film deposited at 300 °C and patterned at room temperature with $\Lambda = 100$ μm. Tuning of the peak wavelength from 616 nm to 654 nm was realized with an applied voltage of 60 V. The tuning
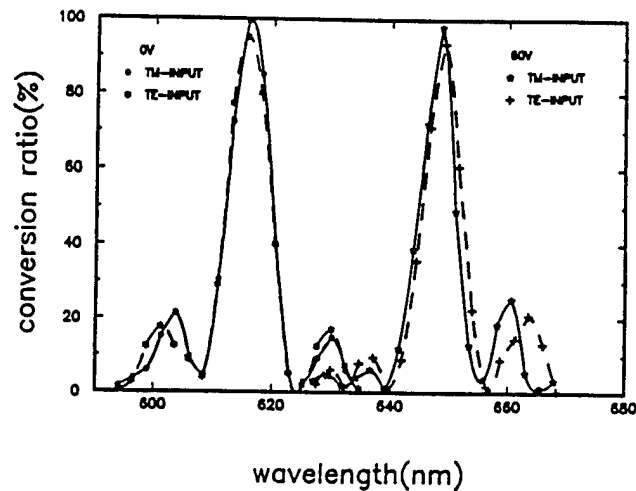

Fig. 5. Spectral response of polarization converter at V = 0 and 60 volts.

is controlled by adjusting the waveguide birefringence through r_c electro-optic coefficient [26]. The 17 nm full width of the pass band between the first minima is obtained through a 5.5 mm long tuning region.

Electro-optically Tunable Channel-Dropping Filter

The use of polarization coupling by the SSO effect can be extended to produce a channel-dropping electro-optic tunable filter (EOTF) using a four-port interferometer configuration. The use of SSO effect for polarization coupling

Crystal Growth of Novel Electronic Materials

makes it possible to combine the electro-optic birefringence section region with the polarization coupling region. This leads to a more efficient utilization of the crystal length for tuning compared to devices where polarization coupling is achieved electro-optically [27].

A schematic diagram of a four-port polarization independent EOTF [28] is shown in Fig. 6. It consists of two polarization splitters (PS) near the input and output ends that are joined by a pair of tunable SSO converters in the center. If the
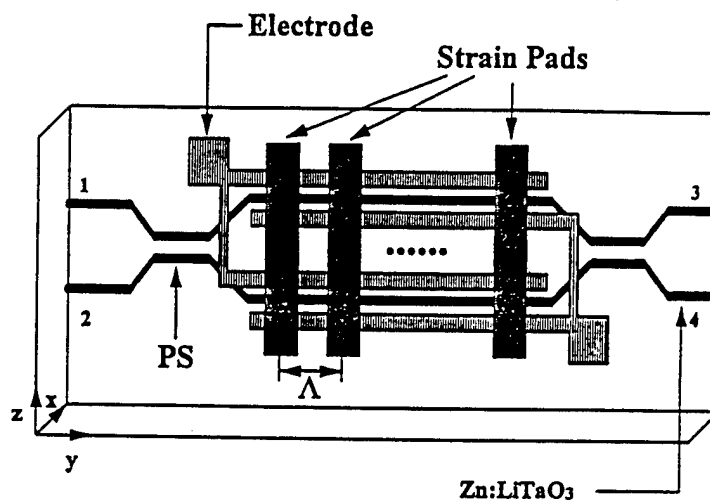

Fig. 6. Polarization independent electrooptically tunable channel-dropping filter.

wavelength of a light beam entering at one of the input ports (e.g., #1) satisfies the phase matching condition of the converter section, the TE and TM components which get separated by the PS undergo polarization rotation then recombine and emerge from port #4 at the output. The induced off-diagonal index n_5 responsible for coupling is given by (3), as before. Wavelength tuning can be accomplished by adjusting the birefringence electro-optically in the converter section through r_c coefficient.

Optical test results for an EOTF produced in $LiTaO_3$ are shown in Fig. 7. The waveguides are fabricated by Zn vapor diffusion. The strain-inducing pads were produced from a 1.9 μm thick SiO_2 film deposited at 300 °C and patterned at room temperature with a spatial periodic separation of 100 μm. The spectral response is shown for the untuned (0 V) and tuned (60 V) filter conditions. A
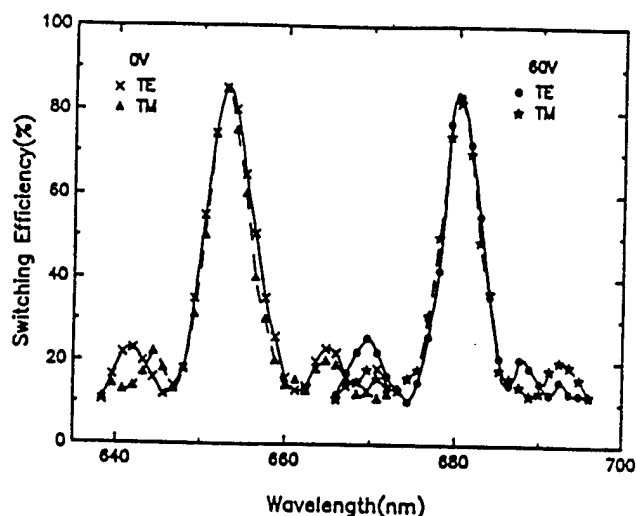
Fig. 7. Spectral response of EOTF at V = 0 and 60 volt.

total shift of 37 nm for the peak wavelength with an applied voltage of 90 V was achieved. The incomplete extinction is due to the splitters providing only 95% separation between TE and TM polarizations, and the TE-TM polarization conversion being limited to 96%. Narrower wavelength passbands could be realized in $LiTaO_3$ through an increase in the converter section, or by the use of substrates with larger birefringence (e.g., BSTN with $\Delta n = 0.0235$ in contrast to $LiTaO_3$ of $\Delta n = 0.0035$). The use of tungsten bronze crystals with large r_{33} coefficient, such as SBN or BSTN, could also provide a means for increasing the tunable bandwidth.

CONCLUSION

The usefulness of ferroelectric oxide crystals in electro-optics technology is apparent in the large variety of devices that have been produced in these materials. Although $LiNbO_3$ based devices are now commercially available, a large interest lies in producing guided-wave devices in materials with higher linear electro-optic coefficients. The tungsten bronze family of ferroelectrics offers several attractive choices for such needs with exceptionally large r_{33} coefficient values. Advances in growing large-diameter optical-quality tungsten bronze crystals of various composition, coupled with the recent development of low-loss optical waveguides in several of these crystals, makes their use for commercial applications a feasible

228

possibility. The waveguides are produced using the static strain-optic effect. The static strain results from the large thermal expansion mismatch between a substrate and a thick film of SiO_2 that is deposited at elevated temperature and patterned at room temperature. Longitudinal strain has been used to produce low-loss optical waveguides in SBN:60, BSTN, $LiNbO_3$, $LiTaO_3$ and $BaTiO_3$. Propagation losses < 1 dB/cm in SBN, < 2 dB/cm in BSTN, and electrooptic modulation in both crystals at frequencies > 100 MHz at 1.3 μm wavelength have been demonstrated. A value of V_π < 1 V has been achieved in SBN at 0.81 μm wavelength, which is a record low for guided-wave modulators in ferroelectrics. The SSO effect from shear-strain has been used in Zn diffused $LiTaO_3$ waveguides to produce electro-optically tunable polarization converter and channel-dropping filter. The use of tungsten bronze SBN and BSTN crystals for making channel-dropping EOTFs is an attractive possibility as the large r_{33} coefficients in these substrates will make it possible to access a large number of channels through birefringence tuning.

REFERENCES

[1] H.F. Taylor, "Applications of guided-wave optics in signal processing and sensing," *Proc. IEEE*, vol. 75, pp. 1524-1535, 1987.

[2] L. Thylén, "Integrated optics in $LiNbO_3$: Recent developments in devices for telecommunications," *J. Lightwave Technol.*, vol. 6, pp. 847-861, 1988.

[3] R.V. Schmidt and I.P. Kaminow, "Metal diffused optical waveguides in $LiNbO_3$," *Appl. Phys. Lett.*, vol. 25, pp. 458-460, 1974.

[4] M.L. Sah, "Optical waveguides in $LiNbO_3$ by ion exchange techniques," *Appl. Phys. Lett.*, vol. 26, pp. 652-653, 1975.

[5] J.L. Jackel, "Optical waveguides in $LiTaO_3$: Silver lithium ion exchange," *Appl. Opt.*, vol. 19, pp. 1966-1969, 1980.

[6] D.W. Yoon and O. Eknoyan, "Characterization of vapor diffused $Zn:LiTaO_3$ optical waveguides," *J. Lightwave Technol.*, vol. 6, pp. 877-880, 1988.

[7] R.R. Neurgaonkar, W.F. Hall, J.R. Oliver, W.W. Ho, and W.K. Cory, "Tungsten bronze $Sr_{1-x}Ba_xNb_2O_6$: A case history of versatility," *Ferroelectrics*, vol. 87, pp. 167-179, 1988.

[8] R.R. Neurgaonkar, W.F. Hall, J.R. Oliver, and W.K. Cory, "Ferroelectric tungsten bronze oxides:a case study of optoelectronic materials," pp. 81-105, Chemistry of Advanced Materials, C.N.R. Rao, Blackwell Scientific Publications, 1992.

[9] J.M. Marx, Z.Tang, O. Eknoyan, H.F. Taylor, and R.R. Neurgaonkar, "low-loss strain induced optical waveguides in strontium barium niobate ($Sr_{0.6}Ba_{0.4}Nb_2O_6$) at 1.3 μm wavelength," *Appl. Phys. Lett.*, vol. 66, pp. 274-276, 1995.

[10] J.F. Nye, Physical Properties of Crystals, p. 243, Oxford, New York, 1957.

[11] I.P. Kaminow, Introduction to Electrooptic Devices, p. 112, Academic Press, New York, 1974.

[12] R.V. Schmidt, P.S. Cross, and A.M. Glass, "Optically induced cross talk in LiNbO$_3$ waveguide switches," *J. Appl. Phys.* , vol. 51, pp. 90-93, 1980.

[13] D.A. Bryan, R. Geson, and E.H. Tomaschke, "Increased optical damage resistance in lithium niobate," *Appl. Phys. Lett.*, vol. 44, pp. 847-849, 1984.

[14] T.R. Volk, V.I. Pryalkin, and N.M. Rubinima, "Optical-damage-resistant LiNbO$_3$:Zn crystal," *Opt. Lett.*, vol. 15, pp. 996-998, 1990.

[15] I.P. Kaminow and J.R. Carruthers, "Optical waveguiding layers in LiNbO$_3$ and LiTaO$_3$," *Appl. Phys. Lett.*, vol. 21, pp. 326-328, 1973.

[16] O. Eknoyan, H.F. Taylor, Z. Tang, V.P. Swenson, and J.M. Marx, "Strain induced optical waveguides in lithium niobate, lithium tantalate, and barium titanate," *Appl. Phys. Lett.*, vol. 60, pp. 407-409, 1992.

[17] M. Minakata, S. Saito, M. Shibata, and S. Miyazawa, "Precise determination of refractive-index changes in Ti-diffused LiNbO$_3$ optical waveguides," *J. Appl. Phys.*, vol. 49, pp. 4677-4682, 1978.

[18] W.K. Burns, P.H. Klein, E.J. West, and L.E. Plew, "Ti diffused in Ti:LiNbO$_3$ planar and channel waveguides," *J. Appl. Phys.*, vol. 50, pp. 6175-6182, 1979.

[19] O. Eknoyan, W.K. Burns, R.P. Moeller, and N.J. Frigo, "Broadband LiTaO$_3$ guided-wave TE-TM mode converter," *Appl. Opt.*, vol. 27, pp. 114-117, 1988.

[20] O. Eknoyan, C.H. Bulmer, H.F. Taylor, W.K. Burns, A.S. Greenblatt, L.A. Beach, and R.R. Neurgaonkar, "Vapor diffused optical waveguides in strontium barium niobate (SBN:60)," *Appl. Phys. Lett.*, vol. 48, pp. 13-15, 1986.

[21] O. Eknoyan, D.W. Yoon, and H.F. Taylor, "Low-loss optical waveguides in lithium tantalate by vapor diffusion," *Appl. Phys. Lett.*, vol. 51, pp. 384-386, 1987.

[22] O. Eknoyan, V.P. Swenson, J.D. Quinn, and R.R. Neurgaonkar, "Low-voltage interferometric modulator in zinc -diffused strontium barium niobate (SBN:60)," *Appl. Phys. Lett.*, vol. 59, pp. 28-30, 1991.

[23] J.L. Jackel, C.E. Rice, and V.J. Veselka, "Proton exchange for high-index waveguides in LiNbO$_3$" *Appl. Phys. Lett.*, vol. 41, pp. 607-608, 1982.

[24] W.B. Spillman, Jr., N.A. Sanford, and R.A. Soref, "Optical waveguides in LiTaO$_3$ by proton exchange," *Opt. Lett.*, vol. 8, pp. 497-498, 1983.

[25] Z. Tang, O. Eknoyan, H.F. Taylor, and V.P. Swenson, "Tunable guided-wave optical polarization convertor in lithium tantalate," *Appl. Phys. Lett.*, vol. 62, pp. 1059-1061, 1993.

[26] Z. Tang, O. Eknoyan, H.F. Taylor, and V.P. Swenson, "Electrooptically tunable wavelength selective polarization converter in LiTaO$_3$," *Electron. Lett.*, vol. 28, pp. 2248-2249, 1992.

[27] W. Warrzanskyj, F. Heismann, and R.C. Alferness, "Polarization-independent electro-optically tunable narrow band wavelength filter," *Appl. Phys. Lett.*, vol. 53, pp. 13-15, 1988.

[28] Z. Tang, O. Eknoyan, and H.F. Taylor, "Polarization-independent electrooptically tunable wavelength filters in LiTaO$_3$," *Electron. Lett.*, vol. 30, pp. 1758-1759, 1994.